EXPERIMENTAL INVESTIGATION AND MODELING OF PRECAST PRESTRESSED HOLLOW-CORE SLABS WITH A STRUT-AND-TIE MODEL

BY

Muneer K. Said

A Thesis Presented to the
DEANSHIP OF GRADUATE STUDIES

KING FAHD UNIVERSITY OF PETROLEUM & MINERALS

DHAHRAN, SAUDI ARABIA

In Partial Fulfillment of the
Requirements for the Degree of

MASTER OF SCIENCE

In

Civil Engineering

April 2009

KING FAHD UNIVERSITY OF PETROLEUM AND MINERALS
DHAHRAN 31261, SAUDI ARABIA

DEANSHIP OF GRADUATE STUDIES

This thesis, written by **Muneer Kaid Said Abdo** under the direction of his Thesis advisor and approved by his Thesis committee, has been presented to and accepted by the Dean of Graduate Studies, in partial fulfillment of the requirements for the degree of **MASTER OF SCIENCE IN CIVIL ENGINEERING.**

Thesis Committee

Prof. Mohammed H. Baluch (Advisor)

Dr. Muhammed K. Rahman (Co – Advisor)

Dr. Ali Hassan Al – Gadhib (Member)

Dr. Ahmed S. Al – Gahtani (Member)

Dr.Maher A. Bader (Member)

Dr. Husain J. Al –Gahtani
Department Chairman

Dr. Salam A. Zummo
(Dean of Graduate Studies)

16/6/09
Date

عمادة الدراسات العليا
DEANSHIP OF GRADUATE STUDIES

This thesis is dedicated to

my parents and my wife

for their

Innumerable prayers , encouragement and patience

ACKNOWLEDGEMENTS

My thanks and gratitude go first to God, my Creator, for his endless blessing. Then, I would like to thank my advisor Dr. Mohammed Baluch, for his continued attention, guidance, and support throughout this work. I also would like to express my sincere gratitude to Dr. M.K.Rahman, my co-advisor, for his guidance, efforts and valuable support. I also would like to thank the thesis committee members, Dr.Ali H.Al.Gadhib, Dr.Ahmed S. Al.Gahtani and Dr.Maher A. Bader, for their valuable suggestions and comments. I am grateful to the laboratory personnel, Mr.Omar and Mr.Essa, for their help and assistance.

Finally, thanks to my parents, my wife, and my son, Aiman. This work would not have been completed without their love, patience, and encouragement.

I am also grateful to SEGIA Gulf Precast Company for providing the hollow core slabs , and to MAPEI of Dammam for the supply of CFRP Sheets and glue materials.

TABLE OF CONTENTS

LIST OF TABLES……xi

LIST OF FIGURES……...….xiii

NOMENCLATURE ……..……xix

THESIS ABSTRACT ……xxii

THESIS ABSTRACT (ARABIC)…….…… ….xxiii

CHAPTER 1 INTRODUCTION.....1

1.1 OVERVIEW OF SYSTEM OF PRECAST PRESTRESSED HOLLOW ..

CORE SLABS 1

1.2 STRUT-AND-TIE MODEL.....2

1.2.1 Introduction 2

1.2.2 Assumptions of Strut-and-Tie Models.....3

1.2.3 Strut-and-Tie Model for RC Members 4

1.3 OBJECTIVES AND SCOPE OF RESEARCH 6

1.4 PHASES OF THE RESEARCH 8

1.4.1 Phase 1: Literature Review and Mobilization for Testing of

PPHC Slabs.....8

1.4.2 Phase 2: Full-Scale Load Testing of Hollow-Core Slabs.....9

1.4.3 Phase 3: Development of Strut-and-Tie Model for PPHC Slabs.....10

1.4.4 Phase 4: Analysis of Data 10

1.5 OUTLINE OF THE CONTENTS IN THESIS 10

CHAPTER 2 LITRATURE REVIEW 12

2.1 INTRODUCTION 12

2.2 FULL SCALE LOAD TESTING OF FRP STRENGTHENED SLABS 13

2.2.1 FRP Strengthened One -Way & Two -Way Slabs 13

2.2.2 Full-Scale Load Tests On PPHC Slabs 15

2.2.3 FRP Strengthened PPHC Slabs 16

2.3 STRUT-AND-TIE MODEL 17

2.3.1 Background 17

2.3.2 Truss Analogy for Design of B-Region 19

2.3.2.1 Compression Field Theory 20

2.3.2.2 Modified Compression Field Theory 21

2.3.3 Components of Strut-and-Tie Model 22

2.3.3.1 Struts 22

2.3.3.2 Ties 25

2.3.3.3 Nodes 27

2.3.4 The Strut-and-Tie Method for Analysis and Design 29

CHAPTER 3 EXPERIMENTAL PROGRAM 36

3.1 TEST ARRANGEMENT 36

3.2 MATERIAL 39

3.2.1 Concrete *39*

3.2.2 Prestressing Strands *39*

3.2.3 Carbon Fiber Reinforced Polymer (CFRP) Sheet *40*

3.3 INSTRUMENTATIONS **40**

3.3.1 Strain Gauges ***41***

3.3.2 Linear Variable Displacement Transducers (LVDT) ***43***

3.3.3 Linear Motion Transducers LMT ***44***

CHAPTER 4 STRUT –AND-TIE METHOD APPROACH FOR PPHC SLABS **45**

4.1 INTRODUCTION **45**

4.2 **EFFECTIVE FACTOR MODELS IN THE STM** **46**

4.3 PROPOSED STRUT- AND-TIE MODEL APPROACH **48**

4.3.1 Introduction ***48***

4.3.2 Strut-and-Tie Model for PPHC Slabs without CFRP ***48***

4.3.2.1 Selecting the Struts and Ties Centerlines 48

4.3.2.2 Dimensioning the Struts and Ties 50

4.3.2.3 Applying the Effect of Prestressing Force 51

4.3.2.4 Adjusting the Centerline and Width of Horizontal Struts 53

4.3.2.5 Checking Stress Ratios in Strut-and-Tie Elements 54

4.3.3 An example of Strength Prediction Process by Using the Proposed STM ***55***

4.3.4 Strut -and-Tie Model for PPHC Slabs with CFRP ***60***

4.3.4.1 Selecting the Struts and Ties Centerlines 60

4.3.4.2 Dimensioning the Struts and Ties 61
4.3.4.3 Applying the Effect of Prestressing Force 62
4.3.4.4 Adjusting the Centerline and Width of Horizontal Strut 62
4.3.4.5 Checking the Stress Ratios in Strut and Tie Elements 63
4.3.5 An example of Strength Prediction Process for Strengthened PPHC Slab by Using the Proposed STM 63
CHAPTER 5 RESULTS AND DISCUSSION 70
5.1 ANALYTICAL RESULTS 70
5.1.1 General 70
5.1.2 Design of PPHC Slabs 70
5.1.2.1 Flexural Load Capacity of Hollow Core Slabs 71
5.1.2.2 Shear Load Capacity of Hollow Core Slabs 72
5.1.2.2.1 Flexural Shear Capacity 72
5.1.2.2.2 Web shear capacity 74
5.1.3 Detailed Example of Analytical Calculations 75
5.1.3.1 Cracking Moment for Slab S4-B 75
5.1.3.2 Ultimate Moment Capacity for Slab S4-B 76
5.1.3.3 Ultimate Shear Capacity for Slab S4-B 78
5.1.3.4 Cracking Moment for Slab S8-D 79
5.1.3.5 Ultimate Moment Capacity for Slab S8-D 80
5.1.3.6 Ultimate Shear Force for Slab S17-H 82
5.2 EXPERIMENTAL RESULTS 85

5.2.1 Introduction *85*

5.2.2 Test Results of PPHC Slabs with length of 5m *88*

5.2.2.1 Test Results for Slab S1-A 88

5.2.2.2 Test Results for Slab S2-A 91

5.2.2.3 Test results for specimen S3-B 93

5.2.2.4 Test results for specimen S4-B 96

5.2.2.5 Test results for specimen S5-C 98

5.2.2.6 Test results for specimen S6-C 101

5.2.2.7 Test results for specimen S7-C 103

5.2.2.8 Test results for specimen S8-D 106

5.2.2.9 Summary of the Experimental Results of PPHC Slabs with Length of 5m 109

5.2.3 Test Results of PPHC Slabs with Length of 2.5m *111*

5.2.3.1 Test Results for Slab S9-E 111

5.2.3.2 Test Results for Slab S10 -E 113

5.2.3.3 Test Results for Slab S11-E 115

5.2.3.4 Test Results for Slab 12-F 118

5.2.3.5 Test Results for Slab S13-F 120

5.2.3.6 Test Results for Slab S14-G 122

5.2.3.7 Test Results for Slab S15-G 124

5.2.3.8 Test Results for Slab S16-G 126

5.2.3.9 Test Results for Slab S17-H 127

5.2.3.10 Summary of the Experimental Results of PPHC Slabs with Length of 2.5m.....130

5.3 The STRUT-AND-TIE MODEL RESULTS 131

5.4 EFFECT OF STRANDS SLIP ON THE FAILURE MODE of PPHC SLABS.....136

CHAPTER 6 SUMMARY , CONCLUSION & RECOMMENDATIONS 140

6.1 SUMMARY 140

6.2 CONCLUSIONS.....141

6.3 RECOMMENDATIONS FOR FUTURE STUDY.....143

REFERENCES.....144

VITA.....151

LIST OF TABLES

Table 1.1: Details of Tested Hollow-Core Slabs 9

Table 3.1: Results From the Tensile Strength of Strands 40

Table 3.2: Properties of the CFRP Sheets 40

Table 4.1: Effective Factor Models 46

Table 4.2: Distribution of Effective Prestressing Force along Strand's Transfer Length 58

Table 4.3: Dimensions of Strut-and-Tie Elements for Strengthened PPHC Slabs 62

Table 4.4: Dimensions of Strut-and-Tie Model Elements for Slab SD-8 66

Table 4.5: Distribution of Effective Prestressing force over the transfer length 66

Table 4.6: Dimensions of STM for PPHC Slabs, mm 68

Table 4.7: Area of Horizontal Struts of PPHC Slabs, mm^2 68

Table 4.8: Width and Thickness Scale Factor of Horizontal Struts 69

Table 5.1: Analytical Results of Tested PPHC Slabs 85

Table 5.2: Test Setup and Analytical Failure Loads for the Tested Slabs 86

Table 5.3: Maximum Strains in the Slab S1-A 91

Table 5.4: Maximum Strains in Slab S2-A 93

Table 5.5: Maximum Strains in the Slab S3-B 95

Table 5.6: The Maximum Strains in the slab S4-B 98

Table 5.7: Maximum Strains in The slab S5-C 101

Table 5.8: Maximum Strains in the Slab S7-C 106

Table 5.9: Summary of the Experimental Results for PPHC slabs with Length of 5m 109

Table 5.10: Summary of the Experimental Results of PPHC Slabs with Length of 2.5m 130
Table 5.11: Strut-and-Tie Model Results for Tested PPHC Slabs..... 131
Table 5.12: Comparison between the Analytical and Experimental Results..... 132
Table 5.13: Comparison between the Experimental Failure Loads and the Results Obtained by New Proposed Eqn. (5.17) 136
Table 5.14: Comparison between the STM Results and the Experimental Results... 136
Table 6.1: Summary of Analytical, Experimental and STM Failure Loads, kN 141

LIST OF FIGURES

Figure 1.1: Hollow Core Slabs.....2

Figure 1.2: Strut-and-Tie Model for Deep Beam.....5

Figure 1.3:Examples of Strut-and-Tie Models for Common D-Regions: (a) Beam-column joint, (b) Coupling beam in a coupled structural wall, (c) Non-slender wall, (d)Dapped-beam end , (e) Pile cap under combined axial load and moment (f) Prestressed concrete beam end. 7

Figure 1.4: B-Regions and D-Regions.....7

Figure 1.5: Schematic Diagram Showing the Front View of the Experimental Setup 9

Figure 2.1: Shear Stress between Cracks (MacGregor, 1997).....18

Figure 2.2: Mode of Failure of Deep Beams, a/d=0.5 to 2.5 (MacGregor, 1997).....18

Figure 2.3: Truss Analogy (MacGregor, 1997) 21

Figure 2.4: Stress-strain Relationships for Cracked Concrete (Collins et al. 1996) 22

Figure 2.5: Idealized Stress Fields in Struts: (a) Prismatic (b) Bottle-shaped (c) Fan-shaped (Adapted from Schliach et al. 1987). 24

Figure 2.6: Typical Stress-Strain Relationship for Concrete in Uniaxial Compression and the Idealization Used in the STM. 25

Figure 2.7: Effective Width of Tie.....27

Figure 2.8 : Basic Node Types: a) CCC b) CCT c) CTT d) TTT 28

Figure 2.9: Examples of Shape Idealization of a Nodal Zone with Four Struts Intersecting: a) Force Acting on the Node b) Simple Shape c) Hydrostatic Shape d) Modified Hydrostatic Shape. 29
Figure 3.1 Frame Used for Testing PPHC Slabs 36
Figure 3.2 : Fabricated I Beams for Application of Line Loads 37
Figure 3.3: Loading Tools, Hydraulic Jack and Load Cell 37
Figure 3.4: The complete Setup for Testing of Hollow Core Slab 38
Figure 3.5: Data Tools: Power Supply, Data Logger and Computer 38
Figure 3.6: Four-Point Loading System for Hollow Core Slabs in Flexure. 39
Figure 3.7: Four-Point Loading System for Hollow Core Slabs in Shear. 39
Figure 3.8: Two LVDTs Placed Under the Slab to Measure Deflection 44
Figure 3.9 : LMT to Measure the Slip of Strand 44
Figure 4.1: Inappropriate Strut-and-Tie Model for PPHC slab 48
Figure 4.2: Proposed Strut-and-Tie Model of PPHC Slabs 49
Figure 4.3: Modeling Prestressing Force of Pre-tensioned Member 53
Figure 4.4: Acceptable Model for Prestressing Force of Pre-tensioned member 53
Figure 4.5: Determining the New Width of Top Horizontal Strut 54
Figure 4.6: Setup Test for Slab S4-B 56
Figure 4.7: Centerlines of STM for Slab S4-B 56
Figure 4.8: Simplified Strut-and-Tie Model of PPHC Slab with CFRP 61
Figure 4.9: Designations of Strut and Tie Elements 61
Figure 4.10: Setup Test for Slab S8-D 64
Figure 4.11: Centerlines of STM for Slab S8-D 65

Figure 4.12: Gradual Effect of Prestressing Force on Slab S8-D 67

Figure 4.13: Direct Effect of Prestressing Force on Slab S8-D 67

Figure 5.1: Cross-Sections of PPHC Slabs 70

Figure 5.2: Ultimate Moment Capacity of PPHC Slab by the Strain Compatibility Method 76

Figure 5.3: Cracking During the Testing of Slab S1-A 89

Figure 5.4: Location of Strain Gauges on Slab S1-A 89

Figure 5.5: Load-Deflection Curves for Slab S1-A 90

Figure 5.6: : Load-Strain Curves for Slab S1-A 90

Figure 5.7: Cracking During the Testing of S2-A 91

Figure 5.8: Location of Strain Gauges on the Slab S2-A 92

Figure 5.9: Load-Deflection Curve for Slab S2-A 92

Figure 5.10: Load-Strain Curves for Slab S2-A 93

Figure 5.11: Cracking During the Testing of Slab S3-B 94

Figure 5.12: Location of Strain Gauges on the Slab S3-B 94

Figure 5.13: Load-Deflection Curves for Slab S3-B 95

Figure 5.14: Load-Strain Curves for Slab S3-B 95

Figure 5.15: Cracking During the Testing of Slab S4-B 96

Figure 5.16: Location of Strain Gauges on Slab S4-B 97

Figure 5.17: Load-Deflection Curves for Slab S4-B 97

Figure 5.18: Load-Strain Curves for Slab S4-B 98

Figure 5.19: Cracking During the Testing of Slab S5-C 99

Figure 5.20: Location of Strain Gauges on Slab S5-C 99

Figure 5.21: Load-Deflection Curves for Slab S5-C 100

Figure 5.22: Load-Strain Curves for Slab S5-C..... 100

Figure 5.23: Cracking During the Testing of Slab S6-C 101

Figure 5.24: Location of Strain Gauges on Slab S6-C..... 102

Figure 5.25: Load-Deflection curves for Slab S6-C 102

Figure 5.26: Load-Strain Curves for Slab S6-C..... 103

Figure 5.27: Cracking During the Testing of Slab S7-C 104

Figure 5.28: Location of Strain Gauges on Slab S7-C..... 104

Figure 5.29: Load-Deflection Curves for the Slab S7-C 105

Figure 5.30: Load-Strain Curves for the Slab S7-C..... 105

Figure 5.31: Strengthening the Slab S8-D with One Layer of CFRP..... 107

Figure 5.32: Cracking During the Testing of Slab S8-D 107

Figure 5.33: Locations of Strain Gauges: a) on concrete b) on CFRP 108

Figure 5.34: Load-Deflection curves for the Slab S8-D..... 108

Figure 5.35: Load-Strain Curves for the Slab S8-D 109

Figure 5.36: Load-Mid Span Deflection Curves for the PPHC Slabs with Length of 5m 110

Figure 5.37: Load-Compressive Strains for the PPHC Slabs with Length of 5m 110

Figure 5.38: Cracking During the Testing of Slab S9-E..... 111

Figure 5.39: Location of Strain Gauges on Slab S9-E..... 112

Figure 5.40: Load-Deflection Curves for Slab S9-E 112

Figure 5.41: Load-Strain Curves for Slab S9-E..... 113

Figure 5.42: Cracking During the Testing of Slab S10-E..... 113

Figure 5.43: Location of Strain Gauges on Slab S10-E.....114

Figure 5.44: Load-Deflection Curves for Slab S10-E 114

Figure 5.45: Load-Strain Curves for Slab 10-E.....115

Figure 5.46: Cracking During the Testing of Slab S11-E.....116

Figure 5.47: Location of Strain Gauges on the Slab S11-E.....116

Figure 5.48: Load-Deflection Curves for Slab 11-E.....117

Figure 5.49: Load-Strain Curves for Slab S11-E.....117

Figure 5.50: Cracking During the Testing of Slab 12-F 118

Figure 5.51: Location of Strain Gauges on the Slab S12-F 118

Figure 5.52: Load-Deflection Curves for the Slab S12-F.....119

Figure 5.53:Load-Strain Curves for Slab S12-F 119

Figure 5.54: Cracking During the Testing of Slab S13-F.....120

Figure 5.55: : Location of Strain Gauges on the Slab S13-F.....120

Figure 5.56: Load-Deflection Curves for slab S13-F 121

Figure 5.57: Load-Strain Curves for S13-F 121

Figure 5.58: Cracking During the Testing of Slab S14-G 122

Figure 5.59: Location of Strain Gauges on the Slab S14-G 122

Figure 5.60: Load-Deflection Curves for Slab S14-G.....123

Figure 5.61: Load-Strain Curves for Slab S14-G 123

Figure 5.62: Cracking During the Testing of Slab S15-G 124

Figure 5.63: : Location of Strain Gauges on the Slab S15-G 124

Figure 5.64: Load-Deflection Curves for Slab S15-G.....125

Figure 5.65: Load-Strain Curves for Slab S15-G 125

Figure 5.66: Load-Deflection Curves for Slab S16-G 126

Figure 5.67: Load-Strain Curves for Slab S16-G 127

Figure 5.68: Shear Strengthening of Slab S17-H 128

Figure 5.69: Cracking During the Testing of Slab S17-H 128

Figure 5.70: Load-Deflection curves for Slab S17-H 129

Figure 5.71: Load-Strain Curves for Slab S17-H 129

Figure 5.72: Load-Mid Span Deflection Curves for the PPHC Slabs with length of 2.5 m 131

Figure 5.73: Relation between k Factor and a/d Ratio 134

Figure 5.74: Relation between a/d and Applied Load by Using ACI Code Expressions 135

Figure 5.75: Relation between a/d and Applied Load by Using New Proposed Equation 135

Figure 5.76 : Load-Slip Curves for Slabs S12,S13&S14 137

Figure 5.77: Load-Slip Curves for Slabs S5, S6 &S7 138

Figure 5.78: Load-Slip Curves for Slabs S14 ,S15 &S16 138

Figure 5.79: Load-Slip Curves for Slabs S9, S10 &S11 139

NOMENCLATURE

ABBREVIATIONS

AASHTO	American Association of State Highway and Transportation Officials
ACI	American Concrete Institute
ASCE	American Society of Civil Engineers
CAST	Computer Aided Strut-and-Tie
CFRP	Carbon Fiber Reinforced Polymer
LFRD	Load and Resistance Factor Design
MCFT	Modified Compression Field Theory
PPHCS	Prestressed Precast Hollow Core Slab
STM	Strut-and-Tie Model

ENGLISH AND GREEK SYMBOLS

a	Shear Span, measured from the center of loading to center of support
A_{dst}	Effective cross-sectional area of a diagonal strut
A_{frp}	Area of CFRP
A_{dtie}	Effective cross-sectional area of a diagonal tie
A_{hst}	Effective cross-sectional area of a horizontal strut
A_{dtie}	Effective cross-sectional area of a diagonal tie
A_{htie}	Effective cross-sectional area of a horizontal tie
A_p	Area of prestressing strands
A_{ps}	Cross-sectional area of bonded prestressed reinforcement of a tie
C	Compressive force in concrete

d Effective depth of a PPHC slab , measured from the extreme compression fiber to the centroid of longitudinal tension reinforcement

d_{tie} Effective depth of a PPHC slab with CFRP strengthening, measured from the extreme compression fiber to the new level of longitudinal tension tie.

E_c Tangent or secant modulus of elasticity of concrete

E_s Modulus of elasticity of steel

e Distance from neutral axis to centroid of prestressing reinforcement

f_c' Specified compressive strength of concrete

f_{cr} Cracking strength of concrete

f_{frp} Stress in CFRP

f_{cr} Cracking strength of concrete

f_{pu} Specified tensile strength of prestressing steel

f_y Specified yield strength of non-prestressed reinforcement in tension or compression.

I Cross-sectional moment of inertia

M_n Nominal flexural strength

P_e Effective force in prestressing strands after all losses

P_i Initial prestressing force

S_b Sectional modulus

T_s Tensile force in prestressing strands

T_{frp} Tensile force in prestressing strands

V_{ci} Flexural shear resistance of concrete

V_{cw} Web shear resistance of concrete

∇f_p Remaining stress in prestressed reinforcement to resist tension

ε_1 Principal average tensile strain

ε_2 Principal average compressive strain

ε_c Compressive strain in uniaxial compressive stress-strain curve of concrete , also compressive strain in stress-strain curve of a strut

ε_{cu} Strain at ultimate in uniaxial compressive stress-strain curve of concrete

ε_{se} Initial strain in prestressed reinforcement

ε_{ps} Total strain in prestressed reinforcement

ε_{frp} Strain in CFRP

ϕ Strength reduction factor

ν Effectiveness factor

θ_s Smallest angle between the strut and the adjoining ties

THESIS ABSTRACT

Full Name	**Muneer Kaid Said Abdo**
Title of Study	**Experimental Investigation and Modeling of Precast, Prestressed Hollow-Core Slabs With A Strut-and-Tie Model**
Major Field	**CIVIL ENGINEERING (STRUCTURES)**
Date of Degree	**APRIL 2009**

The strut-and-tie model provides one of the most useful design methods for shear critical concrete structures, and it gives a better understanding of the force flow in cracked reinforced concrete members, with struts representing the flow of compressive stresses and ties representing the flow of tension stresses. Prestressed precast hollow core slabs are used extensively for floors and roofs in precast concrete construction. For these prestressed concrete members without web reinforcement, shear can be critical for certain load configurations. The strut and tie model provides a tool for predicting the flexural and shear capacity of these slabs. This study presents a new strut-and-tie model to predict the ultimate load-carrying capacity of prestressed precast hollow core slabs and also to indicate the associated mode of failure. It is important to incorporate concrete tension elements (concrete ties) in the truss model to carry the diagonal tension forces in these members. An experimental program involving full-scale load-testing of 17 hollow core slabs, 4.7 m and 2.2 m in span and having three different depths, 200 mm, 250 mm and 300 mm was conducted by using the four point load test. The flexural and shear strength of 17 prestressed precast hollow core (PPHC) slabs with different shear span-to-depth (*a/d*) ratio were investigated experimentally and analytically. The results obtained from the proposed strut-and-tie model have been compared with experimental results The proposed strut-and-tie model provides good agreement with the experimental results, and it can be employed for the analysis and design of hollow core slabs.

MASTER OF SCIENCE
KING FAHD UNIVERSITY OF PETROLEUM AND MINERALS
Dhahran, Saudi Arabia
April 2009

ملخص الرسالة

الاسم منير قائد سعيد عبده

عنوان الرسالة التحقيق المخبري والنمذجه للبلاطات المجوفه المسبقة الصب والاجهاد المعرضه لقوى الانحناء والقص باستخدام نموذج سترت – تاي

التخصص هندسه مدنيه (إنشاءات)

تاريخ التخرج ابريل 2009

نموذج سترت – تاي قدم واحده من افضل الطرق المفيده للمنشات الخرسانيه المعرضه للقوى القص الحرجه. واعطى فهم اوضح لطريقة انسياب القوى في العناصر الخرسانيه المسلحه المتشققه باعتبار الاجهادات الضاغطه سترت و االإ جهادات الشاده تاي . البلاطات المجوفه المسبقة الاجهاد والصب تستخدم كأسقف او اسطح بشكل واسع في المشات المسبقة الصب. تعتبر قوى القص حرجه بالنسبه للعناصر المسبقة الاجهاد التي لاتحتوى على تسليح القص تحت تأثير نوع محدد من الحمولات . هذه الدراسه تقدم نموذج سترت – تاي جديد لحساب حمولة التحمل القصوى للبلاطات المجوفه المسبقة الاجهاد والصب و لتحديد الية الانهيار المرافقه . من المهم استخدام العناصر الخرسانيه المعرضه للشد (تاي من الخرسانه) لتحمل القوى الشاده المائله في تلك العناصر. اجريت التجارب المعمليه ل 17 بلاطه مجوفه مسبقة الإجهاد والصب` ذات بحور (4.7 m , 2.7 m) وسماكات مختلفه (200mm , 250mm , 300mm) باستخدام حموله رباعية النقاط . اجرى التحقيق المعملي والتحليلي لدراسة مقاومة للبلاطات المجوفه المسبقة الإجهاد والصب ذات نسب مجاز القص الى العمق مختلفه للانحناء وللقص . تمت مقارنة النتائج التي تم الحصول عليها باستخدام نموذج سترت – تاى مع النتائج المخبريه . الأنموج المقترح سترت – تاي اعطى نتائج متوافقه بشكل جيد مع النتائج المعمليه ويمكن استخدامه لتحليل وتصميم البلاطات الجوفه المسبقة الإجهاد والصب.

ماجستير العلوم

جامعة الملك فهد للبترول والمعادن

الظهران ، المملكه العربيه السعوديه

ابريل 2009

CHAPTER 1

INTRODUCTION

1.1 OVERVIEW OF SYSTEM OF PRECAST PRESTRESSED HOLLOW-CORE SLABS

Precast prestressed hollow-core slab is one of the most commonly used structural systems to cover large spans. Continuous voids are formed through each unit to reduce weight and improve structural performance. Hollow-core slabs are being used extensively in Saudi Arabia in both commercial and residential buildings. Due to extensive usage of PPHC, it is appropriate that designers have more detailed information about their performance under flexure and shear loading. One of the advantages of using hollow-core slab is that its construction is very fast and the floor/roof of buildings can be completed in a short time with high quality. In precast concrete construction, the slab systems comprise principally hollow-core slabs of spans ranging from 4 to 6 meters. Figure 1.1 shows typical hollow core slabs used in roof and floor systems. The main objectives of this research are: (i) to conduct an experimental investigation of hollow-core slab of depths ranging from 200 mm to 300 mm in flexure and shear with and without strengthening using CFRP sheets, and (ii) to develop a strut-and-tie model that will predict the response of PPHC slabs. The results of full-scale slab testing from this work and the research completed earlier at KFUPM (Mohiuddin (2006) and Mahmud (2008)) will be used to verify the validity of the strut-and-tie model.

Figure 1.1: Hollow Core Slabs

1.2 STRUT-AND-TIE MODEL

1.2.1 Introduction

Strut-and-Tie Modeling (STM) is a method of design for reinforced and prestressed concrete that reduces complex states of stress within a structure to a collection of simple stress paths. The stress paths result in truss members loaded with uniaxial stress that is parallel to the axis of the stress path. Truss members that are in compression are called struts, while the force paths that are in tension are named ties. The intersections of struts and/or ties form the nodes. The collection of struts, ties and nodes is called a truss mechanism or model. The forces within a strut-and-tie model can be calculated by using static equilibrium if the truss is statically determinate. Such a reduction in complexity allows for simple design of structural concrete. With the forces in each strut and tie having been determined from basic statics and any necessary compatibility conditions, only the stresses within these elements (struts, ties, and nodes) need to be compared with permissible stresses. To determine the allowable stress for a strut or node, empirical observations of their behavior must be made. The empirical observations of the strength of isolated members can be

combined with truss mechanisms to develop an accurate model for prediction of the strength of the concrete member.

1.2.2 Assumptions of Strut-and-Tie Models

The basic assumptions followed in the development of the strut-and-tie models used in this study are:

- Static equilibrium must be satisfied.
- The concrete resists compression and has an effective concrete compression strength which prevents diagonal crushing of the concrete prior to yielding of the steel.
- For reinforced concrete members with web reinforcement, compression forces are resisted by concrete (compression struts) and tension forces are resisted by reinforcing steel (tension elements). For reinforced concrete beams without web reinforcement, concrete tension elements are used to resist the tension forces in the members.
- The effective prestressing forces represented by equivalent external loads are gradually introduced along the tendon's transfer length in the nearest strut-and-tie model joints. The pretensioned strands act as the tension chord, and they carry only axial stresses.
- The precast prestressed hollow-core slab will be idealized in such a way that the external loads are applied only at the truss joints.
- The truss members are connected at the joints by frictionless pins. The centerline of each truss member and the lines of action of all external loads at the joint must coincide. This concurrent force system makes the assumption of a pinned joint reasonable.

- Proper detailing of the member is required to ensure the development of the proposed truss model. The designer must provide adequate mechanical anchorage or development length so that the tension truss member forces can be developed at the required locations. Adequate bearing plates must also be provide at supports and points of application of heavy concentrated loads. Proper detailed truss models will result in a discrete stress field which satisfies the lower-bound theorem in plasticity.

1.2.3 Strut-and-Tie Model for RC Members

A strut-and-tie model (STM) consists of elements in pure tension or compression. Appropriate reinforcement must be provided in the portions of the structure where tension is indicated by the strut-and-tie model or where additional strength, confinement, or both, are required by the struts. By using a simple truss model, an estimation of strength of a structural element can be made and, the element can be appropriately detailed.

Strut-and-tie modeling is most useful as a design tool when applied to structures, or portions of structures, in which plane sections do not remain planar after the application of load. The behavior of such elements (corbels, deep beams, dapped-end beams, or post-tension anchorage zones) is not dominated by flexural deformations. The difficulty in analyzing these types of elements often arises from the inability to apply kinematic compatibility. STM disregards kinematic constraints. Overall equilibrium and equilibrium of the nodes are considered during the analysis stage. The constitutive relationships are determined by empirical observation of struts, ties and nodes to establish the yield conditions for those elements. STM, therefore, conforms to the lower bound theory of plasticity, which requires that only equilibrium and yield conditions be satisfied. According to Nielson (1998), the lower bound

theory of plasticity states that, if the load has such a magnitude that it is possible to find a stress distribution corresponding to stresses within the yield surface and to maintain internal and external equilibrium, then this load will not cause a collapse of the body. In other words, the capacity of a structure as estimated by a lower bound method will be less than, or at most equal to, the actual collapse load of the structure in question. The most appealing quality of a lower bound theory is its inherent conservatism.

Strut-and-tie model is considered a rational and consistent basis for designing the cracked reinforced concrete structures. The successful application of a strut-and-tie model depends on a reliable visualization of the path of the force flows. In a typical strut-and-tie analysis, the force distribution is visualized as compressive struts and tensile ties, respectively. Figure 1.2 provides a simple strut-and-tie model applied to a simply supported deep beam. In this figure, the lighter shaded regions represent concrete compressive struts, the steel reinforcing bar represents a tensile tie, and the dark shaded regions represent nodal zones.

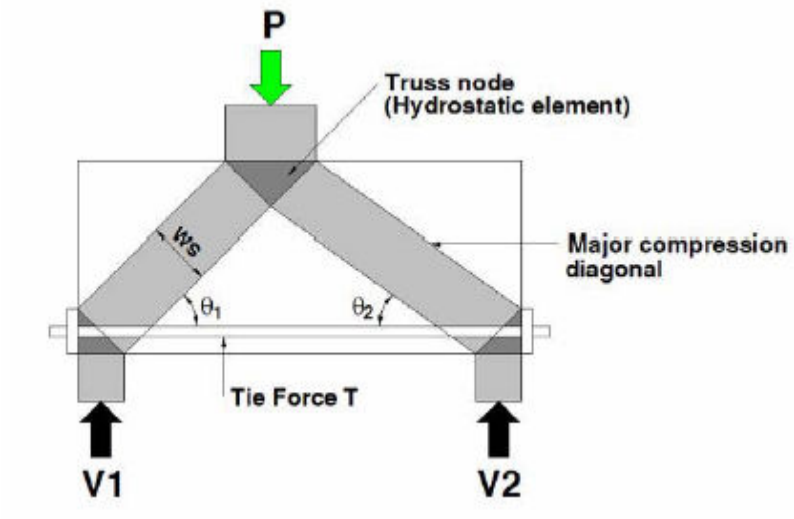

Figure 1.2: Strut-and-Tie Model for Deep Beam

Strut-and-tie modeling was first introduced into American code provisions in the AASHTO Guide Specifications for Design and Construction of Segmental

Concrete Bridges in 1989. In the segmental guide specification, STM can be used to design shear and torsion as well as the forces induced by the anchorage of post-tensioned prestressing forces. In recent years STM has become an increasingly popular method for design and detailing of structural concrete members. Code provisions for STM have been adopted for design by both ACI 318-05 and the AASHTO LRFD Bridge Design Specifications (2005).

Strut-and-tie models are often divided into two categories based on the regions of the structure to which they apply. The distinction is based on the basic stress distribution within the structure. While elastic stresses are not necessarily representative of the stress distribution within the structure, they are utilized to characterize different areas of the structure. The elastic state of stress in the member may be characterized by the use of stress trajectories (contour of principal stress). At concentrated loads and at supports, where the stresses are "disturbed", the areas are defined as D-regions. Figure 1.3 shows examples of strut-and-tie models for a few typical D-regions. Between D-regions, the linear strain profile assumptions of Bernoulli are applicable. These areas are defined as B-regions as shown in Figure 1.4.

1.3 OBJECTIVES AND SCOPE OF RESEARCH

The need for this research exists for reasons which can be summarized as follows:

- Precast prestressed hollow-core slab is being used extensively in Saudi Arabia in both commercial and residential buildings.
- Shear strength of PPHC slabs has not been investigated in detail.

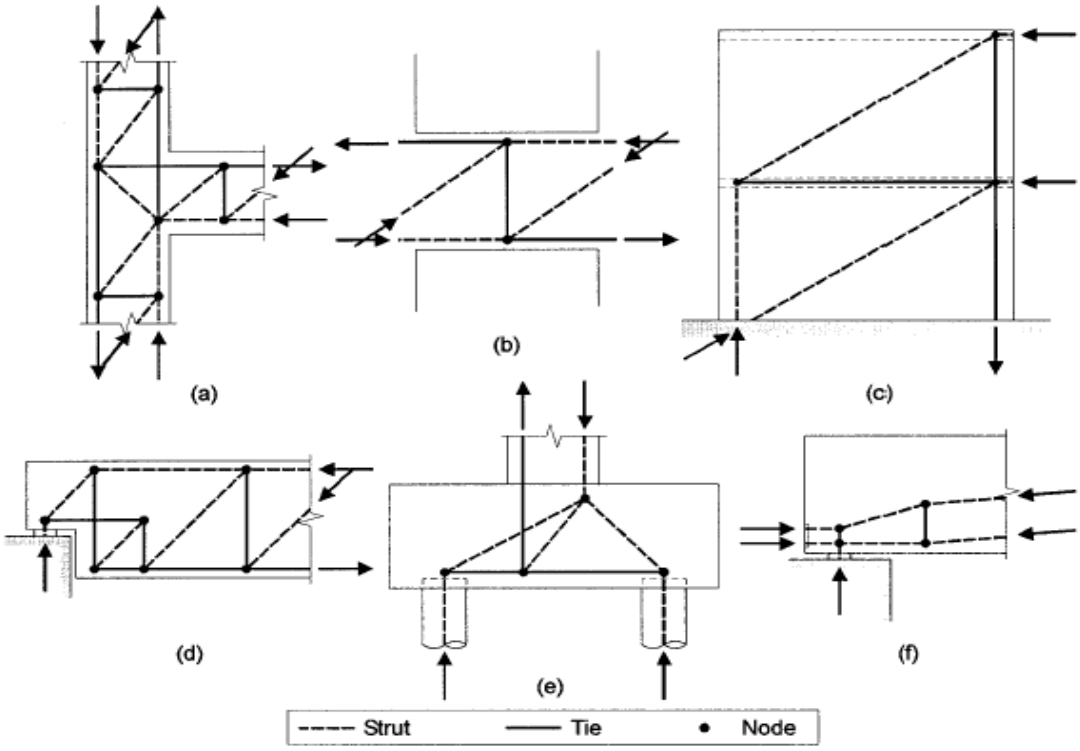

Figure 1.3:Examples of Strut-and-Tie Models for Common D-Regions: (a) Beam-column joint, (b) Coupling beam in a coupled structural wall, (c) Non-slender wall, (d)Dapped-beam end , (e) Pile cap under combined axial load and moment (f) Prestressed concrete beam end.

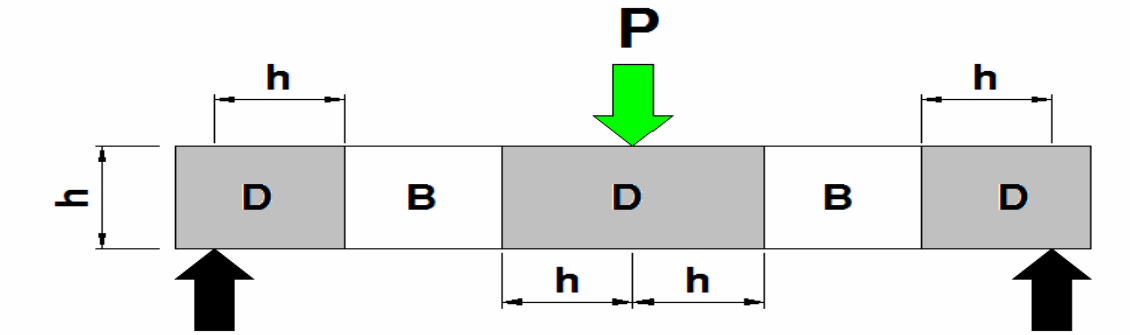

Figure 1.4: B-Regions and D-Regions

- The analytical models for prestressed hollow-core slabs design proposed in the literature sometimes are contradictory.
- The strut-and-tie model is increasingly being used for design of concrete members but the STM for PPHC slabs has not yet been proposed and has to be investigated as it provides a very convenient method.

- The design approach for strengthening prestressed hollow-core slabs by using externally bonded CFRP is far from complete and straightforward. Therefore, there is a need to develop a computational model for the CFRP strengthened stressed hollow-core slabs to be used in industry for the investigation and design of concrete structures.

The specific objectives of this study are:

- To study the experimental behavior in flexure and shear of full-scale PPHC slabs with depths ranging from 200mm to 300mm.
- To study the influence of shear span-to-depth ratio on failure mode of precast prestressed Hollow Core Slabs
- To ascertain the degree of strut-and-tie modeling implementation for PPHC slabs.
- To develop a strut-and-tie model for PPHC slabs with and without CFRP strengthening.
- To develop design recommendations for the CFRP strengthened PPHC slabs to be used in industry.

1.4 PHASES OF THE RESEARCH

The research program has five major phases. Those phases can be summarized as follows:

1.4.1 Phase 1: Literature Review and Mobilization for Testing of PPHC Slabs

A literature search has been conducted to obtain recent information regarding similar studies conducted elsewhere. The literature search will focus on strut-and-tie modelling of reinforced concrete elements prestressed and strengthened by CFRP.

The frame in the Heavy Equipment Laboratory at the Department of Civil Engineering was modified for the testing of the hollow-core slabs in flexure and shear. The testing arrangement is shown schematically in Figure 1.5.

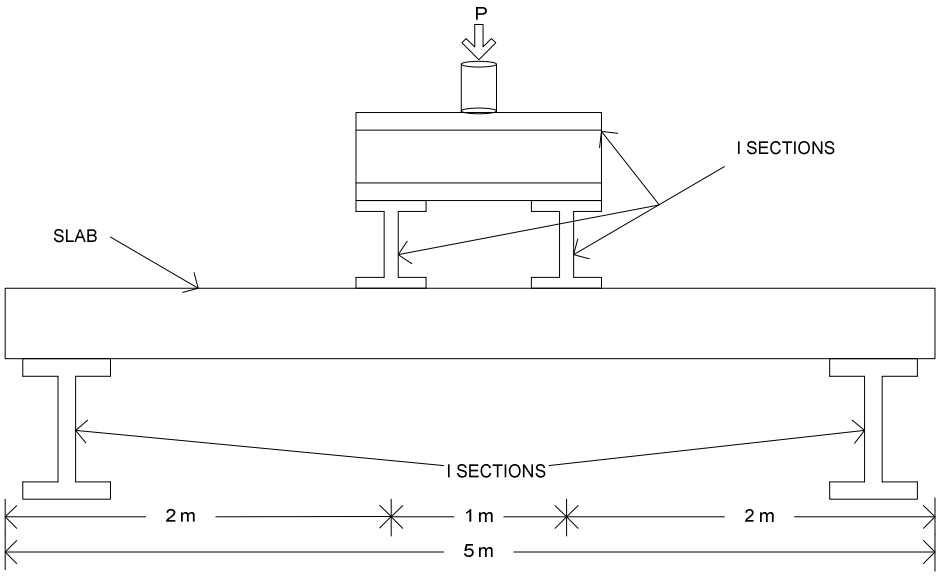

Figure 1.5: Schematic Diagram Showing the Front View of the Experimental Setup

1.4.2 Phase 2: Full-Scale Load Testing of Hollow-Core Slabs

The details of hollow-core slabs to be tested are shown in Table 1.1.

Table 1.1: Details of Tested Hollow-Core Slabs

S.N.	Code of Slab	Length (m)	Thickness (mm)	Type of Strengthening	No. of Strands
1	S1-A	5	200	-	6 strands
2	S2-A	5	200	-	6 strands
3	S3-B	5	250	-	6 strands
4	S4-B	5	250	-	6 strands
5	S5-C	5	300	-	6 strands
6	S6-C	5	300	-	8 strands
7	S7-C	5	300	-	8 strands
8	S8-D	5	250	Flexure	6 Strands
9	S9-E	2.5	200	-	4 strands
10	S10-E	2.5	200	-	4 strands
11	S11-E	2.5	200	-	4 strands

12	S12-F	2.5	250	-	6 strands
13	S13-F	2.5	250	-	6 strands
14	S14-G	2.5	300	-	6 Strands
15	S15-G	2.5	300	-	8 Strands
16	S16-G	2.5	300	-	8 Strands
17	S17-H	2.5	250	Shear	8 strands

* The Slab is strengthened with CFRP sheets in flexure.
** The Slab is strengthened with CFRP sheets in shear.

1.4.3 Phase 3: Development of Strut-and-Tie Model for PPHC Slabs

The important task in the thesis is developing a strut-and-tie model for the various categories of hollow-core slab and predicting the results of the experiments. The model, which will take into consideration all the possible failure modes of strengthened hollow-core slabs with CFRP and of non-strengthened slabs, is validated by comparison with experimental data that will be generated during the phase of this work and other previous experimental work at KFUPM.

1.4.4 Phase 4: Analysis of Data

The data on failure loads, strains, deflection and failure mode were analyzed and graphs were plotted. Comparison between the experimental results and the strut-and-tie model is also developed in this phase.

1.5 OUTLINE OF THE CONTENTS IN THESIS

This part presents a brief review of the contents of this thesis. Chapter 1 introduces a brief overview of precast, prestressed, hollow core slabs with an introduction to strut and tie model approach. The main objective and scope of this research are introduced. Chapter 2 reviews the literature related to FRP strengthened reinforced concrete members and to the strut-and-tie approach for structural concrete members. In chapter 3, experimental program is presented, including material used in

the study. Chapter 4 presents the proposed strut-and-tie model for PPHC slabs, with two detailed examples. In chapter 5, the experimental results, the analytical results and the strut-and-tie model results are presented. Chapter 6 presents the summary and conclusion.

CHAPTER 2

LITERATURE REVIEW

2.1 INTRODUCTION

In Saudi Arabia and the Gulf Region, there is a boom in the construction industry, and precast concrete is being widely used for construction of commercial and residential buildings. This system is adopted because its construction and can be completed in a short time with high quality. In precast concrete construction, the slabs systems comprise principally hollow-core slabs of spans ranging from 4 to 6 meters.

Hollow-core slabs act as diaphragms to transmit lateral earthquake and wind loads in precast concrete and cast-in-place concrete structures. With the implementation of the mandatory Saudi Building Code currently being developed, seismic retrofitting of hollow-core slabs may be needed. The primary reasons for the continuing deterioration of the civil infrastructure are increase of service load, inadequate maintenance, and environmental deterioration. Tens of thousands of existing civil infrastructures identified as substandard highlight the need for effective civil infrastructure rehabilitation. Fiber reinforced polymer (FRP) composites are the best answer .

Therefore, CFRP strengthening of structures is now widely used due to its many incomparable advantages over other materials employed for the repair and strengthening of existing concrete structures. In this chapter, the literature related to FRP strengthened slabs and the strut-and-tie method approach for structural concrete members are reviewed.

2.2 FULL SCALE LOAD TESTING OF FRP STRENGTHENED SLABS

2.2.1 FRP Strengthened One -Way & Two -Way Slabs

A review of the available literature showed that very little research had been conducted on the strengthening of slabs. Wight and Erki (2003) tested six one-way reinforced concrete slabs to investigate the effectiveness of prestressed carbon fiber reinforced polymer (CFRP) sheets used to strengthen the slabs subjected to fatigue loading. The slabs were 3000 × 1000 × 90 mm and reinforced with 11.3 mm diameter reinforcing steel bars. The slabs were tested in two groups of three slabs. In each group, one slab was unstrengthened and used as a control specimen, the second slab was strengthened with non-prestressed FRP sheets, and the third slab was strengthened with prestressed sheets. The first group of slabs was subjected to a higher load amplitude but lower mean stress than the second group. The CFRP strengthened slabs of the second group were externally loaded while applying the CFRP sheets, in order to simulate the sustained load that may be associated with field strengthening conditions. The test results confirmed that strengthening reinforced concrete slabs with bonded CFRP sheets, especially prestressed CFRP sheets, increases fatigue life.

Eraki and Heffernan (1995) conducted an experimental program on eight reinforced concrete slabs (1000 × 1000 × 50 mm). Two-way reinforcing steel was used to reinforce six of the slabs and, one-way reinforcing steel was used to reinforce the remaining two. The two-way slabs were simply supported on all four edges, and the one-way slabs were simply supported on two parallel sides. One one-way and two two-way slabs were tested as controls, and the remaining five were externally reinforced on their tension face with fiber-reinforced plastic (FRP). Those anothers found that FRP sheets externally bonded to the tension face of the member can

significantly improve the load-carrying capacity of the slabs. The additional reinforcement provided by the FRP sheets increased the flexural stiffness of the slabs, delaying the onset of flexural cracking to higher loads, and thereby increasing the punching shear failure loads.

Limam et al. (2003) conducted a study on CFRP-strengthened two-way slabs of size 1700 × 1300 × 70 mm. The slabs were strengthened with CFRP strips, 1.4 mm thick, 50 mm wide and 1500 mm long in the longitudinal direction and 1000 mm long in the transverse direction. The CFRP strips were spaced at 150 mm. The ultimate loading capacity of the control slab (unstrengthened) was about 48 kN, whereas the ultimate load capacity of the strengthened slab increased to about 120 kN. The results of the experimental study indicated that externally-bonded CFRP plates can be efficiently used to strengthen two-way RC slabs.

Kolizadeh and Saadatmanesh (2003) conducted a experimental study on strengthening of steel-concrete composite girders by using carbon fiber reinforced polymers sheets. They tested three large-scale composite girders made of W255×13.6 A36 steel beam and 75 mm thick by 910 mm wide concrete slabs. They used different numbers of layers of CFRP to strengthen the slabs. They reported that the ultimate load-carrying capacities of the girders significantly increased by 44, 51 and 76% for one-, three-, and five-layer retrofitting systems, respectively. They also reported that, as the number of CFRP layers increases, the efficiency for utilizing the CFRP sheet decreases. Stress in the CFRP laminate for the one-layer system was 75% of its ultimate strength, while it dropped to 42% in the five-layer system. Mosallam and Mosallam (2002) conducted a study on strengthening of two-way concrete slabs with FRP composite laminates for evaluating the ultimate response of unreinforced and reinforced concrete slabs repaired and retrofitted with FRP. They found that the use of

FRP systems resulted in an appreciable upgrade of the structural capacity of the as-built slabs.

Ebead and Marzouk (2004) conducted an experimental study on two-way slabs of size 1900×1900×150 mm. The slabs were strengthened with CFRP strips. They reported that the load-carrying capacity of the strengthened slab was increased by up to 40% as compared to the unstrengthened slab. They also reported that the debonding between FRP materials and the concrete was the main cause of failure. Slabs failed soon after debonding occurred due to exceeding flexural capacity.

2.2.2 Full-Scale Load Tests On PPHC Slabs

Yang (1992) used the results of 59 different tests for PPHC slabs conducted by the Technical Research Center of Finland (VTT) and found that the web shear strength of tested slabs did not correlate well with the code predictions. Pisanty (1992) investigated the shear strength of ten hollow core slabs, and he found that modifications were needed in FIP code for better prediction of shear capacity on hollow core slabs. Pajari (1998) analyzed the VTT test results of 49 PPHC slabs with depths ranging from 200 mm to 500 mm, and he observed that in the Eurocode 2 (1992) the mean shear strength for all slabs was overestimated. He proposed a new equation to calculate the web shear strength of PPHC slabs. Hawkins and Ghosh (2006) reported the results of 28 tests conducted by various precast concrete manufacturers for hollow core slabs ranging from 200 mm to 400 mm in depth. They observed that the web shear strength of PPHC slabs with depths greater than 300 mm can be less than the strengths computed by using Equation (11-12) of the ACI 318 code.

2.2.3 FRP Strengthened PPHC Slabs

Hosny et al. (2003) conducted an experimental program to study the flexural behavior of precast, prestressed hollow-core slabs strengthened by carbon fiber reinforced polymer (CFRP) laminates and sheets. The program consisted of testing nine precast slabs with 4.8 m span, 200 mm thickness and 1.2 m width. The slabs were tested under monotonic four-point loading up to failure. The variables in the test program were the type of CFRP laminates (strips with 1.2 mm thickness and sheets with 0.38 mm thickness) and reinforcement ratio of CFRP laminates. Use of CFRP sheets is more efficient than CFRP strips due to the better bond characteristics of the sheets. The ultimate load increased by 26% for slabs with strips and 49% for slabs with sheets. They also found that adding end anchorage for the CFRP strips could not prevent the bond failure; however, it delayed the failure of the slabs. The number of cracks and the loads at which the cracks were stabilized increased for the slabs with CFRP sheets due to the good bond behavior of this material.

Mohiuddin (2006) conducted an experimental program to study the flexural and shear behavior of precast, prestressed hollow-core slabs strengthened by carbon fiber reinforced polymer (CFRP) sheets. The program consisted of testing nine precast slabs, seven in flexure and two in shear, with 4.7 m span, 200 mm thickness and 1.2 m width. The slabs were tested under monotonic four-point loading up to failure. The parameters considered in the experimental program were the number of CFRP sheets. He found that the flexural capacity of the slabs strengthened with 0.13 mm CFRP sheets could be increased from 14% for the slabs strengthened with 300 mm width of CFRP to 36% for slabs strengthened with three sheets of CFRP with a total width of 900 mm. The number of cracks for the slabs strengthened with CFRP sheets ranged from 8 to 12 compared to 4 cracks for the unstrengthened specimen.

Mahmud (2008) conducted an experimental program to study the flexural and shear behavior of precast, prestressed hollow-core slabs strengthened by carbon fiber reinforced polymer (CFRP) sheets. The program consisted of testing 22 precast slabs, 15 in flexure and 7 in shear, with 4.7 m span, 200 mm thickness and 1.2 m width. The slabs were tested under monotonic four-point and three-point loading up to failure. Experimental results were verified with mechanistic and finite element models. The mechanistic model was based on the ACI ultimate strength approach, whereas the finite element modeling made use of the commercial software DIANA. He found that increasing the number of layers of CFRP resulted in a significant increase in flexural strength. With up to 35% increase in the flexural capacity, further strengthening of the slab changed the mode of failure from flexure to shear failure. Therefore, the shear strength of the slab limited the increase in its flexural strength for use of CFRP.

2.3 STRUT-AND-TIE MODEL

2.3.1 Background

In a cracked concrete beam (Figure 2.1), the shear force of the section between two cracks can be expressed as:

$$V = \frac{d(T)}{dx}\, jd + \frac{d(j_d)}{dx} T = V1 + V2 \tag{2.1}$$

where V_1 is the beam action contribution to shear and $V_{2\ is}$ the arch action contribution to the internal shear resistance. The term $\frac{d(T)}{dx}$ in the component V1, the rate of change of the tensile force in steel, is the bond force applied to the flexural reinforcement per unit length of beams. If the internal moment arm length (j_d) remains constant, $\frac{d(j_d)}{dx} = 0 \ \ and V = \frac{d(T)}{dx} j_d.$ Then the shear is transferred by beam action. If the reinforcement is unbounded, or if shear flow transition due to the steel is

prevented by an inclined crack, $\frac{d(T)}{dx} j_d = 0 \quad and V = \frac{d(j_d)}{dx} T$, the shear is transferred by arch action rather than beam action. The shear failure modes widely depend on the relative contributions of beam action and arch action. In deep members with a shear span depth ratio ranges from 0 to 2.5, loads are transferred by arch action. In this case, the steel reinforcement serves as tension ties and the cracked concrete serves as a compression strut, as shown in figure 2.2. In slender members with a shear span depth ratio greater than 2.5, loads are carried by both arch action and beam action. Since arch action generally enhances the strength of a section, the behavior of a slender member is governed by beam action.

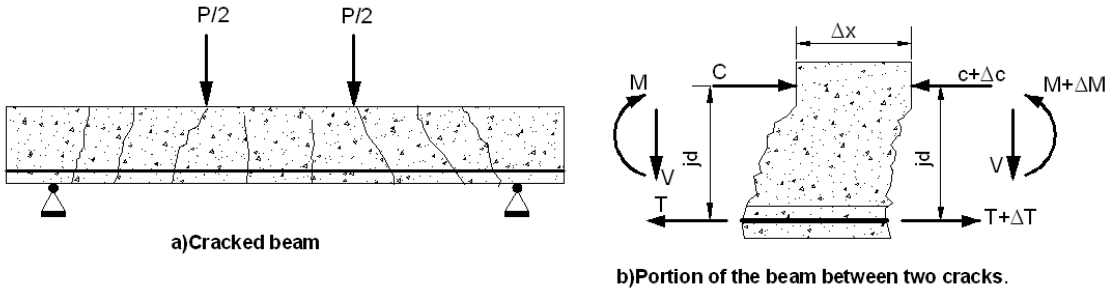

Figure 2.1: Shear Stress between Cracks (MacGregor, 1997)

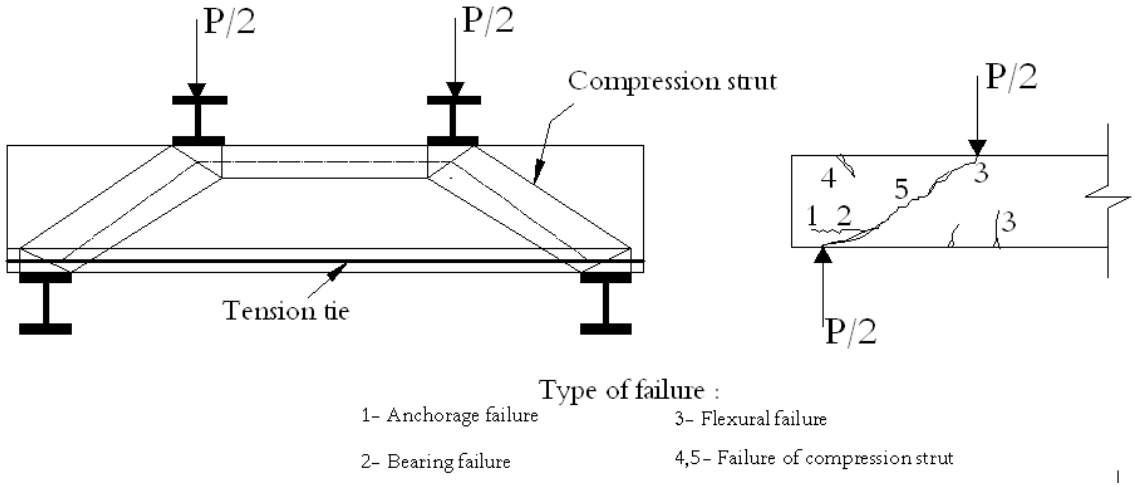

Figure 2.2: Mode of Failure of Deep Beams, a/d=0.5 to 2.5 (MacGregor, 1997)

The Bernoulli hypothesis states “Plane sections remain plane after bending.” This hypothesis is the basic assumption of flexural design of structural concrete by allowing linear variation in strain over the depth of the cross section. According to the Bernoulli hypothesis, any concrete structure may be subdivided into two regions. One is the B-region in which the Bernoulli hypothesis is applicable, where the B stands for beam or Bernoulli. Another is D-region in which the Bernoulli hypothesis is not applicable, where the D stands for discontinuity or disturbed. Based on the principle of St. Venant, the dimensions of the B and D regions are obtained. St.Venant’s principle states “The local distribution of forces acting on a small portion of a body subject to a stress field may be changed without changing the stress field in the body at some distance away from the point where the distribution was made.” This principle suggests that local disturbance extends about one member depth each way from concentrated loads, reaction, or sudden changes in direction or section (MacGregor 1997). B-regions carry load by beam action and, D-regions carry load primarily by arch action involving inplane force (MacGregor, 1997).

2.3.2 Truss Analogy for Design of B-Region

The truss analogy is the shear design approach for reinforced concrete. The truss model introduced by Willhelm Ritter in 1899 has been developed and adopted by most design specifications as the standard shear design method. The general design procedure for concrete consists of selecting the concrete dimension, determining the size and the placing of reinforcement, and finally checking the serviceability (Marti, 1985). In the second step, the truss analogy is used to investigate the equilibrium of the external loads and internal force in the concrete and reinforcement. The truss model approach provides an excellent conceptual framework to show the internal forces that exist in a cracked structural concrete member.

2.3.2.1 Compression Field Theory

This method is based on the lower-bound theorem of plasticity which states that "If an equilibrium distribution of stresses can be found which balances the applied load and is everywhere below yield or at yield, the structure will not collapse. Since the structure can carry at least this applied load, it is a lower bound to the load-carrying capacity of the structure."

Inclined cracks in the reinforced concrete develop a vertical tension force in the vertical reinforcements, horizontal tensile forces in the horizontal reinforcements, and inclined compressive forces in the concrete between the cracks. These internal forces form the indeterminate truss.

The determinate truss system can be formed by lumping all of the stirrups cut by section A-A (Figure 2.3) into one vertical member b-c and all the diagonal concrete members cut by section B-B into one diagonal member e-f (MacGregor,1997).

Dashed lines and solid lines represent compressive force in the concrete and tensile force in the reinforcement respectively.

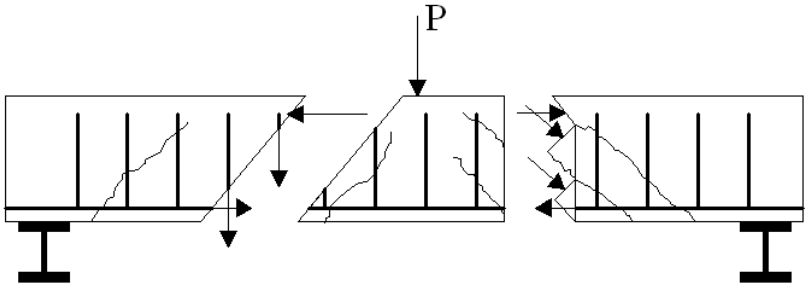

a) Internal Forces in a Cracked Beam

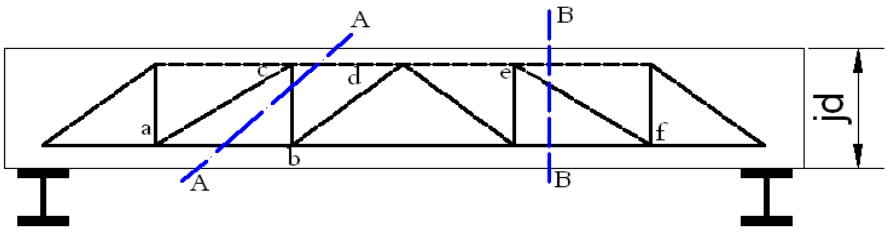

b) Pin-Jointed Truss

Figure 2.3: Truss Analogy (MacGregor, 1997)

2.3.2.2 Modified Compression Field Theory

Tests of reinforced concrete panels subjected to pure shear demonstrated that after cracking, friction or the aggregate interlock stress in the inclined crack increase the ability of reinforced concrete to resist shear stresses (Vecciho and Collins, 1986). The modified compression field theory (MFCT) considers this shear contribution of concrete (V_c) to the shear resistance. This design method introduced by Collins and Mitchell (1991) has been adopted by the AASHTO LRFD specification.

The softened compressive stress f_2 due to transverse tensile strain in the cracked concrete is expressed as a function of both the principal compressive strain ε_2 and the principal tensile strain ε_1 in the following equation (Figure 2.4).

$$f_2 = f_{2\max}\left(2\varepsilon_2/\varepsilon_c' - \left(\varepsilon_2/\varepsilon_c'\right)^2\right) \tag{2.2}$$

where

$$f_{2\max 2} = f_c'/(0.8+170\varepsilon_1) \le f' \tag{2.3}$$

ε_c' can be taken as 0.002

The average principal tensile stress f_1 is expressed as follows

$$f_1 = f_{cr} / \left(1 + \sqrt{500\varepsilon_1}\right) \tag{2.4}$$

before yielding of reinforcement at the crack

$$f_1 = \nu_{ci} \tan\theta \tag{2.5}$$

after yielding of some of the reinforcement at the crack

where shear stress is the function of the crack width w and the aggregate size as follows:

$$\nu_{ci} = 2.16\sqrt{f_c'} / \left(0.3 + 24w/\left(a + 0.63\right)\right) \quad \text{psi and in.} \tag{2.6}$$

Collins et al. (1996) also formulated shear contribution carried by concrete by using stree-strain relationship in the cracked concrete. It is assumed that shear stresses over the effective shear area $b_v d_v$ are uniform. The concrete contribution to the nominal shear strength can be expressed as

$$V_c = f_1 b_v d_v \cot\theta = \beta\sqrt{f'c} b_v d_v \tag{2.7}$$

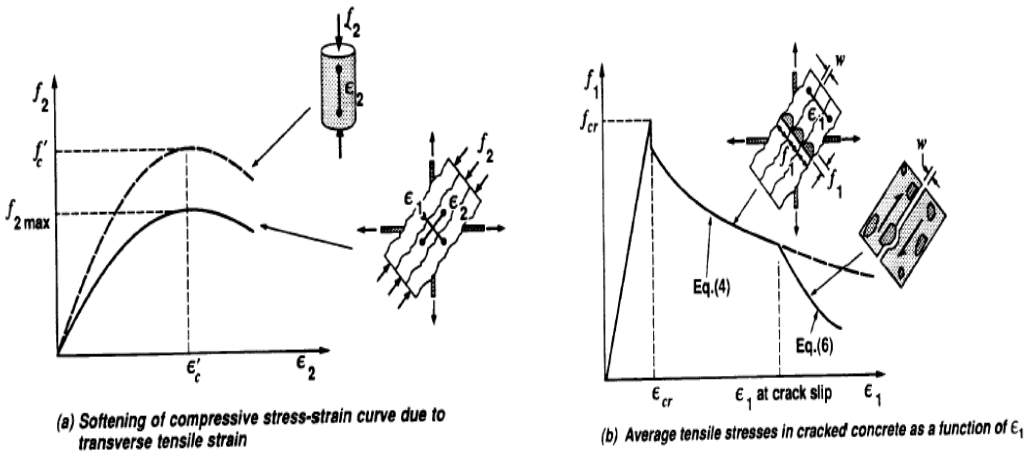

Figure 2.4: Stress-strain Relationships for Cracked Concrete (Collins et al. 1996)

2.3.3 Components of Strut-and-Tie Model

2.3.3.1 Struts

Struts represent concrete compressive stress fields whose principal stresses are predominantly along the centerline of the struts. The shape of the strut stress field in planar D-regions may be idealized as prismatic, bottle-shaped, or fan-shaped as shown in figure 2.5 (Schlaich et al, 1987). Struts may be strengthened by ordinary steel reinforcement, and if, so, they are termed reinforced struts.

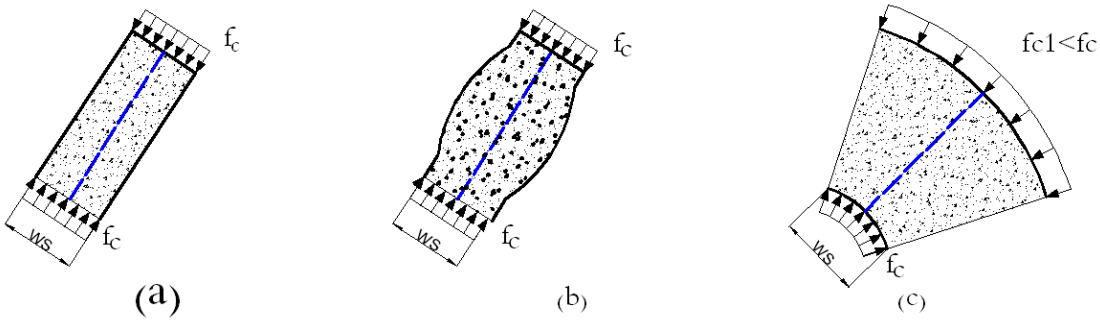

Figure 2.5: Idealized Stress Fields in Struts: (a) Prismatic (b) Bottle-shaped (c) Fan-shaped (Adapted from Schliach et al. 1987).

In general, the stress limit of a strut is not the same as the uniaxial concrete compressive strength obtained from cylinder tests, f_c'. It is defined as

$$f_{cu} = \nu f_c', \tag{2.8}$$

where f_{cu} = stress limit of a strut, commonly referred to as effective strength, and ν = *effectiveness factor,* also known as *efficiency factor* or *disturbance factor* (typically between 0 and 1.0).

The effectiveness factor, ν, is an empirical factor that is used to justify the application of limit analysis concept to structural concrete. It accounts for the difference in the post yielding response between the uniaxial compressive stress-strain curve used for deriving the limit analysis theorem, namely the (rigid or elastic) perfectly plastic curve, and that of typical concrete as shown in Figure 2.6. If the uniform stress distribution is selected, the effective strut capacity is simply

$$f_{cu} = A_c f_{cu,} \tag{2.9}$$

where A_c is termed the effective cross-sectional area given by $A_c = w_c t$. With the same assumption, the effective capacity of reinforced concrete struts is

$$f_{cu} = A_c f_{cu} + A_s f_{y,} \tag{2.10}$$

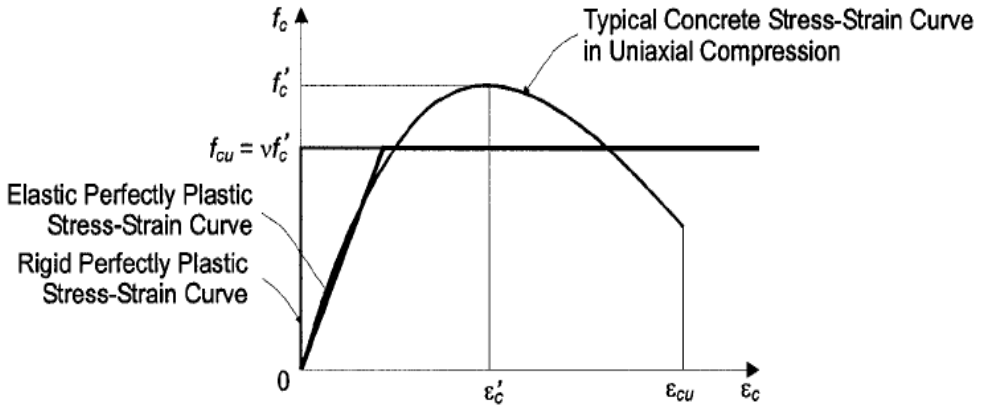

Figure 2.6: Typical Stress-Strain Relationship for Concrete in Uniaxial Compression and the Idealization Used in the STM.

where A_s and f_y are the cross-sectional area and the compressive yield strength of ordinary steel reinforcement, respectively.

2.3.3.2 Ties

Ties typically represent one or multiple layers of ordinary steel, in the form of flexural reinforcement, stirrups, or hoops. Ties can occasionally represent a prestressing steel or concrete stress field with principle tension predominant in the tie direction. The effective capacity of a tie consisting only of non-prestressed reinforcement is given by

$$f_{tu} = A_s f_{y,} \tag{2.11}$$

where A_s = area of ordinary reinforcing steel, and f_y = yield strength of ordinary steel reinforcement in tension. As can be observed from Eq. 2.10, strain hardening and tension stiffening effects are neglected. The effective prestressing force and its

effects may be introduced as a set of statically equivalent external forces acting on the D-region under consideration (Schliach et al. 1987). If this approach is applied to bonded pretesting, the capacity of a tie consisting of non prestressed and prestressed reinforcement is given as

$$f_{tu} = A_s f_y + A_{ps} \nabla f_p , \tag{2.12}$$

where A_{ps} = area of bonded prestressing steel, $\nabla f_p = f_{ps} - f_{se}$ = remaining prestressing steel stress available to resist tension, f_{ps} = stress in prestressing steel at nominal strength, and f_{se} = effective stess in prestressing steel after losses. If the prestressing is introduced as a tie with an initial tensile force of $A_{ps} f_{se}$, the maximum prestressing force , $A_{ps} f_{se}$, replace $A_{ps} \nabla f_p$ in Eq. 2.12.

The tie reinforcement is usually assumed to be enclosed and uniformly distributed in a prism of concrete (smeared reinforcement). Termed *tie effective cross-sectional area*, the cross sectional area of the concrete prism, A_t, $A_t = w_t t$, where w_t is the *tie effective width* as shown in Figure 2.7. The tie capacities given in Eqs. 2.10 and 2.11 can be rewritten in terms of equivalent stress assumed to be uniformly distributed across the effective cross- sectional area as

$$f_{tu} = r_s f_{y,} \tag{2.13}$$

and

$$f_{tu} = r_s f_{y,} + r_{ps} \nabla f_p , \tag{2.14}$$

respectively, where $r_s = A_s / A_t$, and $r_{ps} = A_{ps} / A_t$ are geometrical ratios of non-and prestressed reinforcement ratios, respectively.

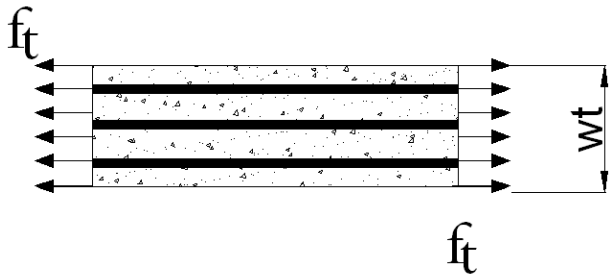

Figure 2.7: Effective Width of Tie

2.3.3.3 Nodes

Analogous to the joints in a structural steel truss, nodes represent regions in which forces are transferred between struts and ties. These regions are usually called nodal zones or nodal regions. Some literature (e.g. ACI 318-08) uses these terms slightly differently; a node refers to the meeting point of the strut axes, tie axes, and body forces acting on the node whereas a nodal zone or nodal region refers to the finite dimension of a node.

Depending on the types of forces being connected, there are four basic types of nodes with three members intersecting, namely CCC, CCT, CTT, and TTT, as illustrated in Figure 2.8, where F_c and F_t in the figure denote strut and tie forces, respectively. Originally used for nodes with three members framing the terms CCC, CCT, and TTT are extended herein for convenience to include nodes with more than three members framing as follows: CCC nodes are those in which all the framing members are struts, CCT nodes are those in which one of the framing members is a tie, CCT nodes are those in which two or more of the framing members are ties, and TTT nodes are those in which are those in which all the framing members are ties.

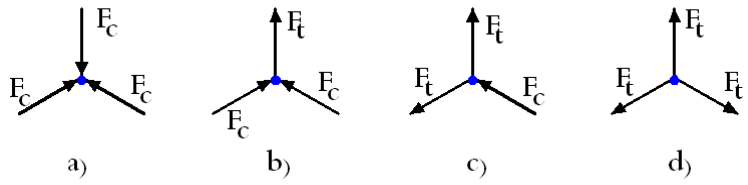

Figure 2.8 : Basic Node Types: a) CCC b) CCT c) CTT d) TTT

Schlaich et al.(1987) classify nodal zones as either *continuous* (or *smeared*), if all the stress fields meeting at the node are wide, or *concentrated* (or *singular)*, if one of the framing fields meeting at the node are wide , or *concentrated* (or *singular*), if one of the framing struts or ties is a concentrated stress field. Smeared nodes are not critical, and thus their strength does not need to be checked. There is no clear definition, however, to help assess nodal zones quantitatively according to this classification.

In 2-D design problems, the stresses in nodal zones are biaxial and are limited to the yield criterion for plane stress problems. The stress distribution in a nodal region depends on the idealized shape, which in turn depends on the effective width and direction of the strut or tie stress field entering the node. An example of this construction for a nodal zone with four struts intersecting is shown in Figure 2.9. The state of stress in these nodal zones is typically complex and difficult to determine. Variants of constructing nodal zone shapes have been proposed to simplify the stress distribution in these regions. These include the hydrostatic approach (Figure 2.9(c)) (e.g. Marti 1985 and Nielson 1998) and modified hydrostatic approach (Figure 2.9 (d)) (Schlaich and Anagnostou 1990). Different effective bearing strength of nodes have been proposed to account for the influencing factors, such as the number and type of intersecting truss members(struts or ties), distribution of tie reinforcement, confinement and use of fibers, level of transverse straining, volume and condition of surrounding concrete, and conditions of ties.

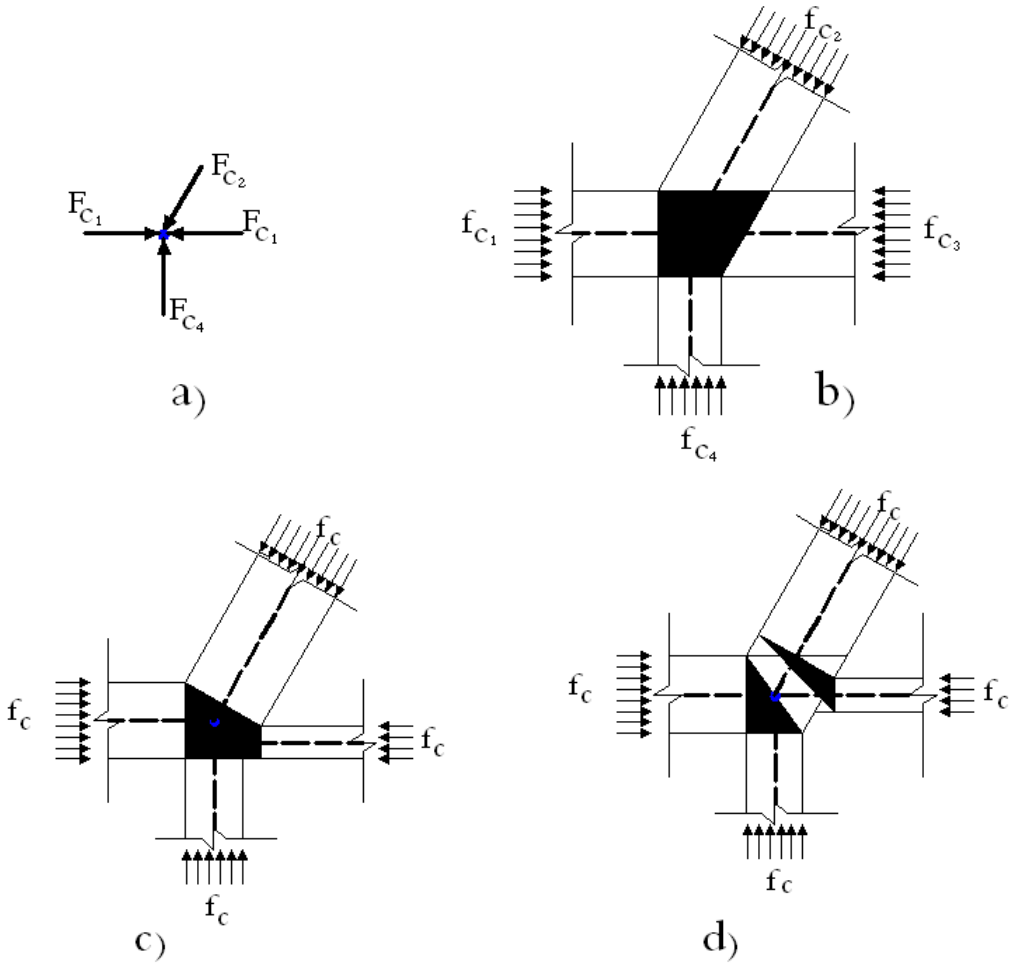

Figure 2.9: Examples of Shape Idealization of a Nodal Zone with Four Struts Intersecting: a) Force Acting on the Node b) Simple Shape c) Hydrostatic Shape d) Modified Hydrostatic Shape.

2.3.4 The Strut-and-Tie Method for Analysis and Design

The strut-and-tie models have been widely used as effective tools for designing reinforced concrete structures. The idea of a Strut-and-Tie Model came from the truss analogy method introduced independently by Ritter (1899) in the early 1900s for shear design. This method employs the so-called Truss Models as its design basis. The model was used to idealize the flow of force in a cracked concrete beam. In parallel with the increasing availability of the experimental results and the development of limit analysis in the plasticity theory, the truss analogy method has been validated and improved considerably in the form of full-member or sectional

design procedures. The Truss Model has also been used as the design basis for torsion.

Schlaich and Weischede (1981) introduced the concept of D-regions and B-regions where D stands for discontinuity or disturbed regions and B stands for beam or Bernoulli. In D-regions, extending a distance equal to the member depth away from discontinuity such as a change in cross section or concentrated loads, the strain distribution is significantly nonlinear.

Later, Schlaich et al. (1987) generalized the application of the truss analogy concept to all parts of reinforced and prestressed concrete structures in the form of Strut-Tie system and suggested using the Strut-Tie system as a primary load-carrying mechanism in such regions. As a guideline for the development of a Strut-Tie model, they recommended visualizing the internal forces flow according to a linearly elastic analysis and orienting the struts and ties within 15 degrees of the elastically determined stresses.

Several theoretical and experimental studies had been carried out to analyze the shear failure of reinforced concrete beams. During the past few years, design codes ACI 318-08 and AASHTO (2005) have adopted strut-and-tie principles for the design of deep beam members.

Hwang et al. (2000) have related the stress limits with the transverse strain perpendicular to the stress direction so as to consider the softening effect of concrete compressive strength. However, it may not be appropriate to apply the smeared crack model concept to the D-region, that is, the disturbed region where the conventional plane-section-remains-plane principle is not valid.

Tan et al. (2001,2003) have developed a direct STM for simply supported deep

beams, which can consider the effects of different web reinforcement configurations (vertical, horizontal, or inclined), and prestressing tendons.

Nielson et al. (1978) have used the theory of plasticity for computation of the inclination of compressive struts in the truss model. The reinforcement was assumed to be rigid, perfectly plastic and unable to resist lateral forces.

Ramirez and Breen (1991) have recently proposed the inclusion of concrete contribution in the variable-angle truss model for use in American sectional design practice. A lower limit of 30 degrees was suggested for the angle of inclination of diagonal struts to ensure adequate safety for reinforced concrete beams failing in shear.

Ong et al. (2004) proposed a strut-and-tie model to calculate the ultimate tensile loads of precast concrete joints with two-to-one loop connections subjected to static uniaxial tensile loading.

Bakir and Boduroglu (2005) discussed the application of the softened truss and strut-and-tie models on short beams. The model has two important characteristics. The first is the non-linear association of stress and strain. The second is the softening of concrete in compression due to tensile strains in the perpendicular direction.

Young (2000) presented an interactive computer graphics program for implementing the nonlinear strut-tie model approach for the practical design and analysis of disturbed regions in structural concrete. The design result showed that the nonlinear strut-tie model, combined with the graphics program, produces simple and effective solutions by providing accurate details on structural concrete.

Tong (1997) has developed a simple and direct strut-and-tie model for non prestressed deep beams, which takes account of different web reinforcement

configurations. Comparison of predictions with 116 experimental results shows that the proposed model is consistent and safe for non prestressed deep beams.

Various models for shear strength estimation have been proposed. Among them, the softened truss model developed by Hsu and Mo (1985) can achieve accurate predictions of shear strength of squat walls. This model assumes a uniform distribution of stress. On the other hand, Hwang et al. (2001) proposed the softened strut-and-tie (SST) model for determining the shear strength of squat walls. Both the softened truss model (1985) and the SST model (2001) offered analytical formulations; yet there exist fundamental discrepancies in their perspective on the distribution of stress. The former assumes that the state of stresses in the central panel is uniform, whereas the latter assumes that compressive stress is concentrated along the paths of concrete struts and tension ties, rather than uniformly distributed, although both models can predict accurately the shear strength of squat walls.

Young and Julio (1996) developed general approaches for determining the effective stress levels of concrete struts and for verifying the bearing capacity of nodal zones in strut-and-tie models.

Tjhin and Kuchma (2002) developed a computer program CAST (Computer Aided Strut-and-Tie) for design and analysis of reinforced and prestressed concrete members.

Ning and Kang (2007) presented a modified strut-and-tie model (STM) for determining the shear strength of reinforced deep beams. The modified model is based on Mohr Coulomb's failure criterion.

Hyo-Gyoung and Sang-Hoon (2006) have introduced a method to determine strut-and-tie models in reinforced concrete (RC) structures by using evolutionary structural optimization (ESO). The introduced optimization procedure also showed

the availability of determining optimal strut-and-tie models of RC structures with complicated geometry, such as corbel structures and deep beams with openings, for which the classical strut-and-tie approach has limitations in application. However, the availability of the proposed method for RC structures with complicated loadings should be checked. Further theoretical research, including the effect of material property on the optimal strut-and-tie models, as well as experimental verifications must be followed to achieve a more rational design approach.

Alshegeir and Ramirez (1992) have developed an iteractive computer graphics program implementing the strut-tie model approach for analysis and design of reinforced and prestressed concrete members. The program provides the direction of principal compressive stresses, which gives guidance in the development of strut-tie models.

AbdulKadir (2005) has used the strut-and-tie model to design the hammerhead piers and compared the results with the strength method.

Basil (1974) presented a theoretical model to idealize structural concrete cracked sections under combined loads. This model, called the variable angle space truss, is capable of predicting the post-cracking response of rectangular reinforced and prestressed concrete beams subjected to a combination of vertical shear, lateral shear, vertical bending, lateral bending, torsion and axial load.

Liang et al. (2006) developed a strut-and-tie design methodology for three-dimensional reinforced concrete structures. The unknown strut-and-tie model is realized through the machinery of a refined evolutionary structural optimization method. Stiffness of struts and ties is computed from an evolved topology of a finite element model to solve statically indeterminate strut-and-tie problems. In addition,

compressive strength for struts and nodal zones is evaluated by using Ottosen's four-parameter strength criterion.

Chun (2002) developed a 3D indeterminate strut-and-tie model for the analysis of the footing system. Five different levels of stiffness were used to cover the lower and upper bounds for both cracked and uncracked situations. By following the sequence of construction, the model predicted the stresses of the members at different stages. Finite-element solid modeling was also conducted to verify the strut-and-tie model.

Yun and Ramirez (1996) have assumed the effective strength of struts in a concrete continuum to be the normal stress component parallel to the strut axis. Thus FE analyses are required to quantify the deviation of the principal compressive stress direction from the strut axis. MacGregor (2002) decomposed the effectiveness factor, υ, into a product of $\upsilon_1 \upsilon_2$, where υ_1 = factor accounting for concrete strength and υ_2 = factor accounting for strut disturbances.

Richard (1995) has developed a strut-and-tie model for the punching shear behavior of a concrete slab. This model provides a quick and simple approach to punching shear behavior. It is applicable for both normal and high strength concrete under symmetric and non-symmetric loading with and without shear reinforcement.

Marco (1994) has tested four reinforced deep beams to determine the impact of stirrups spacing and steel fiber content on the concrete compression strut capacity. Efficiency factors and a model for compression strut capacity for use with the strut-and-tie model were proposed.

Colloti et al. (2004) have presented a unified global model based on the truss analogy, to predict the failure modes of RC beams strengthened by externally bonded plates to flexure and/or shear. The model incorporates the load transfer mechanism by

bond to reflect the plate debonding phenomenon and associated forms of cracking. The model validated the test results of 124 RC beams strengthened to flexure and 75 RC beams strengthened to shear, reported in the published literature. It is shown that the proposed model gives consistently good correlation with test data.

Hong and Jeung-Hwan (2007) have developed the strut-and-tie models of a total of (14) concrete deep beams with varying size and location of web opening by using a topology optimization approach. They used both von Mises stress and displacement sensitivity numbers as deletion criteria, with the aim of maximizing the material efficiency and overall stiffness of the structural beam. They evaluated the performance indices in terms of von Mises and nodal displacement to monitor the optimization process and to determine the optimal topology which is transformed to the strut-and-tie model.

CHAPTER 3

EXPERIMENTAL PROGRAM

3.1 TEST ARRANGEMENT

The flexural frame in the Heavy Equipment Laboratory at the Department of Civil Engineering was utilized for the testing of the hollow core slabs in flexure and shear as shown in Figure 3.1. Special I-sections were fabricated in the laboratory for application of line loads, as shown in Figure 3.2. The hollow core slabs were supported on two I-sections of 40 cm height and 20cm width. Load was applied on the slab by using two I-sections at approximately third point. A hydraulic jack was used to apply the load, and a load cell of 1000 kN capacity was used to measure the applied load, as shown in 3.3. The complete setup for testing of the hollow core slab is shown in Figure3.3. All data is captured by using a data logger and a computer as shown in Figure 3.5.

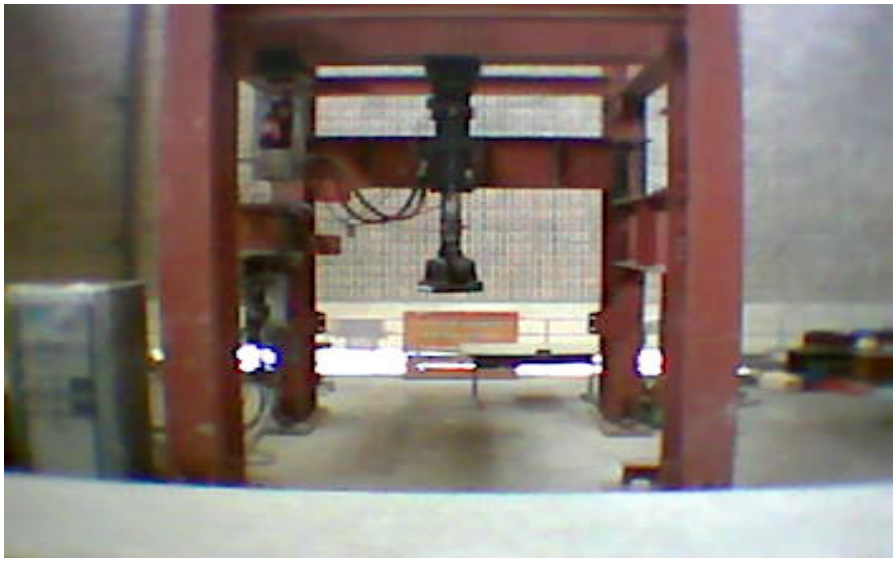

Figure 3.1 Frame Used for Testing PPHC Slabs

Figure 3.2 : Fabricated I Beams for Application of Line Loads

Figure 3.3: Loading Tools, Hydraulic Jack and Load Cell

Figure 3.4: The complete Setup for Testing of Hollow Core Slab

Figure 3.5: Data Tools: Power Supply, Data Logger and Computer

The specimen was moved to its location by crane, and its alignment was checked. The fabricated I beams were lifted by crane to their position over the specimen. The hydraulic jack was carried to its location over I beams by crane. The load cell was put on the hydraulic jack. The flexural load tests and shear load tests were conducted by using four-point test loads as shown in Figure 3.6 and Figure 3.7 respectively.

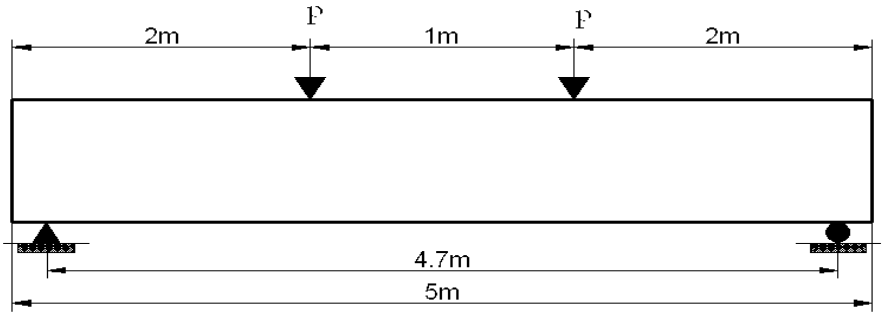

Figure 3.6: Four-Point Loading System for Hollow Core Slabs in Flexure.

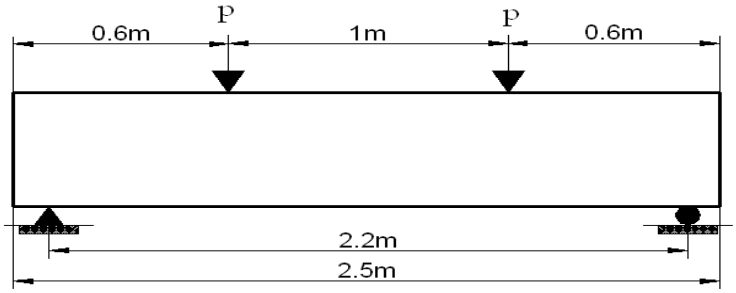

Figure 3.7: Four-Point Loading System for Hollow Core Slabs in Shear.

3.2 MATERIAL

3.2.1 Concrete

Portland cement Type 1 was used in the concrete. Designed concrete strength was 40 MPa. The mix design details are listed below:

- Gray cement – type 1 420 kgs
- Aggregate 3/8 in 473 kgs
- Aggregate ½ in 667 kgs
- Fine sand 800 kgs
- Water 120-130 litres
- Admixture 3 litres

3.2.2 Prestressing Strands

The mechanical properties of the prestressing wire found by testing the strands under tension by using the Universal Testing Machine. A total of three samples were tested.

The length of each specimen was 1000 mm; the prestressing strands are standard strands consisting of 7 wires. The outer six wires have the diameter of 4.27, mm and the central wire has the diameter of 4.43 mm. The average results of tensile strength from the three specimens are tabulated in Table 3.1.

Table 3.1: Results From the Tensile Strength of Strands

Item	Value
$f_y\ (MPa)$	1700
$f_{pu}\ (MPa)$	1961
$E_{ps}\ (MPa)$	193400

3.2.3 Carbon Fiber Reinforced Polymer (CFRP) Sheet

The CFRP sheet used in this research program was MAPE wrap C UNIX –AX 300/40. The roll package of the sheet has 400 mm width, 0.16 mm thickness and 50-meter length. MAPE wrap C UNIX –AX 300/40 is a linear elastic and unidirectional carbon fiber fabric. The detailed properties of MAPE are shown in Table 3.2.

Table 3.2: Properties of the CFRP Sheets

Item	Value
Weight(g/m^2)	300
Thickness (mm)	0.167
Width(mm)	400
Tensile Strength(MPa)	4800
E-Modulus(MPa)	230000
Ultimate Strain (%)	2.1

3.3 INSTRUMENTATIONS

To monitor the behavior of the tested slabs, the strains at concrete surface and the displacements were measured by using different instruments. Instrumentation

of the slabs included electrical resistance strain gauges for strain measurements and linear variable displacement transducers (LVDTs) for deflection and slip measurements. Detailed description of the instrumentation will be presented in this section.

3.3.1 Strain Gauges

Choosing the proper strain gauge is important since the strain gauges affect results significantly. Optimizing the strain performance can help in obtaining accurate and reliable strain measurements. The following are procedure for selecting proper strain gauges :

- Gauge length, the gauge length of a strain gauge is the active or strain-sensitive length of the grid. The strain gauge tends to average the strain over the area covered by the grid.
- Gauge resistance, higher gauge resistance decreases lead-wire effect and reduces temperature sensitivity. But higher gauge resistance leads to higher costs. Thus, a proper resistance must be chosen to satisfy the accuracy requirement and reduce cost. For 60 mm of strain gauge length, the common resistance is 120 ohms.
- S-T-C number, this is the self-temperature compensation (S-T-C) Parameter, which is the approximate thermal expansion coefficient. The thermal expansion coefficient of concrete is about $8*10^{-6.}$ The S-T-C number 11 was chosen for our study. The PL-60-11 strain gauges were chosen for concrete.

Strain gauges can be bonded satisfactorily if the material surface is properly prepared. The purpose of surface preparation is to develop a chemically clean surface having a roughness appropriate to the gauge installation requirement. There are three steps to prepare the material surface, as follows:

The first step is surface abrading. The purpose is to remove any loosely bonded adherents (such as scale, rust, paint, coating, oxides, etc.), and to develop a surface texture suitable for bonding. Place a liberal amount of M-Prep conditioner A in the gauging area, and wet-lap it with proper silicon-carbide paper. Add conditioner A as necessary to keep the surface wet during the lapping process. When the surface is ready, wipe the surface dry with a clean gauze sponge. A sufficiently large area should be cleaned to ensure that contaminants will not be dragged back into the gauging area during the steps to follow. Repeat this step by using finer silicon-carbon paper.

The second step is layout lines. The desired location and orientation of the strain gauge on the test surface should be marked with a pair of crossed perpendicular reference lines. A ball-pen or medium-hard drafting pencil may be used for the concrete surface.

The third step is neutralizing. The optimum alkalinity for micro-measurements strain gauge adhesives should be provided. This can be accomplished by applying M-Prep Neutralizer 5A liberally to the cleaned surface, and scrubbing the surface with a clean cotton-tipped applicator. Then, the surface should be dried with a single slow stroke of a clean gauze sponge.

Through the above steps, the surface is properly prepared for gauge bonding. The performance of the strain gauge is absolutely dependent on the bond between itself and test specimens. The following bond procedure can help ensure satisfactory bonds with adhesive.

(1) Remove the strain gauge from its acetate envelops by grasping the edge of the gauge back with tweezers and placing it on a chemically clean empty gauge box with the bonding side of the gauge down.

(2) Place the appropriate terminals next to the strain gauge solder tabs, leaving a space of approximately 1.5mm between the gauge backing and terminals.

(3) Using a 100-t0-150 mm length of M-line PCT-2A cellophane tape, anchor one end the tape to the empty strain gauge box behind the gauge and terminal. Wipe the tabe firmly down over the gauge and terminal. Pick the gauge and terminals up by carefully lifting one end of the tape from the box. The strain gauge and terminals are attached to the tape.

(4) Position the gauge/tape assembly so the alignment marks on the gauge are over the layout line on the beam. Holding the tape at a shallow angle, wipe the assembly onto the beam surface.

(5) Lift the end of the tape opposite the solder tabs at a shallow angle until the gauge and terminals are free of the beam.

(6) Holding the gauge/tape assembly in a fixed position, apply two or three drops of M-bond adhesive at the junction of the tape and beam surface, about 13 mm outside the actual gauge installation area. Then apply firm thumb pressure to the gauge and terminal area.

(7) The terminals of strain gauges are soldered to the lead-wires and connected to form an electrical circuit.

3.3.2 Linear Variable Displacement Transducers (LVDT)

The deflections at the center of the slabs and at the center line of applied load were measured by two LVDTs attached to the bottom of the slabs as shown in Figure 3.8.

Figure 3.8: Two LVDTs Placed Under the Slab to Measure Deflection

3.3.3 Linear Motion Transducers LMT

The slip occurred in prestressed steel during the test is measured by using two LMTs as shown in Figure 3.9.

Figure 3.9 : LMT to Measure the Slip of Strand

CHAPTER 4

STRUT-AND-TIE METHOD APPROACH FOR PPHC SLABS

4.1 INTRODUCTION

The behavior and strength of prestressed steel ties in the Strut-and-Tie Method can be predicted with certainty. However, there are substantial differences in the rules and guidelines for concrete struts to account for the softening of the concrete after cracking, because of uncertainties associated with defining the characteristics of an idealized truss within a continuum of structural concrete. A total of 17 experimental tests of PPHC slabs are analyzed by the STM approach. The CAST program is used as aided tool to analyze the PPHC slabs. A total of 17 PPHC slabs with and without CFRP strengthening are analyzed by the proposed STM approach.

The STM approach is based on the force flow in PPCH slabs. The PPHC slabs are concrete members without web reinforcement, and so concrete tension elements are used to resist the tension forces in the PPHC slabs. The compression struts are inclined at an angle of 30 deg to the horizontal, whereas the inclination angle of concrete ties is 60 deg to the horizontal. The concrete compression struts and tension ties are intersecting perpendicular to each other. The STM based on these criteria are able to predict the failure loads of PPHC slabs.

This chapter proposes the Strut-and-Tie model approach for PPHC slabs with and without CFRP strengthening, and it gives an example to illustrate the proposed strength prediction procedure. The CAST program, which was developed by the

University of Illinois, is used to draw strut-tie models and to calculate the internal forces of elements in these models.

4.2 EFFECTIVE FACTOR MODELS IN THE STM

In the STM, the behavior and strength of the prestressed steel tie are well defined with certainty. However, it is difficult to predict the structural behavior of cracked concrete strut. There are lots of rules to account for the softening of the concrete after cracking. In general, allowable compressive stress f_{cu} in the struts are chosen as some fraction of the concrete cylinder compressive strength f_c', i.e., $f_{cu} = \phi \nu f_c'$, where ϕ = strength of reduction factor and ν = an effective factor that is less than 1. The effective factor is introduced to reflect the softening effect due to cracking of the struts and transverse tensile strains. Table 4.1 summarizes the effective factor models.

Table 4.1: Effective Factor Models

Effective Factor ν	Comment	Proposed by
$\ln\left(\nu\frac{d}{b}\right) = 3.342 - 0.199\frac{a}{d_c} - 7.471\frac{b}{d}$	a shear span b width of web d effective depth	Batchelor and Cambell (1986)
0.8 0.68 0.51 0.34	Undisturbed and uniaxial state Parallel cracking to the strut Skew crack to the strut's axis Skew crack with extraordinary crack width	Schlaich et al (1987)
$\frac{(0.691-0.25D)(100\rho+2)\left(2-0.4\frac{a}{D}\right)}{\sqrt{f_c'}}$	D height of beam in meters ρ longitudinal reinforcement ratio	Chen(1988)
0.85 0.75 0.5 0.95	confined strut with a/d<2.0 struts forming arch mechanism arch member in prestressed beam undisturbed and highly stressed strut	Alshegeir and Ramiraz (1990)

$1.25-\frac{f_c^{'}}{500}-0.72\frac{a}{d}+0.18\left(\frac{a}{d}\right)^2 \; for \; \frac{a}{d}<2$ $0.53-\frac{f_c^{'}}{500} \; for \; a/d \geq 2$	$f_c^{'}$ is in MPa and compressive strength range from 20 t0 80 MPa	Warwick and Foster(1993)
$\frac{1}{1.0+k_c k_f}$, $where \; k_c=0.35\left(\frac{-\varepsilon_1}{\varepsilon_2}-0.28\right)^{0.80} \geq 1.0$ $k_f=0.1825\sqrt{f_c^{'}} \geq 1.0$ $\frac{1}{1.0+k_c}$, $where \; k_c=0.27\left(\frac{\varepsilon_1}{\varepsilon_0}-0.37\right)$	Model A Function of principal tensile strain to principle compressive strain $\left(\varepsilon_1/\varepsilon_2\right)$ $\varepsilon_1=\varepsilon_x+(\varepsilon_x-\varepsilon_2)/\tan^2\theta$ Model B Strength –only softening model as a function of ε_1	Veccio and Collins(1993)
$\frac{1}{1.14+(0.64+f_c^{'}/470)(a/z)^2}$ $\frac{1}{1.14+0.75(a/z)^2}$	Efficiency factor depends on concrete strength and a/d ratio. $z=d-\Omega/2$ .Further simplified By eliminating conc.Strength effect.	Foster and Gilbert(1996)
$\nu=\nu_1 \; \nu_2$ where $\nu_1=1.0$ $=0.8$ $=0.65$ $=0.6$ $\nu_2=0.55+\frac{15}{\sqrt{f_c^{'}}}$	confined strut with a/d<2.0 struts forming arch mechanism arch member in prestressed beam undisturbed and highly stressed strut	MacGregor(1997)
$\frac{1}{0.8+170\varepsilon_1} \leq 0.85$ $\varepsilon_1=\varepsilon_s+(\varepsilon_s+0.002)\cot^2\alpha_s$	ε_s = The tension strain in the concrete in the direction of the tension tie α_s = The smallest angle between strut and tie.	AASHTO LRFD(2003)
$0.85\beta_s$ *where* $\beta_s=1$ $=0.75$ $=0.6\lambda$ $=0.4$ $=0.6$ $\lambda=1.0$ $=0.85$ $=0.75$	For Idealized prismatic struts For bottle-shaped strut with re-bar For bottle-shaped strut w/o re-bar For tension member For all other cases For normal weight conc. For sand-light weight conc. For all light weight conc.	ACI 318-08

4.3 PROPOSED STRUT- AND-TIE MODEL APPROACH

4.3.1 Introduction

Once an inclined crack is formed, the stress trajectories in a beam are interrupted. The force flow changes direction and a redistribution of forces occur. One possible redistribution of forces for PPHC slab is the STM shown in Figure 4.1. Only concrete compression struts and steel tension ties are used. The predicted failure load found by using this STM is much lower than actual load for PPHC slab. The predicted failure load for this model is controlled by yielding of longitudinal reinforcement or crushing of diagonal strut. This ignores the possibility of concrete diagonal tension failure.

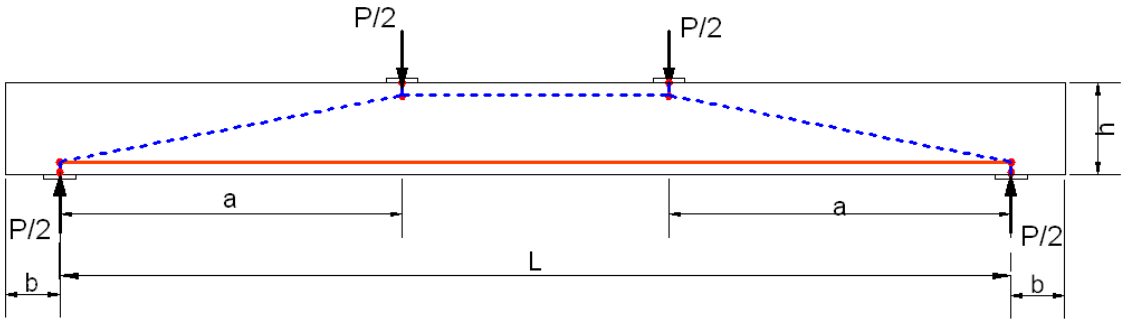

Figure 4.1: Inappropriate Strut-and-Tie Model for PPHC slab

4.3.2 Strut-and-Tie Model for PPHC Slabs without CFRP

4.3.2.1 Selecting the Struts and Ties Centerlines

The proposed Strut-and-Tie model must include a concrete tension member that might fail in tension before the yielding of the flexural reinforcement. The tension member of concrete is necessary for members without web reinforcement to maintain equilibrium for a compression struts. The appropriate angle of inclination for struts and ties is chosen after an iterative process. The proposed STM shown in Figure 4.2 is initiated by constructing the horizontal tie at the level of prestressed steel and the horizontal concrete strut, by assuming the distance from extreme top fiber to the center of the strut to equal the distance from the extreme bottom fiber to the center of

prestressed steel. Two compression struts originate at the node under the applied load in a fan shape. One of the compression struts is inclined with a 30-deg angle to the horizontal, and the other is inclined with a 60-deg angle to the horizontal. The concrete ties are inclined with 60-deg to the horizontal. The tension concrete ties are perpendicular to the diagonal compression concrete struts.

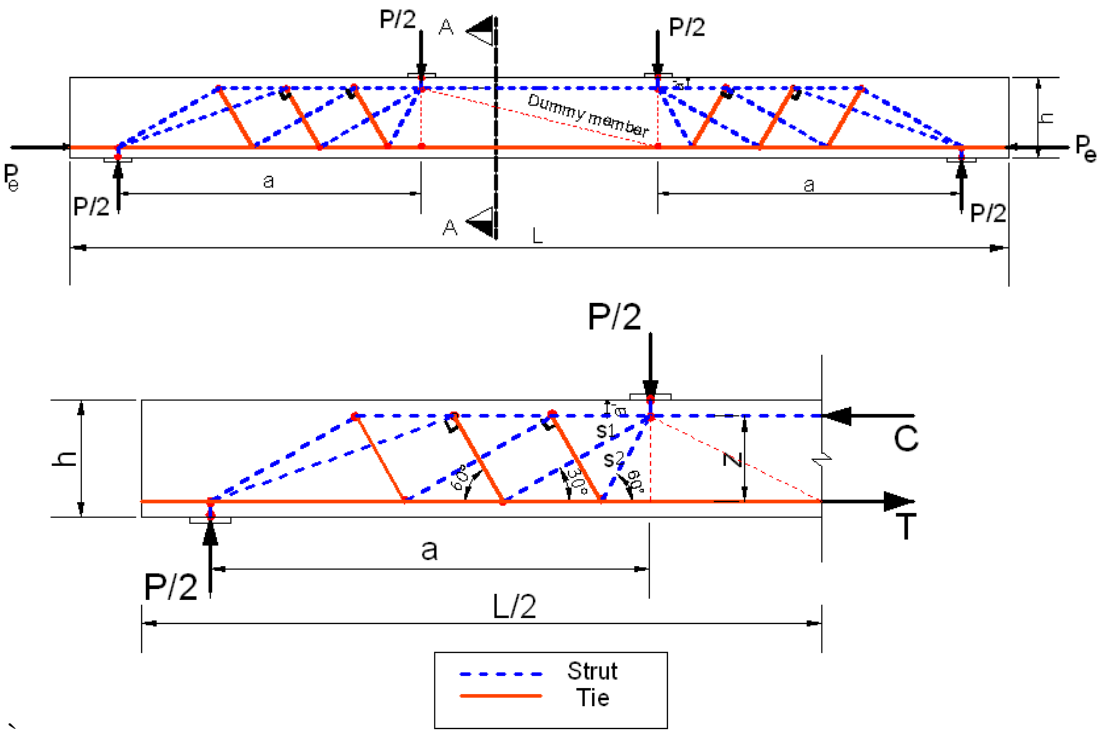

Section A-A

Figure 4.2: Proposed Strut-and-Tie Model of PPHC Slabs

For the truss analysis, it is necessary to add dummy members that are not actually contributing to the structural strength but whose existence ensures the stability of the analytical computations. For example, the STM shown in Figure 4.2 is stable, but, when this problem is being soolved with any numerical model, instability in analysis will occur. To avoid instability, the dashed diagonal member is added.

This member will be a zero member due to symmetry. In some situations, the dummy members might not be zero members. In this case, the area of these members should be set to a relatively small area, in order to make them very flexible to contribute to the load carrying system, or in other words to force them to become zero members.

4.3.2.2 Dimensioning the Struts and Ties

The steel tension tie has constant width, which is given in the following Eq. 4.1

$$w_{stie} = 2(h - d) \tag{4.1}$$

where h is the height of PPHC slab and d is the effective depth of PPHC slab. The width of top concrete strut is assumed to have the same width of the bottom steel tie. A concrete tension tie is assumed to have a constant width, w_{ctie}, which can be taken from the following equation

$$w_{ctie} = z\cos\alpha \tag{4.2}$$

where z is the vertical projection of a concrete tension tie between two nodes as shown in Figure 4.2 and α is the inclination of the compression strut which forms a perpendicular intersection with the tension tie. The third dimension of a concrete tension tie is assumed to be equal to the web width of PPHC slab, which can be calculated from the following equation

$$b_w = b - n\left(\sqrt{\pi r^2}\right) \tag{4.3}$$

where b is the width of PPHC slab , n is the number of circular holes and r is the radius of circular hole. A concrete tension tie is assumed to fail when its maximum tensile stress is equal to the tensile strength of concrete subjected to transverse compression. For normal weight concrete, test results yield a range between 6 and 8 $\sqrt{f_c'}$ psi (0.5 to 0.67 $\sqrt{f_c'}$ MPa) for concrete tensile strength. The value used for

tensile strength of concrete in a transverse compressed field was $4\sqrt{f_c'}$ psi ($0.332\sqrt{f_c'}$ MPa). A diagonal concrete compression strut is assumed to have a constant width w_{strut}, which can be taken from the following equation

$$w_{strut} = w_{ctie} \tan\alpha \tag{4.4}$$

where w_{ctie} the width of a concrete tension of is tie and α is the inclination of the compression strut. The third dimension of a diagonal concrete compression strut is equal to the web width of PPHC slab. If the cross-section areas of two almost parallel concrete struts or concrete ties, placed side-by-side overlap with each other, or if the dimensioned strut-tie model is not compatible with the actual size of the structural concrete, then the strut-tie model itself and/or its geometry must be modified and the procedure repeated until a satisfactory solution is obtained.

4.3.2.3 Applying the Effect of Prestressing Force

The basic concept of reinforced and prestressed concrete construction is that steel reinforcement is placed at those locations where tensile stresses will occur. In prestressed concrete members, this reinforcement is tensioned prior to the application of externally applied dead and live loading. This initial prestressing of the reinforcement precompresses the surrounding concrete which, in turn, improves the ability to resist higher loads prior to cracking. These prestressing forces act as tension forces on the prestressing steel and as compression forces in the concrete.

To model the effect of these forces, Schliach et al.(1987) proposed to treat the prestressing loads as constant permanent loads acting on the concrete member while the bonded prestressing steel are considered to increase the resistance of the member by acting as massive reinforcement like nonprestressed steel. That means all types of prestressed structures can be analyzed, designed and dimensioned like reinforced

concrete structures. The sectional forces in a beam due to prestress, dead and live loads are determined, and the resistance of the cross section is derived as for a reinforced concrete member, with bonded prestressing steel as additional reinforcement:

Normal forces $N = -P + N_L$

Shear forces $V = V_P + V_L$ (4.5)

Moments $M = M_P + M_L$

where

p = prestressing forces immediately after prestressing

M_P, V_P = moment and shear forces due to prestressing

N_L, M_L and V_L = axial, moment and shear forces due to other loads.

In this study, for ultimate consideration, a PPHC slab is treated following Schlaich's proposal except the prestressing forces are considered as the effective prestressing force instead of the initial prestressing load. The prestressing forces are usually transferred to the concrete by bond or mechanical end anchorage. These forces are represented as concentrated loads applied at truss joints. For PPHC slabs, the prestressing force is assumed to be transferred to concrete gradually. The transferred force varies linearly with the distance from the end of the prestressing strand. The distance (l_t) over which the effective prestress is developed is called transfer length as shown in Figure 4.3. Truss joints located within this transfer length will be loaded with concentrated loads which can be determined by linear interpolation as shown in Figure 4.3. In a post-tensioned member, the force is fully developed at the end of the member. Thus, the total prestressing force is applied at the first truss joint. The idea of

proportioning the prestressing force according to the transfer length is also applicable for debonded pretensioned strands.

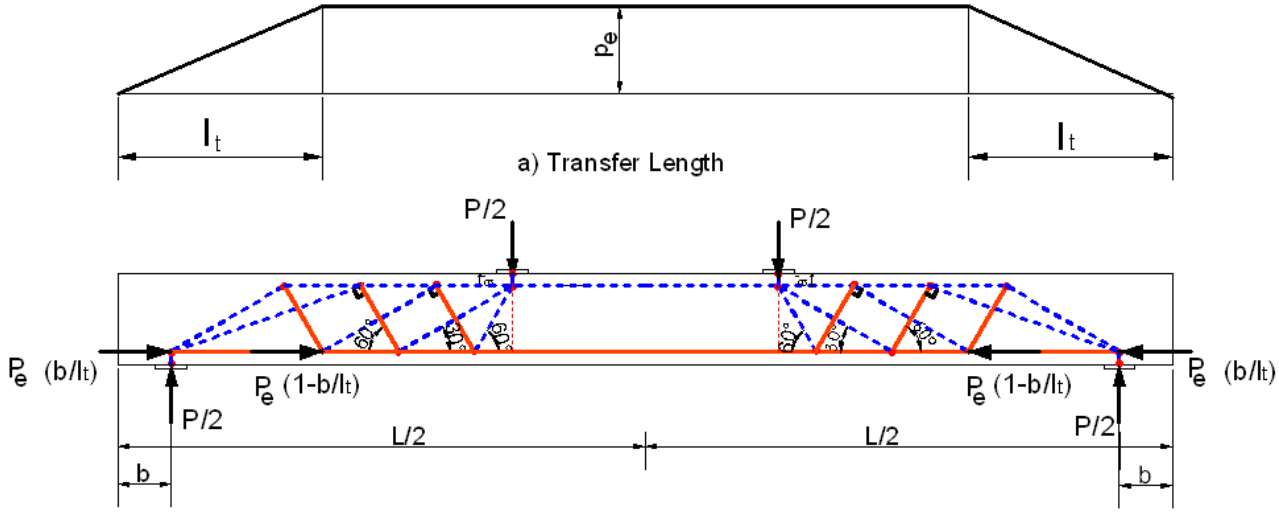

(b) Pretension Model

Figure 4.3: Modeling Prestressing Force of Pre-tensioned Member

IF the model for prestressing force illustrated in Figure 4.3 is substituted by the following model shown in Figure 4.4**,** the results will not be affected more than 5%.

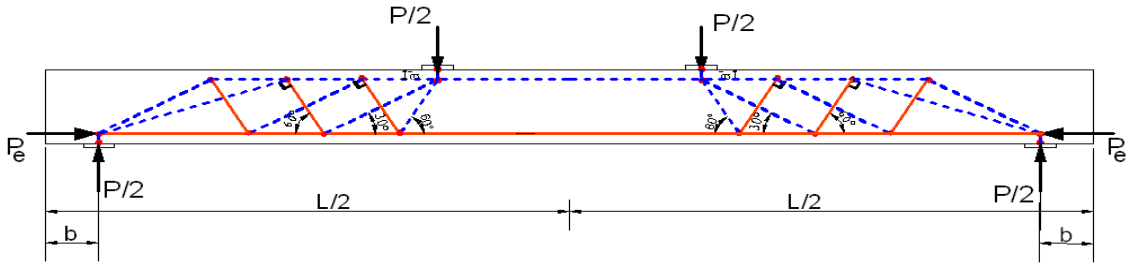

Figure 4.4: Acceptable Model for Prestressing Force of Pre-tensioned member

4.3.2.4 Adjusting the Centerline and Width of Horizontal Struts

In this step, the centerline of the horizontal compressive strut, and its width are adjusted to satisfy the equilibrium with the limit forces of other struts and ties of the STM model as shown in Figure 4.5.

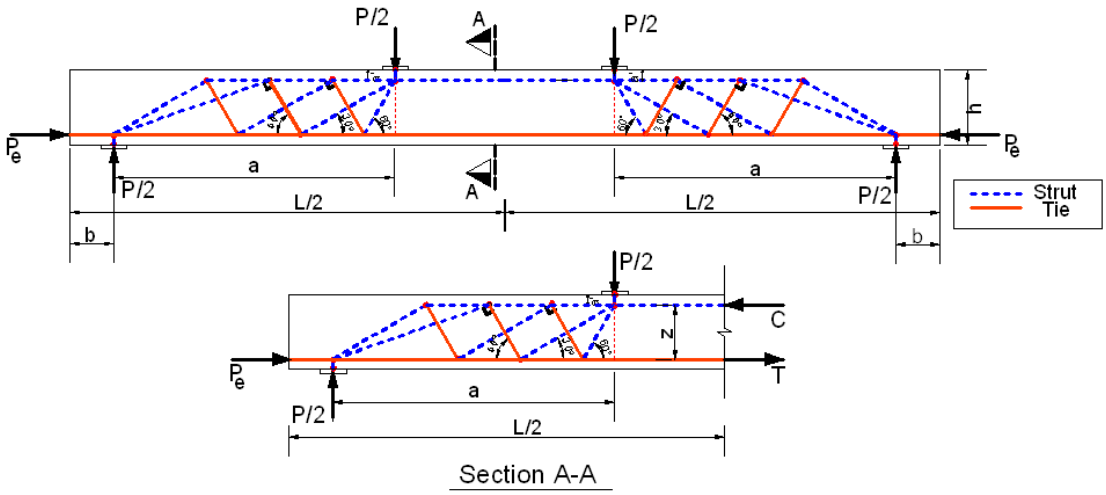

Figure 4.5: Determining the New Width of Top Horizontal Strut

The limit forces for T and C shown in section A-A in Figure can be given by following equations:

$$T = 0.75 A_{ps} \left(f_{pu} - f_{pe} \right) \tag{4.6}$$

$$C = P_e + T \tag{4.7}$$

When the magnitude of C is determined by using Eq. 4.8, one can get the new area of the top horizontal strut.

$$A_{hstr} = \frac{C}{Limit\ \ stress\, in\ \ strut\, or\, nodal\ zone(\ which\, smaller\ )} \tag{4.8}$$

4.3.2.5 Checking Stress Ratios in Strut-and-Tie Elements

After selecting the centerline of the Strut-and-Tie Model and dimensioning the width of struts and ties, a structure analysis is conducted to obtain stress ratios for each strut-and-tie element, where the stress ratio means the ratio of element stress to stress limit. A stress ratio greater than 1.0 points out an overstress (CAST).The applied load is increased until the stress ratio of any one of the struts or ties reaches one. The stress ratio can be given by following equation:

$$\text{Stress ratio} = \frac{f_c}{\phi \nu f_c'} \tag{4.9}$$

where f_c is the element stress, ϕ is strength reduction factor, ν is the effective factor, and f_c' is the compressive stress in concrete. The effective factor reflects the reduction of concrete strength due to cracking and transverse tensile strains of the struts. In this study, the ACI 318-08 effective model is used to account for types of struts. If the maximum tensile stress is equal to the tensile strength of concrete subjected to transverse compression, the shear failure will occur in the concrete tie. The flexural failure can occur due to the yielding or rupturing of prestressing steel or due to compression of concrete.

4.3.3 An example of Strength Prediction Process by Using the Proposed STM

This section shows the strength prediction procedure by using the proposed STM approach for S4-B slab. The effective factor used here is ACI 318-08's effective model.

Step-1: **Selecting the Struts and Ties Centerlines**

The setup and cross section of slab S4-B is illustrated in Figure 4.6.

The proposed STM shown in Figure 4.7 starts with two compression struts originating at the node under the applied load. One of the compression struts is inclined with a 30-deg angle to the horizontal, and the other is inclined with a 60-degree angle to the horizontal. The tension concrete ties are perpendicular to compression concrete struts.

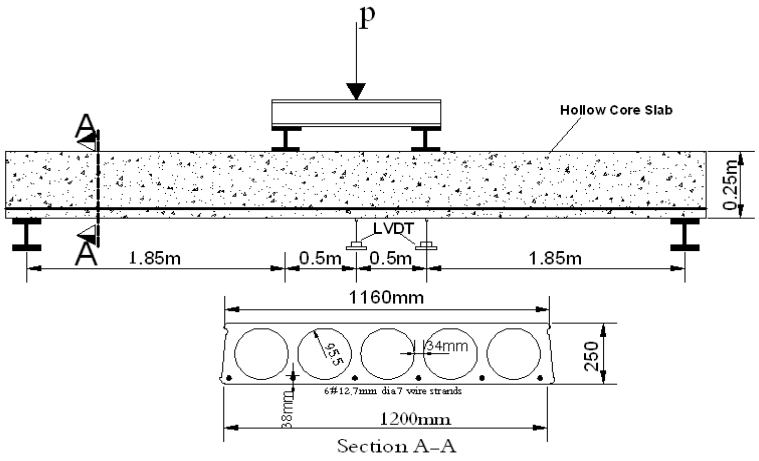

Figure 4.6: Setup Test for Slab S4-B

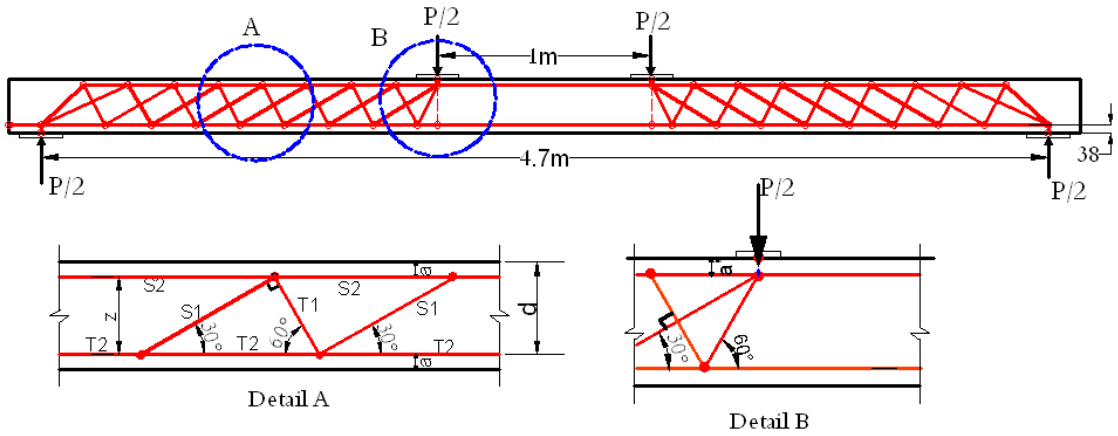

Figure 4.7: Centerlines of STM for Slab S4-B

Step-2**: Dimensioning the Struts and Ties**

The dimensions of struts and ties of slab S4-C can be obtained as follows:

The lever arm $z = h - 2a = 250 - 2 * 38 = 174$

The width of diagonal concrete tie $w_{ctie} = z\cos\alpha = 174 * cos(30) = 150.7\ mm$

The width of diagonal concrete strut $w_{strut} = w_{ctie}\tan\alpha = 150.7 * \tan(30) = 87\ mm$

The depth of diagonal concrete tie = The depth of diagonal concrete strut = $b_w = b - n\left(\sqrt{\pi r^2}\right)$ =1160-5$\sqrt{\pi r^2}$ =1160-5$\sqrt{\pi(95.5)^2}$ =313.65 mm

$$\Rightarrow Thickness\ scale\ \ factor\ \ for\ concrete\ strut\ or\ concrete\ tie = \frac{b_w}{b} = \frac{313.65}{1160} = 0.27$$

The width of horizontal tie = $2a = 2*38 = 76\ mm$ = the width of horizontal strut

If the width of horizontal strut $\geq \left(\frac{h}{2} - r\right)$ then the depth of horizontal strut can be given by the following equation:

$$b_y = b - 2\ n\sqrt{r^2 - \left(w_{hstr} - \frac{h}{2}\right)^2}$$

where b_y is the depth of horizontal strut, b is the width of PPHC slab and w_{hstr} is the width of horizontal strut. If the width of horizontal strut $\leq \left(\frac{h}{2} - r\right)$ then the depth of horizontal strut equals the width of PPHC slab. In this case w_{hstr}=76 mm.

$$b_y = 1160 - 2*5*\sqrt{(95.5)^2 - \left(76 - \frac{250}{2}\right)^2} = 340.3mm.$$

After the depth of horizontal strut had been obtained, the area of the strut can be calculated by the following equations:

If $w_{hstr} \geq \frac{h+2r}{2}$ then $A_{hstr} = b\,w_{hstr} - n\pi r^2$

If $w_{hstr} \leq \frac{h+2r}{2}$ then $A_{hstr} = b\,w_{hstr} - 0.5n\ r^2(\theta - \sin\theta)$

where $\theta = a\cos\left(1 - 0.5\left(\frac{b - b_y}{n\ r}\right)^2\right)$, in this case $w_{hstr} = 76mm \leq 220.5mm$

$$\theta = a\cos\left(1 - 0.5\left(\frac{1160 - 340.3}{5*95.5}\right)^2\right) = 118.26^0$$

$$A_{hstr} = b\,w_{hstr} - 0.5n\ r^2(\theta - \sin\theta)$$
$$= 1160*76 - 0.5*5*(95.5)^2\left(118.26*\frac{\pi}{180} - \sin 118.26\right)$$

$\Rightarrow A_{hstr} = 61181.88\ mm^2$

$\Rightarrow Thickness\ scale\ factor\ for\ horizontal\ strut = \frac{A_{hstr}}{w_{hstr}\ b} = \frac{61181.88}{76*1160} = 0.694$

Step-3: **Applying the Effect of Prestressing Force**

The transfer length of the strand was found as follows:

$$l_t = \frac{f_{se}}{20.7} d_p$$

where:

f_{se} = effective strand stress (MPa)

d_p = nominal diameter of prestressing strand (mm)

f_{se} =1202 MPa

$l_t = \frac{1202}{20.7} * 12.7 = 738$ mm

The value of prestressing force at a distance x from the edge of concrete member $= \frac{p_e\ x}{l_t}$. The prestressing forces that may be developed at the joints located in the range of transfer length are summarized in Table 4.2.

Table 4.2: Distribution of Effective Prestressing Force along Strand's Transfer Length

No. of joint	Distance from edge of PPHC slab (mm)	Prestressing force (kN)
1	150	145
2	448.6	434
3	664	642
4	871	714

Step-4: **Adjusting the Centerline and Width of Horizontal Strut**

The width of horizontal strut adjusted to maintain the equilibrium in the STM model. The new width of horizontal strut can be calculated by using Eq. 4-6 to Eq. 4-8:

$$C = P_e + T$$
$$T = 0.75A_{ps}\left(f_{pu} - f_{pe}\right) = 0.75 * 594 * (1961 - 1202) = 338.13 \text{ kN}$$

$$C = P_e + T = 714 + 338.13 = 1052.13 kN$$

$$A_{hstr} = \frac{C}{\phi\left(0.85\nu f_c^{'}\right)} = \frac{1052.13 * 10^3}{0.75 * 0.85 * 1 * 40} = 41260 mm^2$$

If $A_{hstr} \le b\left(\frac{h}{2} - r\right)$ then $w_{hstr} = A_{hstr} / b$

If $A_{hstr} \ge b\left(\frac{h+2r}{2}\right) - n\pi r^2$ then $w_{hstr} = \left(A_{hstr} + n\pi r^2\right)/b$

If $b(\frac{h}{2} - r) \le A_{hstr} \le b\left(\frac{h+2r}{2}\right) - n\pi r^2$ then $w_{hstr} = \left(A_{hstr} + 0.5nr^2\left(\theta - \sin\theta\right)\right)/b$

$$\theta = a\cos\left(1 - 0.5\left(\frac{b - b_y}{n\ r}\right)^2\right)$$

$$b_y = b - 2\ n\sqrt{r^2 - \left(w_{hstr} - \frac{h}{2}\right)^2}$$

By trail and error

b_y= 782 mm

θ = 46.63°

w_{hstr} = 37.3 mm

$$\Rightarrow Thickness\ scale\ \ factor = \frac{A_{h\,str}}{w_{shtr} * b} = \frac{41260}{37.3 * 1160} = 0.953$$

Step-5: **Checking Stress Ratios in Strut- and-Tie Elements**

The stress ratio of steel tie reached one which means the failure occurred due to yielding of prestressing steel and then by flexural shear crack. The failure load obtained from the STM model was 206 kN. The S8-D slab failed in flexural shear mode.

4.3.4 Strut -and-Tie Model for PPHC Slabs with CFRP

4.3.4.1 Selecting the Struts and Ties Centerlines

The centerline of the Strut-and-Tie Model is selected by vertical positioning of horizontal ties including CFRP ties and vertical positioning of horizontal strut to satisfy equilibrium in the system of the STM model. The center of the vertical tie is assumed to be located at the center of the CFRP sheet if the PPHC slab is strengthened in shear. The diagonal concrete ties and the diagonal concrete struts are inclined respectively with 60-deg and 30-deg to the horizontal and intersecting perpendicular to each other. The new location of horizontal tie, including CFRP sheet, can be located by finding the new effective depth(d_{tie}) as shown in Figure 4.8. The new effective width can be given by Eq. 4.9 by assuming that the strains of both the bottom tensile prestressing steel and the CFRP sheet are the same because of the assumption of perfect bonding between CFRP sheet and concrete:

$$d_{tie} = d + \frac{A_{frp}\,E_{frp}}{A_{frp}\,E_{frp} + A_{ps}\,E_{ps}}\,d_{frp} \tag{4.10}$$

where A_{frp} and A_{ps} are respectively the areas of bottom CFRP and bottom prestressed steel. E_{frp} and E_{ps} are the modulus of elasticity of bottom CFRP and bottom

prestressed steel respectively. d_{frp} is the distance between the center of the bottom prestressing strand and the center of CFRP sheet.

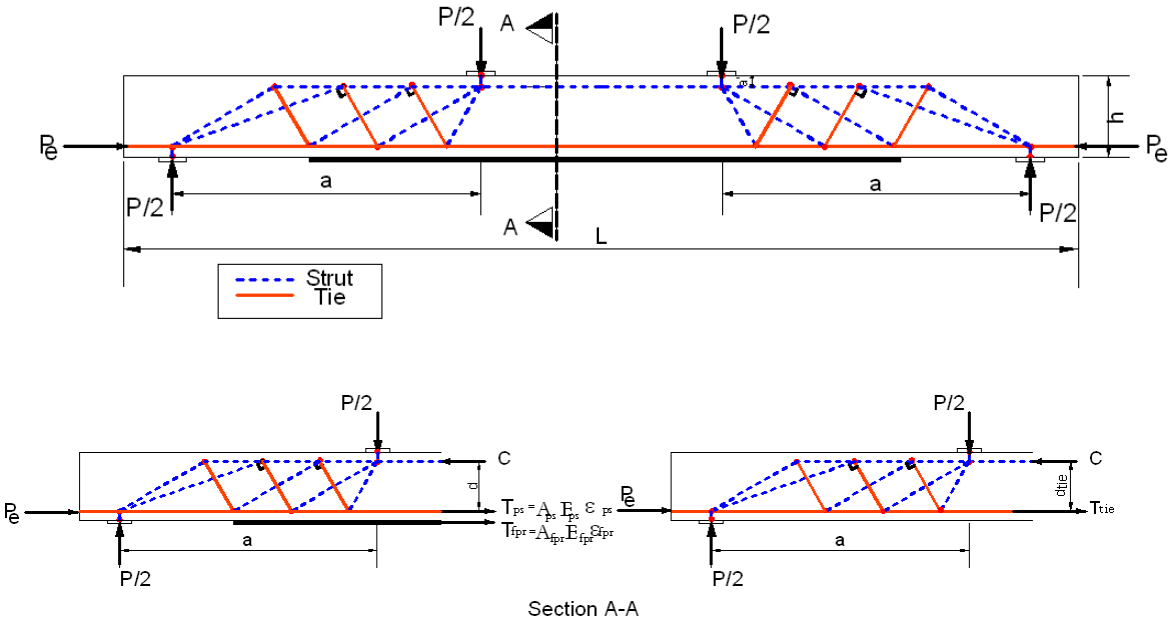

Figure 4.8: Simplified Strut-and-Tie Model of PPHC Slab with CFRP

4.3.4.2 Dimensioning the Struts and Ties

The dimensions of the Strut-and-Tie model elements shown in Figure 4.9 can be calculated by the equations tabulated in Table 4.3:

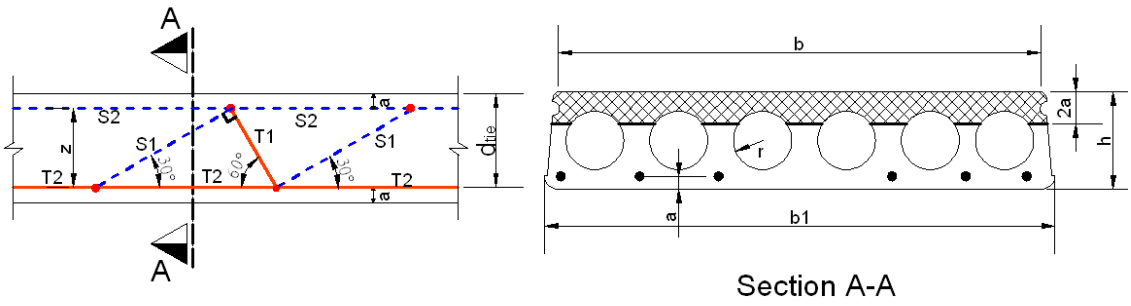

Figure 4.9: Designations of Strut and Tie Elements

It is assumed that the prestressing steel is fully effective. For CFRP, only 75% of their strength is assumed to be effective. The bottom tension tie capacity can be obtained

by adding 75% of prestressing steel reinforcement rupture strength and 75% of CFRP rupture strength.

Table 4.3: Dimensions of Strut-and-Tie Elements for Strengthened PPHC Slabs

ID	Width	Depth
T_1	z Cos 30^0	$b_w = b - n\left(\sqrt{\pi r^2}\right)$
T_2	$2(d\text{-}d_{tie})$	$\alpha_1 b$
S_1	Width of T_1*tan30^0	$b_w = b - n\left(\sqrt{\pi r^2}\right)$
S_2	$2a$	$\alpha_2^* b$

* α_2 is the thickness scale factor for strut *s2* = (the width of cross-section at distance equals *2a) /b*

where n is the number of circular holes in PPHC slab cross-section , α_1 and α_2 are named the thickness scale factor, d is the distance from the extreme compression fiber to the level of prestressing steel, d_{tie} is the new effective depth including the effect of CFRP sheet. In dimensioning the area of tension ties, it is assumed that the prestressing steel is fully effective. For CFRP, only 75% of their strength is assumed to be effective.

4.3.4.3 Applying the Effect of Prestressing Force

The effect of prestressing force for a PPHC slab with CFRP is treated by following the same way for PPHC slab without CFRP, which is explained in detail in 4.3.2.3.

4.3.4.4 Adjusting the Centerline and Width of Horizontal Strut

In this step, the centerline of the horizontal compressive strut, and its width are adjusted to satisfy the equilibrium with the limit forces of other struts and ties of STM model. The bottom tension tie capacity in STM for a PPHC slab with CFRP strengthening is increased by the effect of CFRP strength. Therefore, the width of

horizontal strut should be modified to maintain the equilibrium in STM. The new width of horizontal strut can be determined by using the following Eqns :

$$T = 0.75A_{ps}\left(f_{pu} - f_{pe}\right) + 0.75\,A_{frp}\,f_{frpu} \quad (4\text{-}11)$$

$$C = P_e + T \quad (4\text{-}12)$$

$$A_{hstr} = \frac{C}{\phi\left(0.85vf_c^{'}\right)} = \frac{1293.33*10^3}{0.75*0.85*1*40} = 50718.8\ mm^2 \quad (4\text{-}13)$$

When the area of horizontal compressive strut is determined, its width can be determined as explained previously.

4.3.4.5 Checking the Stress Ratios in Strut and Tie Elements

CAST software was used to analyze the Strut-and-Tie model for PPHC slabs. The stress ratios for STM elements can be obtained, and the failure mode can be detected according to the type of STM element that reaches the stress ratio limit.

4.3.5 An example of Strength Prediction Process for Strengthened PPHC Slab by Using the Proposed STM

The ultimate capacity of S8-D slab by using the proposed STM approach is discussed in the following steps.

Step-1: **Selecting the Struts and Ties Centerlines**

The setup and cross section of slab S8-D is illustrated in Figure 4.10.

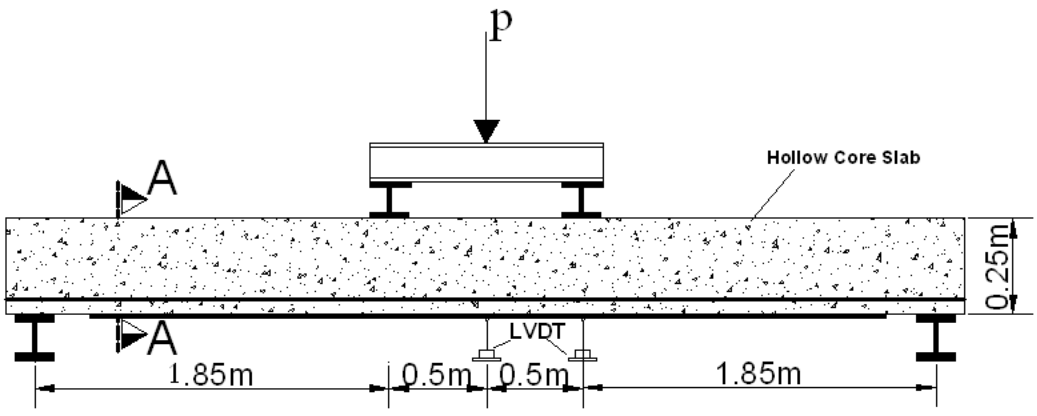

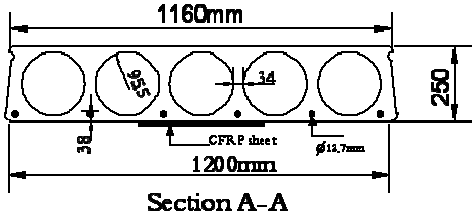

Figure 4.10: Setup Test for Slab S8-D

The centerline of horizontal steel tie can be found by Eq. 4-9 as follows

$$d_{tie} = d + \frac{A_{frp}\,E_{frp}}{A_{frp}\,E_{frp} + A_{ps}\,E_{ps}}\,d_{frp} = 212 + \frac{0.167*400*230*10^3}{0.167*400*230*10^3 + 594*195*10^3}*38$$

$$d_{tie} = 212 + 4.45 = 216.45\ mm$$

Width of steel tie = $2*(h - d_{tie}) = 2*(250 - 216.45) = 67.1$

$$z = 216.45 - \frac{w_{hstr}}{2}$$

where w_{hstr} is the width of top horizontal strut which can be caculated as follows :

$$C = P_e + T$$

$$T = 0.75A_{ps}(f_{pu} - f_{pe}) + 0.75\,A_{frp}\,f_{frpu}$$

$$T = 0.75*594*(1961 - 1202) + 0.75*67*4800 = 579.33kN$$

$$C = P_e + T = 714 + 579.33 = 1293.33\ \ kN$$

$$A_{hstr} = \frac{C}{\phi\left(0.85\nu f_c^{'}\right)} = \frac{1293.33*10^3}{0.75*0.85*1*40} = 50718.8\ mm^2$$

Since

$$b(\frac{h}{2} - r) \le A_{hstr} \le b\left(\frac{h+2r}{2}\right) - n\pi r^2$$

$$1160*(125 - 95.5) \le A_{hstr} \le 1160*\left(\frac{250 + 2*95.5}{2}\right) - 5*\pi*95.5^2$$

$$34220 \le A_{hstr} \le 112519.4$$

$\Rightarrow$

$$w_{hstr} = \left(A_{hstr} + 0.5nr^2(\theta - \sin\theta)\right)/b$$

where

$$\theta = A\cos\left(1 - 0.5\left(\frac{b - b_y}{n\ r}\right)^2\right) \text{ and } b_y = b - 2\ n\sqrt{r^2 - \left(w_{hstr} - \frac{h}{2}\right)^2}$$

By trail and error:

$$w_{hstr} = 52\ mm$$

$$b_y = 544.2\,mm$$

$$\theta = 80.29\ \ mm$$

$$\Rightarrow \quad z = 216.45 - \frac{w_{hstr}}{2} = 216.45 - \frac{52}{2} = 190.45\ mm$$

After selecting the widths of the steel tie and top horizontal concrete strut, the-strut and-tie model can be drawn as shown in Figure 4.11.

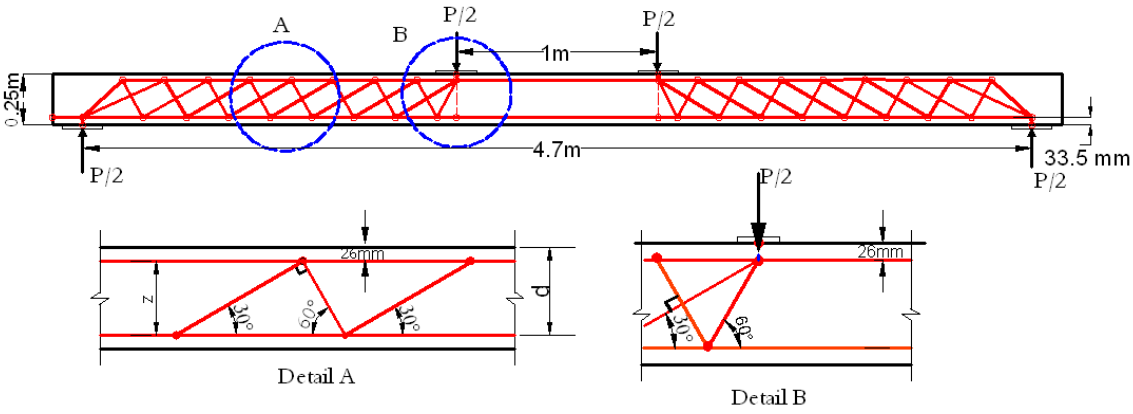

Figure 4.11: Centerlines of STM for Slab S8-D

Step-2: **Dimensioning the Struts and Ties**

The dimensions of Strut-and-Tie model elements can be calculated by the aforementioned equations tabulated in Table 4.3 as follows :

Table 4.4: Dimensions of Strut-and-Tie Model Elements for Slab SD-8

ID	Width(mm)	Depth (mm)	Thickness Scale Factor
w_{ctie}	165	313.65	0.27
w_{stie}	67.1	400.53	0.743
w_{dstrut}	95.26	313.65	0.27
w_{hstrut}	52	544.2	0.843

where w_{ctie} is the width of concrete tie , w_{stie} is the width of steel tie, w_{dstrut} is the width of diagonal concrete strut and w_{hstrut} is the width of horizontal concrete strut.

Step 3**: Applying the Effect of Pestressing force**

The effect of prestressing force for a PPHC slab with CFRP is treated by following the same way for PPHC slab without CFRP.

The transfer length of the strand was found as follows:

$$l_t = \frac{f_{se}}{3} d_p$$

f_{se}=1202 MPa = 174.33 ksi

$$l_t = \frac{174.33}{3} * 0.5 = 29.055 \text{ in} = 738 \text{ mm}$$

The prestressing forces that may be developed at the joints located in the range of transfer length are summarized in Table 4.5.

Table 4.5: Distribution of Effective Prestressing force over the transfer length

No. of joint	Distance from edge of PPHC slab (mm)	Prestressing force (kN)
1	150	145
2	448.6	434
3	664	642
4	871	714

Truss joints located within this transfer length will be loaded with concentrated loads as shown in Figure 4.12.

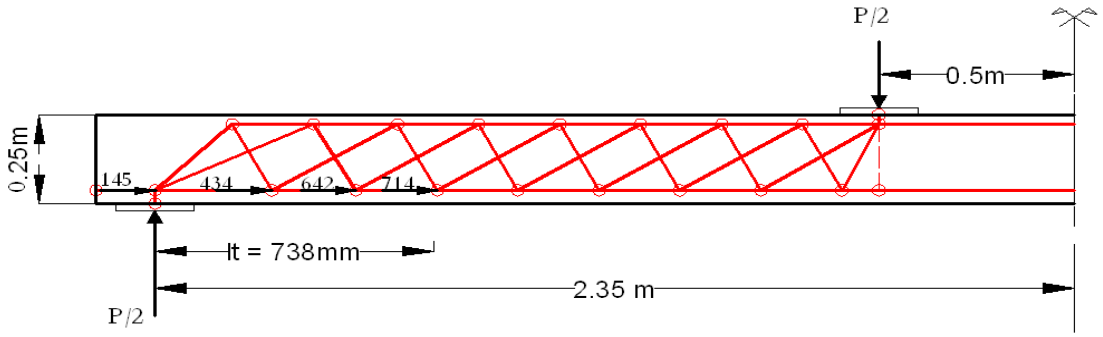

Figure 4.12: Gradual Effect of Prestressing Force on Slab S8-D

The results are not changed more than 5% if the prestressing force is applied directly to the support node as shown in Figure 4.13.

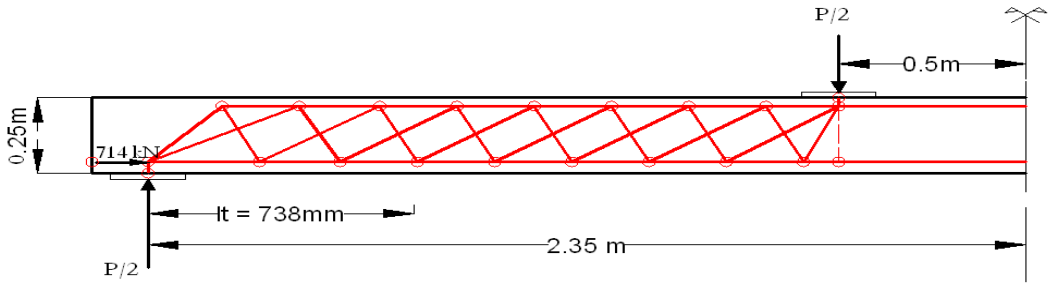

Figure 4.13: Direct Effect of Prestressing Force on Slab S8-D

Step-5: Checking Stress Ratios in Strut-and-Tie Elements

The analysis of the strut and tie model was performed by using CAST software. When the stress ratio of any element of STM reached one, the failure in the STM occurred. Four failure modes may occur for a PPHC slab strengthened with externally-bonded CFRP sheets: concrete crushing, steel yielding followed by concrete crushing, steel yielding followed by CFRP rupture, and shear failure.

4.3.5 Summary

The dimensions of STM elements for PPHC slabs are summarized in Table 4.6. The area of top horizontal concrete strut for each PPHC tested slab that satisfies the equilibrium with the tensile force in the bottom cord are summarized in Table 4.7.

Table 4.6: Dimensions of STM for PPHC Slabs, mm

Slab Name	w_{ctie}	t_{ctie}	w_{stie}	t_{stie}	w_{dstrut}	t_{dstrut}	w_{hstrut}	t_{hstrut}
S1-A	123.8	387.4	76	351.8	71.5	387.4	38	732.6
S2-A	123.8	387.4	76	351.8	71.5	387.4	38	732.6
S3-B	167.1	313.6	76	340.26	96.5	313.6	37.3	781
S4-B	167.1	313.6	76	340.26	96.5	313.6	37.3	781
S5-C	203.1	314.4	76	424	117.3	314.4	55	600.1
S6-C	203.1	314.4	76	424	117.3	314.4	55	600.1
S9-E	129.9	387.4	76	351.8	75	387.4	24	1160
S10-E	129.9	387.4	76	351.8	75	387.4	24	1160
S11-E	129.9	387.4	76	351.8	75	387.4	24	1160
S12-F	167.1	313.6	76	340.26	96.5	313.6	37.3	781
S13-F	167.1	313.6	76	340.26	96.5	313.6	37.3	781
S14-G	203.1	314.4	76	424	117.3	314.4	55	600.1
S15-G	203.1	314.4	76	424	117.3	314.4	55	600.1
S8-D	165	313.6	67.1	400.5	95.26	313.6	52	544.3
S17-H	167.1	313.6	76	340.26	96.5	313.6	37.3	781

The area of the top horizontal concrete strut that satisfy the equilibrium with the tensile force in the bottom cord is summarized in Table 4.7.

Table 4.7: Area of Horizontal Struts of PPHC Slabs, mm^2

Slab Name	Limit force in Steel Tie (kN)	Effecive Prestressed Force(kN)	Force in Horizontal Strut(kN)	Limit Stress in Top Strut (kN)	w_{hstrut} (mm^2)
S1-A	338.1	714	1052.1	25.2	41258.8
S2-A	338.1	714	1052.1	25.2	41258.8
S3-B	338.1	714	1052.1	25.2	41258.8
S4-B	338.1	714	1052.1	25.2	41258.8
S5-C	450.75	951.7	1402.4	25.2	54996.5
S6-C	450.75	951.7	1402.4	25.2	54996.5
S9-E	225.75	475.8	701.55	25.5	27511.76
S10-E	225.75	475.8	701.55	25.5	27511.76
S11-E	225.75	475.8	701.55	25.5	27511.76
S12-F	338.1	714	1052.1	25.2	41258.8
S13-F	338.1	714	1052.1	25.2	41258.8
S14-G	450.75	951.7	1402.4	25.2	54996.5
S15-G	450.75	951.7	1402.4	25.2	54996.5
S8-D	579.3	714	1293.3	25.5	50717.6
S17-H	338.1	714	1052.1	25.2	41258.8

When the area of horizontal struts are determined as illustrated in Table 4.7, the width of the top horizontal concrete strut and the thickness scale factor are obtained and tabulated in Table 4.8 .

Table 4.8: Width and Thickness Scale Factor of Horizontal Struts

Slab Name	Height (mm)	Radius of Circular Hole (mm)	Area of Horizontal Strut(mm^2)	Width of Horizontal Strut(mm)	Thickness Scale Factor
S1-A	200	71.5	41258.8	38	0.9377
S2-A	200	71.5	41258.8	38	0.9377
S3-B	250	95.5	41258.8	37.3	0.954
S4-B	250	95.5	41258.8	37.3	0.954
S5-C	300	118	54996.5	55	0.863
S6-C	300	118	54996.5	55	0.863
S9-E	200	71.5	27511.76	24	1
S10-E	200	71.5	27511.76	24	1
S11-E	200	71.5	27511.76	24	1
S12-F	250	95.5	41258.8	37.3	0.954
S13-F	250	95.5	41258.8	37.3	0.954
S14-G	300	118	54996.5	55	0.863
S15-G	300	118	54996.5	55	0.863
S8-D	250	95.5	50717.6	52	0.843
S17-H	250	95.5	41258.8	37.3	0.954

CHAPTER 5

RESULTS AND DISCUSSION

5.1 ANALYTICAL RESULTS

5.1.1 General

Three types of PPHC slabs are used in the experimental program for this research. The different cross-sections for PPHC slabs are shown in Figure 5.1.

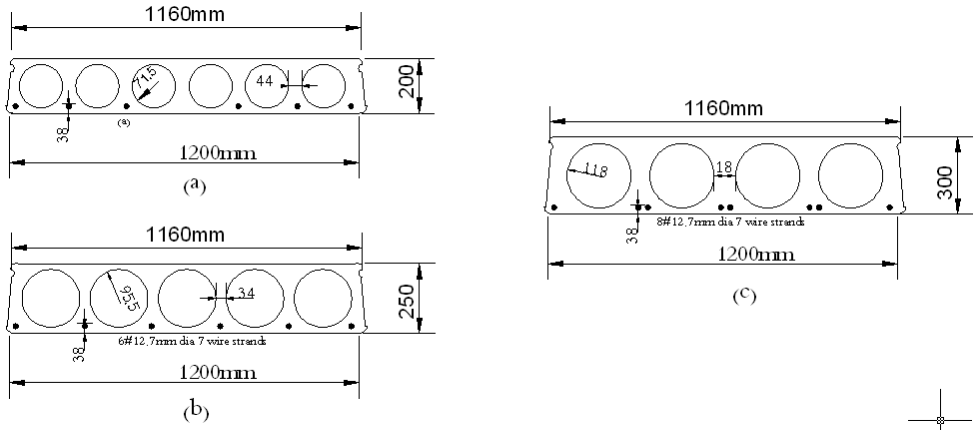

Figure 5.1: Cross-Sections of PPHC Slabs

5.1.2 Design of PPHC Slabs

The design of hollow core slabs in generally done by using the manual for design of hollow-core slabs (1998) which is based on the ACI 318 requirements. In addition, the graphical method and strain compatibility method proposed in the PCI design handbook (PCI, 2005) are also used. The PCI hollow-core slab manual also provides the section properties of several proprietary hollow-core sections together with graphs of safe uniformly distributed loads that can be used for various spans for slabs varying from 150 mm to 375mm in depth.

In precast or steel frame construction, the hollow-core slabs are supported on either precast walls or steel beams, and they act as simply supported prestressed slabs. These slabs are generally designed as simply supported one-way slabs without any negative or torsional moment. The hollow-core slabs may fail by one of the following failure modes (Walravan and Mercx 1983, Pajari 1989, and Girhammar 1992):

- Concrete cracking at top due to prestress transfer
- Concrete cracking at bottom
- Rupture of prestressing strands
- Crushing of concrete at top
- Excessive deflection under loads.
- Flexure shear failure
- Web shear failure
- Bond slip failure of strands

5.1.2.1 Flexural Load Capacity of Hollow Core Slabs

The flexural strength for prestressed concrete slabs is computed by using the following equation:

$$M_u = \phi A_{ps} f_{ps}\left(d_p - \frac{a}{2}\right) \tag{5.1}$$

Where

$$a = \frac{A_{ps} f_{ps}}{o.85 f'_c b_w} \tag{5.2}$$

$$f_{ps} = f_{pu}\left(1 - \frac{\gamma_p}{\beta_1}\rho_p \frac{f_{pu}}{f'_c}\right) \tag{5.3}$$

$$M_u = \phi M_n \tag{5.4}$$

$$M_n = 1.2 M_{cr} \tag{5.5}$$

The flexural cracking strength is given by

$$M_{cr} = \frac{I}{y_b}\left(\frac{P}{A} + \frac{P_e}{S_b} + 0.67\sqrt{f_c'}\right) \quad (5.6)$$

where A_{ps} = area of prestressing steel.

ϕ = strength reduction factor

f_{ps} = stress in prestressed reinforcement at nominal strength

d_p = effective depth of the slab

b_w = net web width of the slab

β_1 = factor depending on concrete strength

ρ_p = $A_{ps}/b_w d_p$ = ratio of prestressing steel

f_{pu} = ultimate tension strength of steel

M_n = Nominal flexural strength

M_{crf} = flexural cracking strength

5.1.2.2 Shear Load Capacity of Hollow Core Slabs

5.1.2.2.1 Flexural Shear Capacity

The flexure shear capacity of PPHC slabs is given as sum of three components

$$V_{ci} = V_{fs} + V_{ds} + V_d \quad (5.7)$$

where: V_{fs} =shear force that initiates flexure shear crack, V_{ds} =additional shear force required to drive the shear crack, V_d = shear due to dead load.

In PPHC slabs loaded by using a four-point loading system, the flexure cracks are first developed in the constant moment zone. These flexural cracks at higher loads extend into regions outside this zone where high moment and shear exists. The flexure-shear cracks initiate from the tip of these previously developed flexural cracks. This region is close to the point load where both high moment and shear

exists, and it is assumed that this occurs at *d/2* distance from the point load. The diagonal shear crack developed coincides with the principal tension plane in concrete and extends into the flexural compression zone. The cracking moment is then given as

$$M_{cr} = M_{max} - V_i\left(\frac{d}{2}\right) = V_i\left(\frac{M_{max}}{V_i} - \frac{d}{2}\right) \tag{5.8}$$

where $M_{\max}$ and V_i are the moment and shear adjacent to the loading (excluding self weight). The shear force V_{fs} that initiates the flexure shear crack is given by

$$V_{fs} = V_i = \frac{M_{cr}}{\frac{M_{max}}{V_i} - \frac{d}{2}} \tag{5.9}$$

The additional shear force required to further drive the diagonal shear crack (V_{ds}), is conservatively approximated by tests reported in University of Illinois Bulletin 493 [9] as

$$V_{ds} = \frac{1}{20}\sqrt{f_c'}\, b_w d \tag{5.10}$$

The flexure shear capacity (V_{ci}) of the hollow core slab is then given as

$$V_{ci} = \frac{1}{20}\sqrt{f_c'}\, b_w d + \frac{M_{cr}}{\frac{M_{max}}{V_i} - \frac{d}{2}} + V_d \tag{5.11}$$

In the ACI 318 code, the term *d/2* is dropped, which results in the ACI Equation 11-12:

$$V_{ci} = \frac{1}{20}\sqrt{f_c'}\, b_w d + \frac{V_i}{M_{max}} M_{cr} + V_d \qquad V_{ci} \geq \frac{1}{7}\sqrt{f_c'}\, b_w d \qquad \text{and} \qquad d \geq 0.8\,h \tag{5.12}$$

$$M_{cr} = \frac{1}{y_b}\left(\frac{1}{2}\sqrt{f_c'} + f_{pe} - f_d\right) \tag{5.13}$$

where:

V_d = shear force at the section due to unfactored dead load

V_i = factored shear force at the section due to externally load occurring with $M_{\max}$

d = effective depth of the slab

b_w = minimum net web width of the slab

f_{pe} = compressive stress in concrete at the bottom of the slab due to effective prestress force only

f_d = stress at the bottom of the slab due to unfactored dead load

M_{cr}= flexural cracking strength

5.1.2.2.2 Web shear capacity

The web shear cracks develop in high shear zone where the principal tensile stress in the web exceeds the tensile strength of the concrete. These inclined cracks initiate in the web of the PPHC slabs where the thickness of web is minimum and the shear stress a maximum (close to the neutral axis). They then propagate in the diagonal direction as the load is increased. A combined state of stress, including compressive stress due to prestressing force and shear stress, exists in the web in this high shear zone. The web shear cracking occurs where the principal tensile stress reaches the tensile strength of the concrete f_t. By using Mohr's circle, this can be expressed as

$$f_t = \sqrt{{v_{cw}}^2 + \left(\frac{f_{pc}}{2}\right)^2} - \left(\frac{f_{pc}}{2}\right) \rightarrow v_{cw} = f_t\sqrt{1 + \frac{f_{pc}}{f_t}} \quad \text{and}$$

$$V_{cw} = \left(f_t\sqrt{1 + \frac{f_{pc}}{f_t}}\right)b_w d \tag{5.14}$$

where v_{cw} is the web shear cracking stress, f_{pc} is the compressive stress in concrete at the centroid of the cross section of the concrete, and V_{cw} is the web shear capacity of the hollow core slab.

By Using a conservative value of the tensile strength f_t of concrete as $f_t = 0.3\sqrt{f_c'}$ and by approximating the term under the square root in Equation (8), the web shear capacity for hollow core slabs with horizontal prestressing steel ($V_p = 0$) can be written as

$$V_{cw} = \left(0.3\sqrt{f'_c} + 0.3 f_{pc}\right) b_w d \qquad (5.15)$$

5.1.3 Detailed Example of Analytical Calculations

The calculation was made for a section (a) in Figure 5.1. The calculations deal with:

- Cracking bending moment
- Ultimate bending moment
- Ultimate shear force

The Excel spreadsheet was used to facilitate the analytical calculations.

5.1.3.1 Cracking Moment for Slab S4-B

- Concrete strength $f_c' = 40\,MPa$
- The concrete area $A_C = 1.47*10^5$ mm^2
- The prestressing steel area $A_{ps} = 594$ mm^2(6 strands 12.7 mm diameter)
- The eccentricity e = 87 mm
- The effective depth d = 212mm
- The moment of inertia I= $1.19*10^9$ mm^4

From stress-strain diagram F_{pu}=1961.8 *MPa*

F_{ps} before loss =0.7*1961.8=1373.26 *MPa*

F_{pe} after loss = 0.875*1373.26 = 1201.6 *MPa*

$P_i = F_{ps} * A_{ps}$=1373.26*594/1000= 815.716 kN

$P_e = F_{pe} * A_{ps} = 1201.6 * 594/1000 = 713.75$ kN

$$M_{cr} = \frac{I}{yb}\left[\frac{p_e}{A} + \frac{P_e e}{S_b} + \frac{1}{2}\sqrt{f_c'}\right]$$

$$M_{cr} = \frac{1.18*10^9}{122.32}\left[\frac{713.75*10^3}{1.47*10^5} + \frac{713.75*10^3*87*122.64}{1.19*10^9} + \frac{1}{2}\sqrt{40}\right]$$

$$M_{cr} = 139.5\ kN.m$$

$$p_{cr} = \frac{139.5*2}{1.85} = 150.8\ kN$$

5.1.3.2 Ultimate Moment Capacity for Slab S4-B

The ultimate moment capacity is obtained by using the strain compatibility method. The details of slab S4-B cross section and, the strains associated with different load stages, are shown in Figure 5.2.

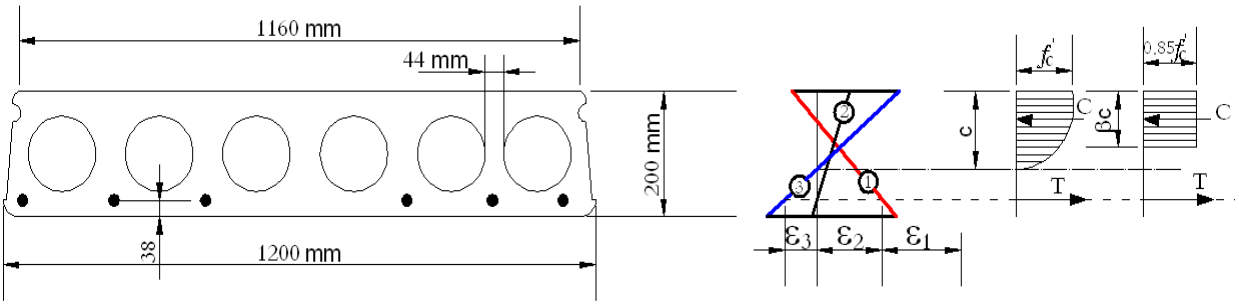

Figure 5.2: Ultimate Moment Capacity of PPHC Slab by the Strain Compatibility Method

Using the stress-strain diagram

$$\varepsilon_1 = 0.0062$$

$$r^2 = \frac{I}{A_c} = \frac{1.19*10^9}{1.47*10^5} = 8027.2\ mm^2$$

$$\varepsilon_2 = \frac{p_e}{A_c E_c}\left(1 + \frac{e^2}{r^2}\right) = \frac{713.75*10^3}{1.47*10^5 * 27000}\left(1 + \frac{87^2}{8077.25}\right) = 3.48*10^{-4}$$

Now from the strain diagram:

$$\frac{c}{0.003} = \frac{d-c}{\varepsilon_3}$$

$$\frac{c}{0.003} = \frac{d-c}{\varepsilon_3}$$

$$\frac{c}{0.003} = \frac{212-c}{\varepsilon_3}$$

$$c(0.003+\varepsilon_3) = 0.636$$

$$c = \frac{0.636}{(0.003+\varepsilon_3)}$$

$$a = \beta c$$

$$\beta = 0.85 \quad for \quad f_c' = 28\,Mpa$$

$$\beta = 0.80 \quad for \quad f_c' = 35\,Mpa$$

$$\Rightarrow \beta = 0.76 \quad for \quad f_c' = 40\,Mpa$$

$$C = 0.85 f_c' * b * \beta c = 0.85 * 40 * 1162 * 0.764 * \frac{0.636}{(0.003+\varepsilon_3)} = \frac{19197.1}{(0.003+\varepsilon_3)}$$

Now by trail and error: Assume ε_3= 0.0152

$$\Rightarrow \varepsilon_{ps} = \varepsilon_1 + \varepsilon_2 + \varepsilon_3$$

$$\Rightarrow \varepsilon_{ps} = 0.0062 + 3.48 * 10^{-4} + 0.0152 = 0.0217$$

$$\Rightarrow f_{ps} = 1774.8\,Mpa$$

$$T = A_{ps} * f_{ps} = 594 * 1774.8/1000 = 1054.2\ kN$$

$$C = \frac{19197.1}{(0.003+\varepsilon_3)} = \frac{19197.1}{(0.003+0.0152)} = 1054.8\ \text{kN}$$

$$Thus\ C = T$$

$$Then\ \ a \approx 0.764c = 0.764 * 34.95 = 26.7 \le 29.5\ \ mm$$

$$Mn = T(d - a/2) = 1054.8 * (212 - 26.7/2)/1000 = 209.5\ \ kN.m$$

Flexural failure load P_n=209.5*2/1.85 = 226.5 kN

5.1.3.3 Ultimate Shear Capacity for Slab S4-B

- Concrete strength $f_c' = 40\,MPa$
- The concrete area A_C = 1.47*10^5 mm^2
- The prestressing steel area A_{ps} = 594 mm^2(6 strands 12.7 mm diameter)
- The eccentricity e = 87 mm
- The effective depth d = 212 mm
- The moment of inertia I = 1.19*10^9 mm^4

To estimate the value of *bw*, the hollow core section was transferred to an equivalent section with square hole. The area of the square hole is equal to the area of the circular holes. From the equivalent section, *bw* = 315.67 mm, the ACI equation for the web shear states that:

$$V_{cw} = \left(0.3\sqrt{f_c'} + 0.3 f_{pc}\right) b_w d + V_P$$

$$f_{pc} = \frac{p_e}{A_c} = \frac{713.75 * 10^3}{1.47 * 10^5} = 4.855\,MPa$$

$$V_p = 0$$

$$\Rightarrow V_{cw} = \left[\left(0.3\sqrt{40} + 0.3 * 4.855\right) * 315.67 * 212 + 0\right]/1000 = 224.4\ kN$$

For the flexural shear, the ACI equation is given as:

$$V_{ci} = \frac{1}{20}\sqrt{f_c'}\ b_w d + \frac{V_i M_{cr}}{M_{\max}} + V_d \geq \frac{1}{7}\sqrt{f_c'}\ b_w d$$

$$V_{ci} = \left(\frac{1}{20}\sqrt{40} * 315.66 * 212 + \frac{139.4 * 10^6}{1850} + 0\right)/1000 = 96.51\ kN$$

$$\frac{1}{7}\sqrt{f_c'}\ b_w d = \frac{1}{7} * \sqrt{40} * 315.66 * 212 = 60.46\ kN$$

Thus , shear failure load Pn = 2*96.5 = 193 kN

5.1.3.4 Cracking Moment for Slab S8-D

- Concrete strength $f_c' = 40\,MPa$
- The concrete area $A_C = 1.47*10^5$ mm^2
- The prestressing steel area $A_{ps} = 594$ mm^2(6 strands 12.7 mm diameter)
- The eccentricity e = 87 mm
- The effective depth d = 212mm
- The moment of inertia I= $1.19*10^9$ mm^4

The slab was strengthened with MAPE wrap sheet of 400 mm width.

- The CFRP area A_{frp} = 66.8 mm2
- The CFRP Modulus E_{frp} = 230000 MPa
- Moment of inertia of transformed section $I_t = 1.19 \times 10^9$ mm4
- Distance to fibers in tension y_b = 121.84 mm

From the stress-strain diagram F_{pu}=1961.8 *MPa*

F_{ps} before loss =0.7*1961.8=1373.26 *MPa*

F_{pe} after loss = 0.875*1373.26 = 1201.6 *MPa*

$P_i = F_{ps} * A_{ps}$=1373.26*594/1000= 815.716 kN

$P_e = F_{pe} * A_{ps}$=1201.6 *594/1000= 713.75 kN

$$M_{cr} = \frac{I}{yb}\left[\frac{p_e}{A} + \frac{P_e e}{S_b} + \frac{1}{2}\sqrt{f_c'}\right]$$

$$M_{cr} = \frac{1.19*10^9}{121.84}\left[\frac{713.75*10^3}{1.47*10^5} + \frac{713.75*10^3*87*121.84}{1.19*10^9} + \frac{1}{2}\sqrt{40}\right]$$

$$M_{cr} = 140.4\ kN.m$$

$$p_{cr} = \frac{140.4 * 2}{1.85} = 151.78\ kN$$

5.1.3.5 Ultimate Moment Capacity for Slab S8-D

From the stress-strain diagram F_{pu}=1961.8 *MPa*

F_{ps} before loss =0.7*1961.8=1373.26 *MPa*

F_{pe} after loss = 0.875*1373.26 = 1201.6 *MPa*

$P_i = F_{ps} * A_{ps}$=1373.26*594/1000= 815.716 kN

$P_e = F_{pe} * A_{ps}$=1201.6 *594/1000= 713.75 kN

From the stress-strain diagram of the prestressing strand:

$$\varepsilon_1 = 0.00616$$

$$r^2 = \frac{I}{A_c} = \frac{1.19 * 10^9}{1.47 * 10^5} = 8027.2\ mm^2$$

$$\varepsilon_2 = \frac{p_e}{A_c E_c}\left(1 + \frac{e^2}{r^2}\right) = \frac{713.75 * 10^3}{1.47 * 10^5 * 27000}\left(1 + \frac{87^2}{8027.2}\right) = 3.5 * 10^{-4}$$

$$\varepsilon_{frp-1} = \frac{p_e}{A_c E_c}\left(1 + \frac{eh}{2r^2}\right)$$

$$\varepsilon_{frp-1} = \frac{p_e}{A_c E_c}\left(1 + \frac{eh}{2r^2}\right)$$

$$\varepsilon_{frp-1} = \frac{713.75 * 10^3}{1.47 * 10^5 * 27000}\left(1 + \frac{87 * 250}{2 * 8027.2}\right) = 4.23 * 10^{-4}$$

Now from the strain diagram:

$$\frac{c}{0.003} = \frac{d - c}{\varepsilon_3}$$

$$\frac{c}{0.003} = \frac{212 - c}{\varepsilon_3}$$

$$c(0.003 + \varepsilon_3) = 0.636$$

$$c = \frac{0.636}{(0.003 + \varepsilon_3)}$$

$$a = \beta c$$

$$\beta = 0.85 \quad for \quad f_c' = 28\,Mpa$$

$$\beta = 0.80 \quad for \quad f_c' = 35\,Mpa$$

$$\Rightarrow \beta = 0.76 \quad for \quad f_c' = 40\,Mpa$$

$$C = 0.85 f_c' * b * \beta c = 0.85 * 40 * 1162 * 0.764 * \frac{0.636}{(0.003 + \varepsilon_3)} = \frac{19197.1}{(0.003 + \varepsilon_3)}$$

Now by trail and error: Assume ε_3= 0.0121

$$\Rightarrow \varepsilon_{ps} = \varepsilon_1 + \varepsilon_2 + \varepsilon_3$$

$$\Rightarrow \varepsilon_{ps} = 0.0062 + 3.48 * 10^{-4} + 0.0121 = 0.0186$$

$$\Rightarrow f_{ps} = 1753.8\,MPa$$

$$\Rightarrow c = \frac{0.636}{(0.003 + \varepsilon_3)} = \frac{0.636}{(0.003 + 0.0121)}$$
$$= 42.12 \text{ mm}$$

$$\varepsilon_{frp-2} = \varepsilon_{cu}\left(\frac{h - c}{c}\right) = 0.003 * \left(\frac{250 - 42.12}{42.12}\right) = 0.0148$$

$$\varepsilon_{frp-1} + \varepsilon_{frp-2} = 4.12 * 10^{-4} + 0.0148 = 0.0152 < 0.021$$

$$T_{ps} = A_{ps}\ f_{ps} = 594 * 1753.8 = 1041.75\ kN$$

$$T_{frp} = A_{frp}\ E_{frp}\left(\varepsilon_{frp-1} + \varepsilon_{frp-2}\right)$$

$$T_{frp} = 66.8 * 230000 * 0.0152 / 1000 = 233.21 \text{ kN}$$

$$T = T_{ps} + T_{frp} = 1041.75 + 233.21 = 1275\ kN$$

$$C = \frac{19197.1}{(0.003 + \varepsilon_3)} = \frac{19197.1}{(0.003 + 0.012059)} = 1275\ kN$$

Thus : $T \approx C$

Then: $a = 0.764c = 0.764 * \frac{0.636}{(0.003 + \varepsilon_3)} = 0.764 * \frac{0.636}{(0.003 + 0.01205)} = 32.26$ mm

Since $a = 32.26\ mm$ is greater than the thickness above the extruded holes, the calculations of the concrete area in compression became a little complicated. To simplify the calculation, an equivalent cross-section was used, in which the extruded holes were converted into a square cross-section with side length of 191 mm (the circle diameter).

$$M_n = 0.85 f_c' a b_1 \left(d_p - \frac{a}{2} \right) + 0.85 f_c' * 29.5 * b_2 \left(d_p - \frac{29.5}{2} \right) + A_{frp} f_{frp} (h - d_p)$$

$$= 0.85 * 40 * 32.26 * 245 * \left(212 - \frac{32.26}{2} \right) + 0.85 * 40 * 29.5 * 955 * \left(212 - \frac{29.5}{2} \right)$$

$$+ 66.8 * 3496 * (250 - 212) = 250.46\ kN.m$$

$$\Rightarrow\ p_n = \frac{2 * 250.46}{1.85} = 270.76\ kN$$

5.1.3.6 Ultimate Shear Force for Slab S17-H

- Concrete strength $f_c' = 40\ MPa$
- The concrete area $A_C = 1.47 * 10^5$ mm^2
- The prestressing steel area $A_{ps} = 594$ mm^2 (6 strands 12.7 mm diameter)
- The eccentricity e = 87 mm
- The effective depth d = 212mm
- The moment of inertia I= $1.19 * 10^9$ mm^4

To estimate the value of bw, the hollow core section was transferred to an equivalent section with square hole. The area of the square hole is equal to the area of the circular holes. From the equivalent section, bw 315.67 mm, the ACI equation for the web shear states that:

$$V_{cw} = \left(0.3\sqrt{f_c'} + 0.3 f_{pc}\right) b_w d + V_P$$

$$f_{pc} = \frac{p_e}{A_c} = \frac{713.75 * 10^3}{1.47 * 10^5} = 4.855\, MPa$$

$$V_p = 0$$

$$\Rightarrow V_{cw} = \left[\left(0.3\sqrt{40} + 0.3 * 4.855\right) * 315.67 * 212 + 0\right] / 1000 = 224.4\ kN$$

For the flexural shear, the ACI equation is given as:

$$V_{ci} = \frac{1}{20}\sqrt{f_c'}\ b_w\, d + \frac{V_i M_{cr}}{M_{\max}} + V_d \geq \frac{1}{7}\sqrt{f_c'}\ b_w\, d$$

$$V_{ci} = \left(\frac{1}{20}\sqrt{40} * 315.66 * 212 + \frac{139.4 * 10^6}{600} + 0\right) / 1000 = 253.5\ kN$$

$$\frac{1}{7}\sqrt{f_c'}\ b_w\, d = \frac{1}{7} * \sqrt{40} * 315.66 * 212 = 60.46\ kN$$

The slab was strengthened with MAPE wrap sheet of 400 mm width.

- The CFRP area A_{frp} = 66.8 mm2
- The CFRP Modulus E_{frp} = 230000 MPa
- Moment of inertia of transformed section $I_t = 1.19 \times 10^9$ mm4
- Distance to fibers in tension y_b = 121.84 mm

IF the slab is wrapped with 0.167 mm thickness CFRP at the maximum shear force region. The additional shear force was:

$$V_{frp} = 2 t_{frp}\, f_{frp}\, d_{frp}$$

The stress level in the CFRP shear reinforcement, f_{frp} , was limited to control shear crack widths . The ultimate stress level in the CFRP shear reinforcement is given by $f_{frp} = \varepsilon_{frpe} E_{frp}$.

where ε_{frpe} is the effective strain of CFRP sheet.

ε_{frpe} can be calculated as follows:

$$A_{frp} = 2 w_{frp} t_{frp}$$

$$= 2 * 600 * 0.167 = 200.4 \; mm^2$$

And the effective anchorage length as:

$$L_e = \frac{25350}{\left(t_{frp} E_{frp}\right)^{0.58}} = \frac{25350}{\left(0.167 * 23 * 10^4\right)^{0.58}} = 55.59 \; mm$$

$$k_1 = \left(\frac{f_c'}{27.65}\right)^{2/3} = \left(\frac{40}{27.65}\right)^{2/3} = 1.279$$

$$k_2 = \frac{d_{frp} - n_e l_e}{d_{frp}} = \frac{250 - 1 * 55.59}{250} = 0.778$$

Note: $n_e = 1$ since U-shaped stirrups are used.

The effective strain is then computed as:

$$\varepsilon_{frpe} = \frac{\alpha \phi_{frp} k_1 k_2}{9525}$$

$$\varepsilon_{frpe} = \frac{0.8 * 0.75 * 1.279 * 0.778 * 55.59}{9525} = 0.00348$$

$$R = \alpha \lambda_1 \left(\frac{f_c'^{2/3}}{\rho_{frp} E_{frp}}\right)^{\lambda_2}$$

$$\rho_{frp} = \left(\frac{2t_{frp}}{b_w}\right)\left(\frac{w_{frp}}{s_{frp}}\right) = \left(\frac{2 * 0.167 * 600}{1200 * 600}\right) = 2.78 * 10^{-4}$$

$$R = 0.8 * 1.35 * \left(\frac{40^{2/3}}{2.78 * 10^{-4} * 230 * 10^3}\right)^{0.3} = 0.649$$

$$\varepsilon_{frpe} = R\varepsilon_{frpu} = 0.649 * 0.021 = 0.0136$$

For design purposes, the effective strain will be the least of 0.004, 0.0136 and 0.00348; Thus, $\varepsilon_{frpe} = 0.00348$.

$$V_{frp} = 2t_{frp} f_{frp} d_{frp}$$

$$= 2 * 0.167 * 0.00314 * 230000 * 250/1000 = 60.3\ kN$$

$$V_n = 224.6 + 60.3 = 285\ k\,N$$

$$\Rightarrow\ p_n = 2 * 285 = 570\ k\,N$$

The analytical results of tested PPHC slabs are summarized in Table 5.1

Table 5.1: Analytical Results of Tested PPHC Slabs

Slab Name	M_{cr} kN.m	P_{cr} kN	Flexural Failure Load(kN)	Shear Force (kN)		Shear Failure Load(kN)
				V_{ci}	V_{cw}	
S1-A&S2-A	99.86	107.95	167.4	74.5	226.3	149.1
S3-B&S4-B	139.4	150.71	226.4	96.5	224.7	193.03
S5-C&S7-C	223.97	242.13	354.6	148	302.5	296.1
S9-E&S10-E&S11-E	73.58	245.25	361.2	143.2	191.9	286.4
S12-F&S13-F	139.4	464.7	698	253.5	224.7	449.25
S14-G& S15-G	223.97	746.6	1093	400.3	302.51	605
S8-D	139.7	150.71	226.4	96.5	224.7	193.03
S17-H	139.4	464.7	698	253.5	285	570

5.2 EXPERIMENTAL RESULTS

5.2.1 Introduction

A total of 17 hollow core slabs were tested during the test program. There are four differences between the tested slabs, summarized as follows:

1. Supported span: Two different spans were used in the experiments which are (4.7m and 2.0 m)

2. Thickness of slabs: Three different thicknesses were used during the experimental program which are (200 mm , 250mm,and 300mm)

3. Number of strands : The hollow core slabs used in the experiments had three configurations of prestressing strands (4 strands , 6 strands , and 8 strands).

4. Type of CFRP in flexure or shear: One type of CFRP was used in strengthening the slabs, MAPE wrap, of different cross-section area. Some of the slabs were tested without CFRP. Therefore, the possible variable for this field is W/OC for slabs without CFRP, W/CF for slab strengthened with CFRP in flexure, and W/CS for slab strengthened with CFRP in shear.

Test arrangements for each specimen, analytical cracking and failure load are listed in Table 5.2.

Table 5.2: Test Setup and Analytical Failure Loads for the Tested Slabs

Name	Test Setup	Analytical Cracking Load (kN	Analytical Cracking Load (kN)
S1-A S2-A	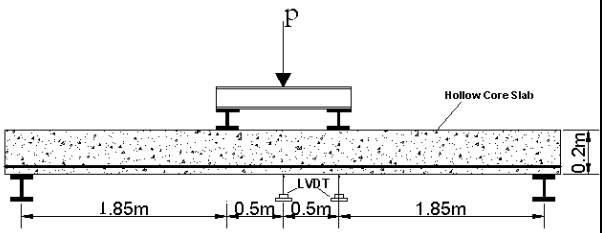	108	167

S3-B S4-B	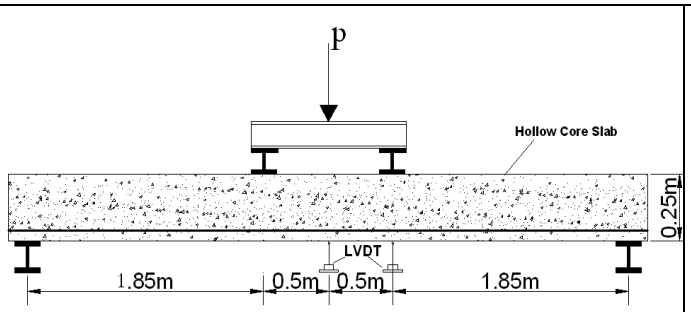	150.7	226.4
S5-C S6-C S7-C	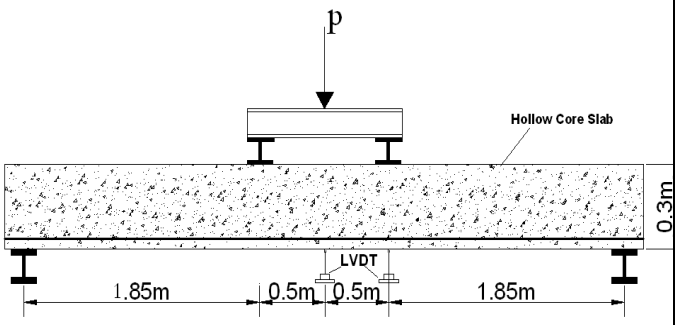	242	354.6
S8-D	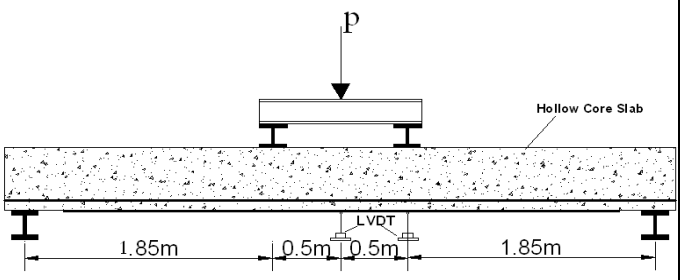	150.7	270
S9-E S10-E S11-E	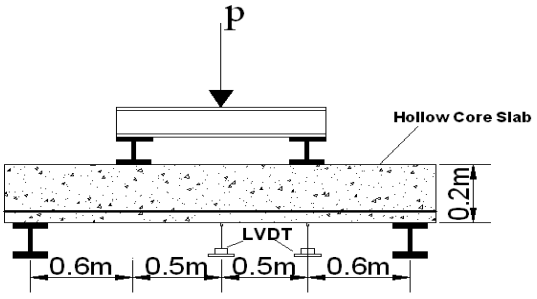	245	286.4

S12-F S13-F	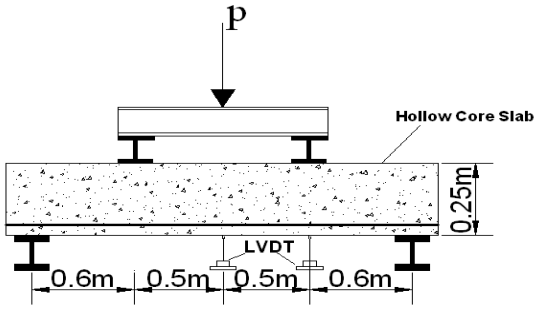	464.7	449.25
S14-G S15-G S16-G	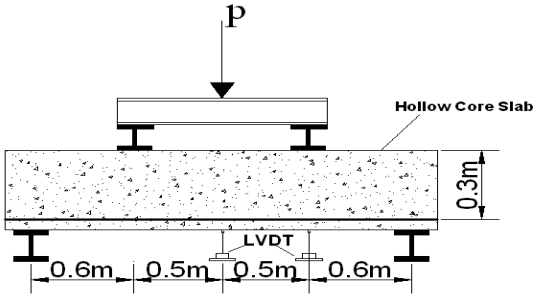	746.6	605
S17-H	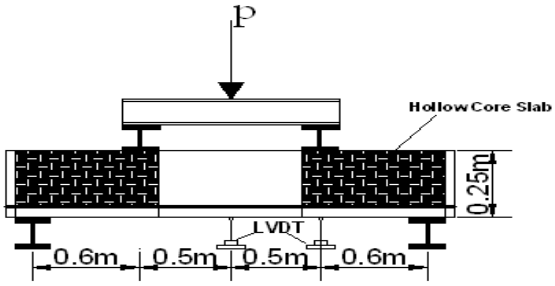	464.7	570

5.2.2 Test Results of PPHC Slabs with length of 5m

5.2.2.1 Test Results for Slab S1-A

The specimen has the overall length of 5000 mm and thickness of 200mm. During the test, the first crack appeared at a loading of 99 kN. The maximum load measured was 160 kN when the test was stopped. The slab had six cracks in the constant moment zone at a varying distance from one another, and five cracks outside the constant moment zone as shown in Figure 5.3. The maximum deflection at mid-span

recorded in the LVDT was 65 mm. The failure of this slab was ductile and caused by the yielding of prestressing strands. The slab failed in pure flexural mode.

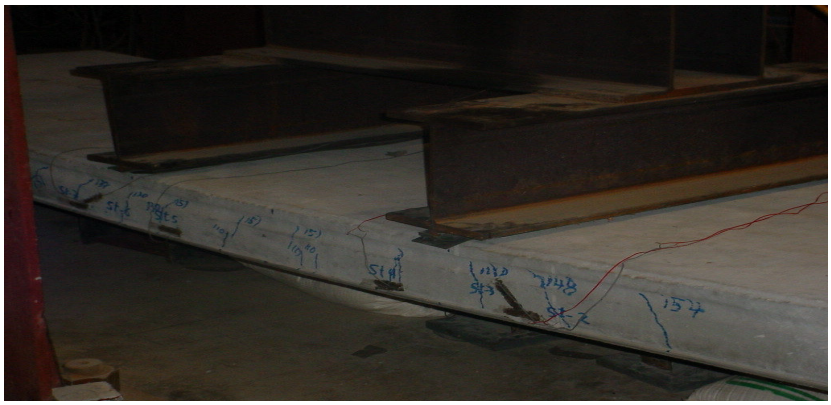

Figure 5.3: Cracking During the Testing of Slab S1-A

Eight strain gauges were attached to the slab to measure the strains on the concrete as shown in Figure 5.4.

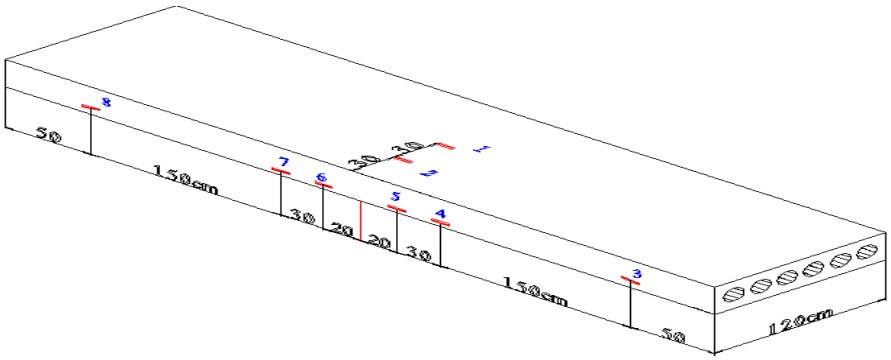

Figure 5.4: Location of Strain Gauges on Slab S1-A

The load-versus-deflection curves are shown in the figure 5.5. The load-strain curves for the gauges are shown in Figure 5.6.

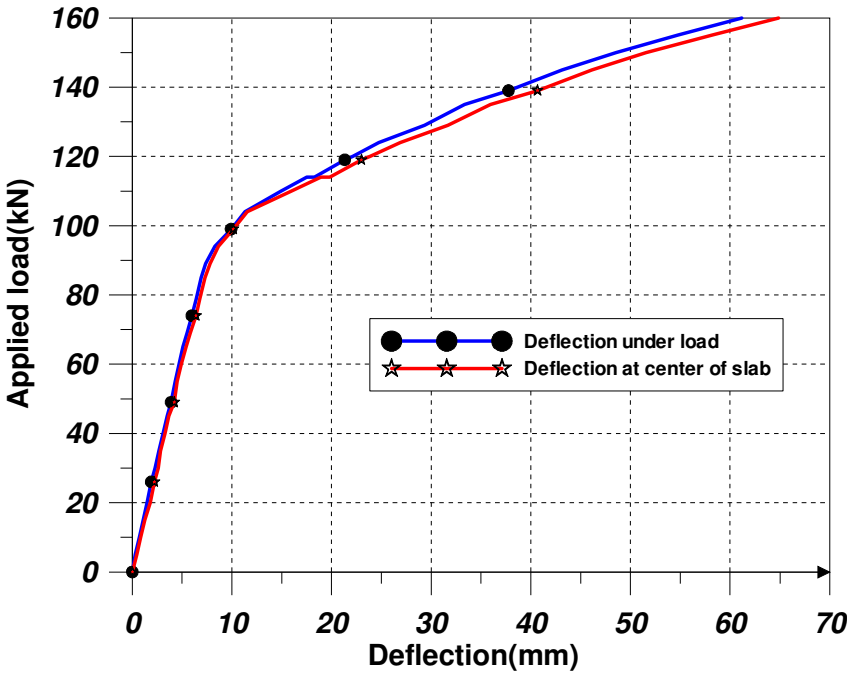

Figure 5.5: Load-Deflection Curves for Slab S1-A

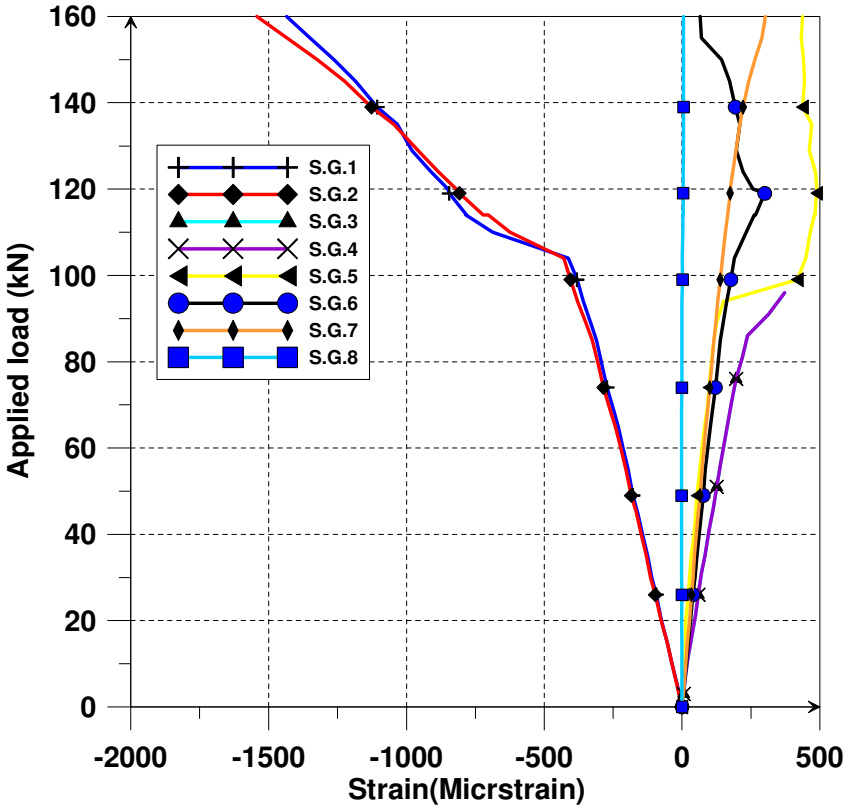

Figure 5.6: : Load-Strain Curves for Slab S1-A

The maximum strains, were recorded by the strain gauges, are listed in the Table 5.3.

Table 5.3: Maximum Strains in the Slab S1-A

Strain Gauge No.	S.G.-1	S.G.-2	S.G.-3	S.G.-4	S.G.-5	S.G.-6	S.G.-7	S.G.-8
Strain(micro strain)	1543	1435	21	189	437	66	302	6

5.2.2.2 Test Results for Slab S2-A

The overall length and the thickness of slab were 5000mm and 200mm respectively. During the test, the first crack appeared at a loading of 101 kN. The maximum load measured was 158 kN when the test was stopped. Six cracks were formed in the constant moment zone at a varying distance from one another, and five cracks outside the constant moment zone as shown in Figure 5.7. The maximum deflection at mid-span recorded in the LVDT was 95.95 mm. The slab failed in pure flexural mode.

Figure 5.7: Cracking During the Testing of S2-A

The locations of strain gauges used to measure the strains on concrete are shown in Figure 5.8.

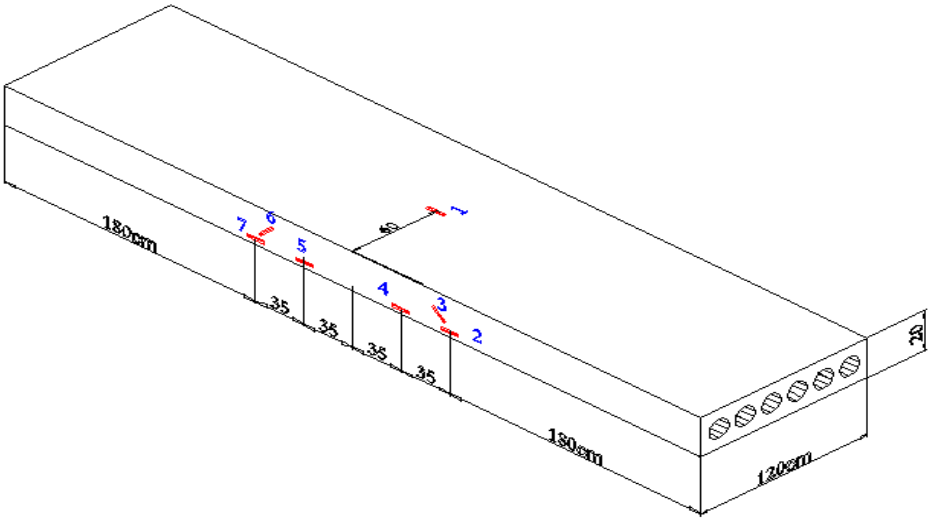

Figure 5.8: Location of Strain Gauges on the Slab S2-A

The load-versus-deflection curves are shown in the figure 5.9. The load-strain curves for the gauges are shown in Figure 5.10.

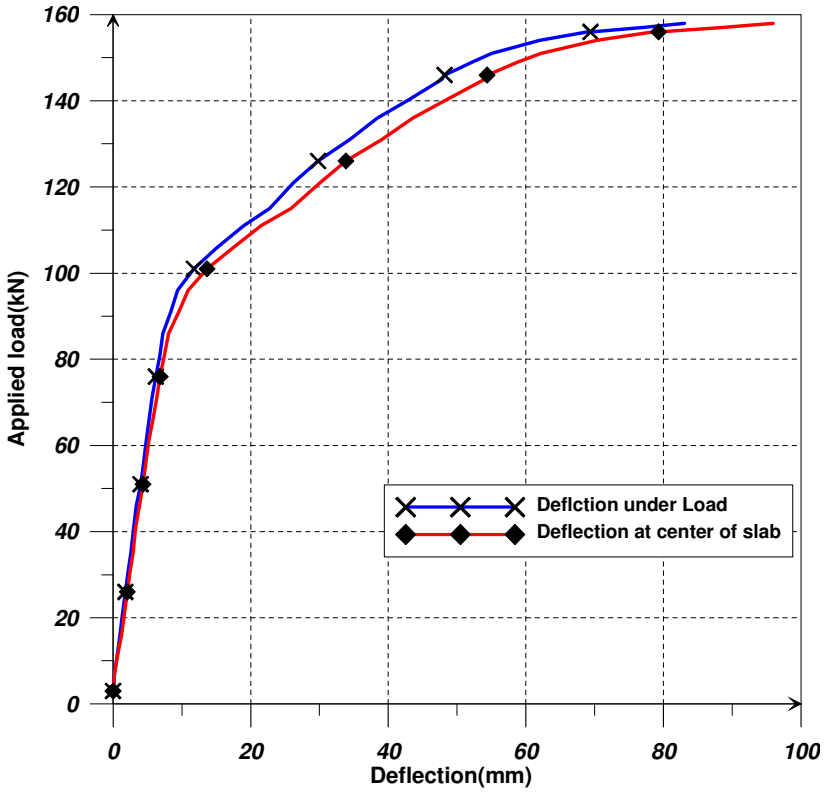

Figure 5.9: Load-Deflection Curve for Slab S2-A

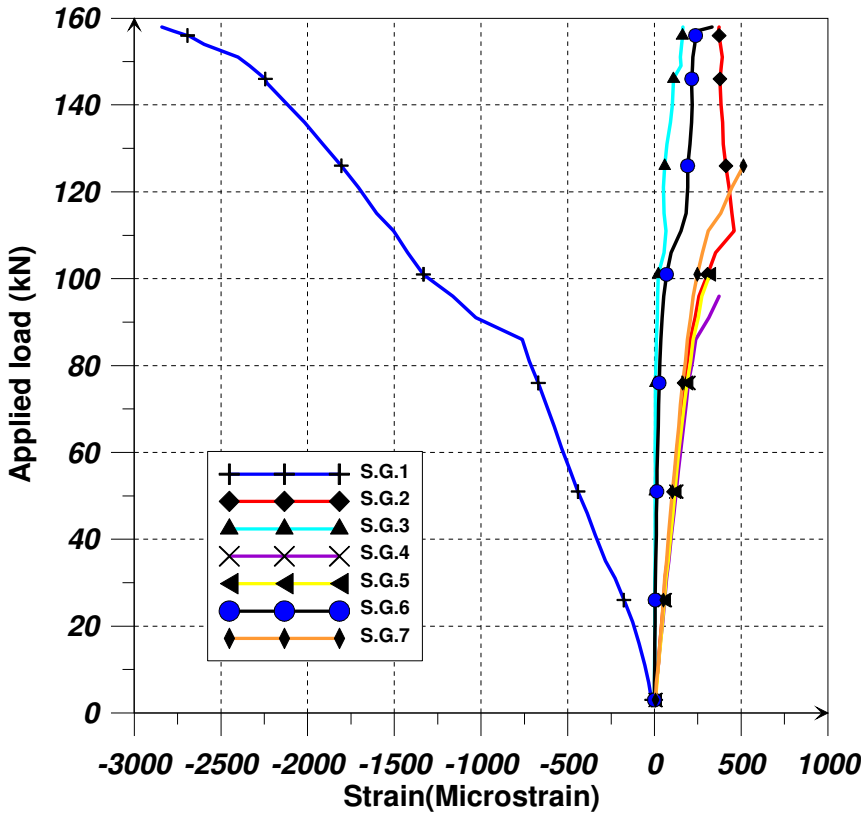

Figure 5.10: Load-Strain Curves for Slab S2-A

The maximum strains obtained from strain gauges are tabulated in Table 5.4.

Table 5.4: Maximum Strains in Slab S2-A

Strain Gauge No.	S.G.-1	S.G.-2	S.G.-3	S.G.-4	S.G.-5	S.G.-6	S.G.-7
Strain(micro strain)	2839	372	169	372	319	331	513

5.2.2.3 Test results for specimen S3-B

The specimen has the overall length of 5000 mm and thickness of 250mm. During the test, the first crack appeared at a loading of 148 kN. The maximum load measured was 226.8 kN when the test was stopped. Five flexural cracks occurred in the constant moment zone between two lines of load at a varying distance from one another, and four flexural shear cracks outside the constant moment zone as shown in Figure 5.11. The slab failed due to the flexural shear cracks. The maximum deflection at mid-span recorded in the LVDT was 50.8 mm. The maximum slip at strands recorded in the

LVDT was 2.21mm. Three strain gauges were used to measure the strains on concrete as shown in Figure 5.12. The maximum strains recorded by the strain gauges are listed in Table 5.5.

Figure 5.11: Cracking During the Testing of Slab S3-B

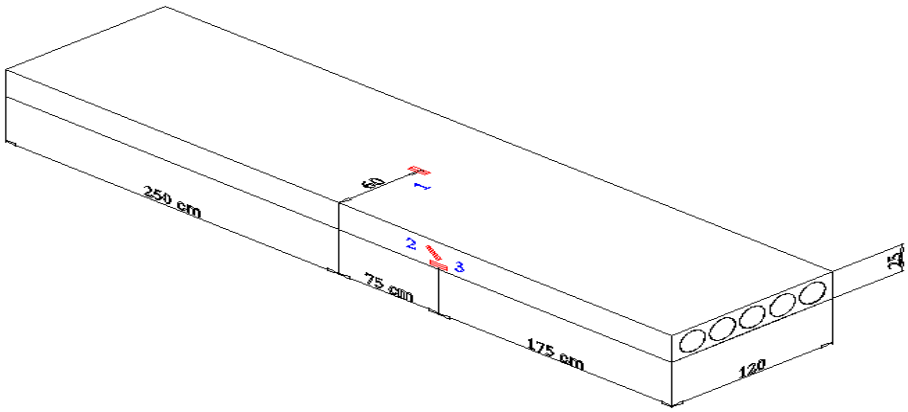

Figure 5.12: Location of Strain Gauges on the Slab S3-B

The load-versus-deflection curves of the slab S3-B are shown in the figure 5.13. The load-strain curves for the strain gauges are shown in Figure 5.14.

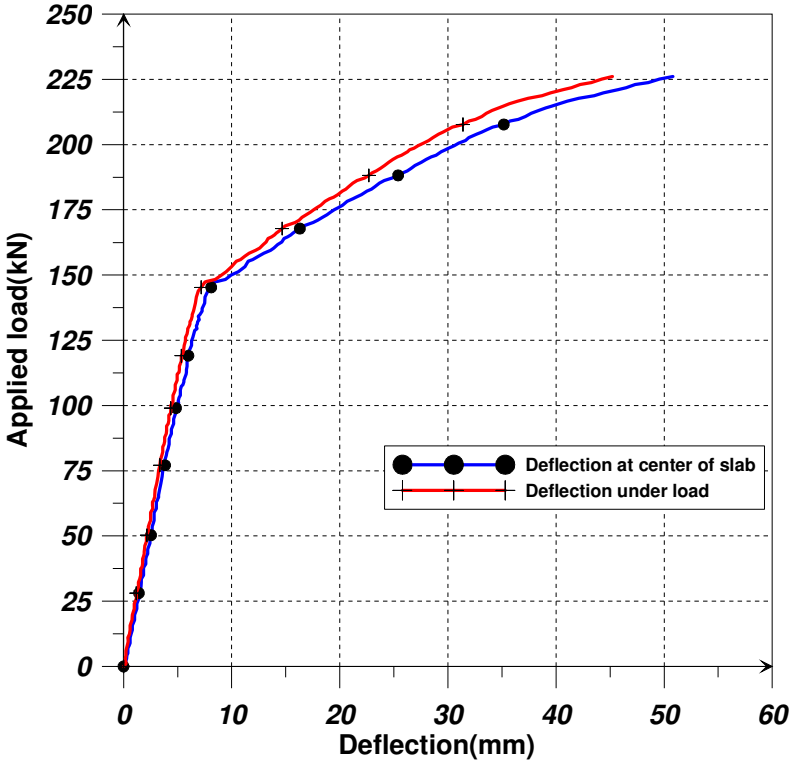

Figure 5.13: Load-Deflection Curves for Slab S3-B

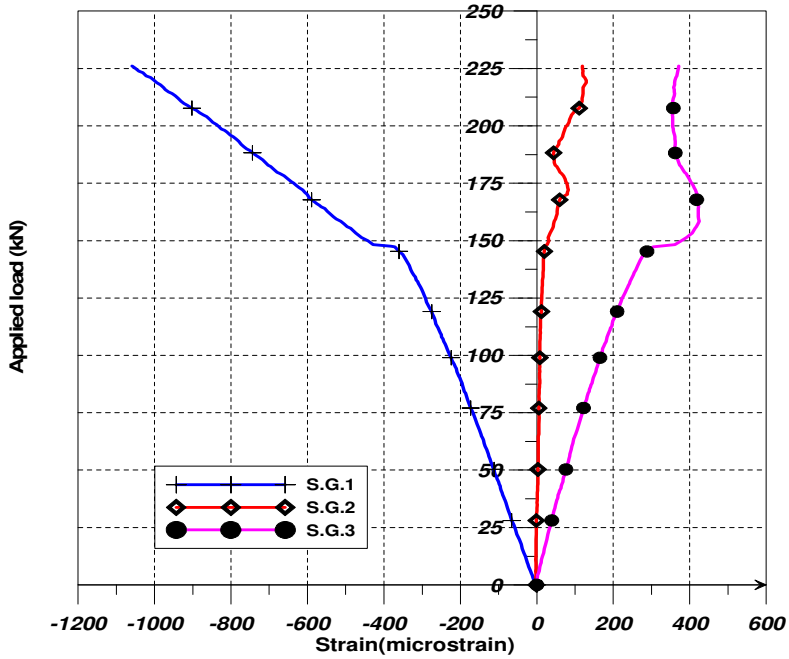

Figure 5.14: Load-Strain Curves for Slab S3-B

Table 5.5: Maximum Strains in the Slab S3-B

Strain Gauge No.	S.G.-1	S.G.-2	S.G.-3
Strain(micro strain)	1050	119	371

5.2.2.4 Test results for specimen S4-B

The specimen has the overall length of 5000 mm and thickness of 250mm. During the test, the first crack appeared at a loading of 148 kN. The maximum load measured was 233.9 kN when the test was stopped. Crack formation was initiated in the flexural span between the two concentrated loads where the flexural stress is highest and shear stress is zero. The cracks were vertical and perpendicular to the direction of the maximum principal tensile stress induced by pure bending. As load increased, additional flexural cracks opened within the shear span. However, because of the dominance of the shear stresses, the cracks became progressively more inclined and propagated towards the load points, leading finally to diagonal tension failure. The slab had six flexural cracks in the constant moment zone at a varying distance from one another, and three flexural shear cracks outside the constant moment zone as shown in Figure 5.15. The maximum deflection at mid-span recorded in the LVDT was 60.45 mm. The maximum slip at strands recorded in the LVDT was 6.96 mm.

Figure 5.15: Cracking During the Testing of Slab S4-B

Figure 5.16 shows the locations of strain gauges used to measure the strains on concrete.

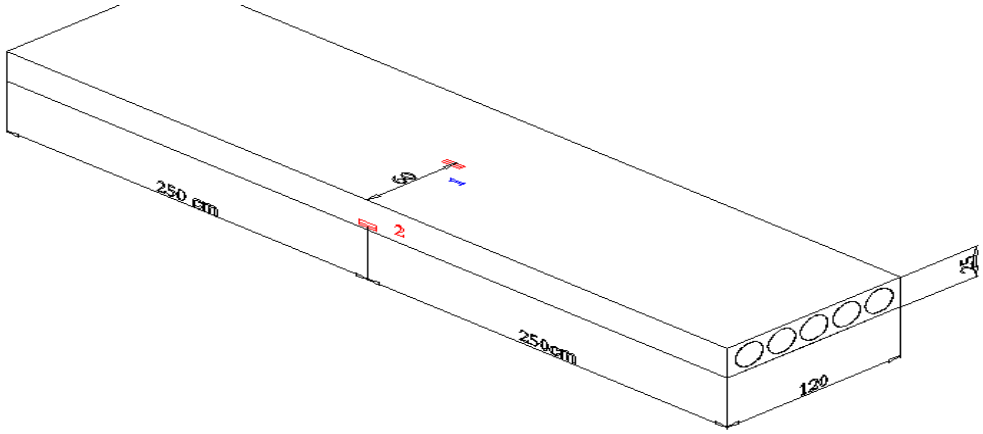

Figure 5.16: Location of Strain Gauges on Slab S4-B

The load-versus-deflection curves of the slab S4-B is shown in the figure 5.17. The Load-strain curves for the strain gauges are shown in Figure 5.18.

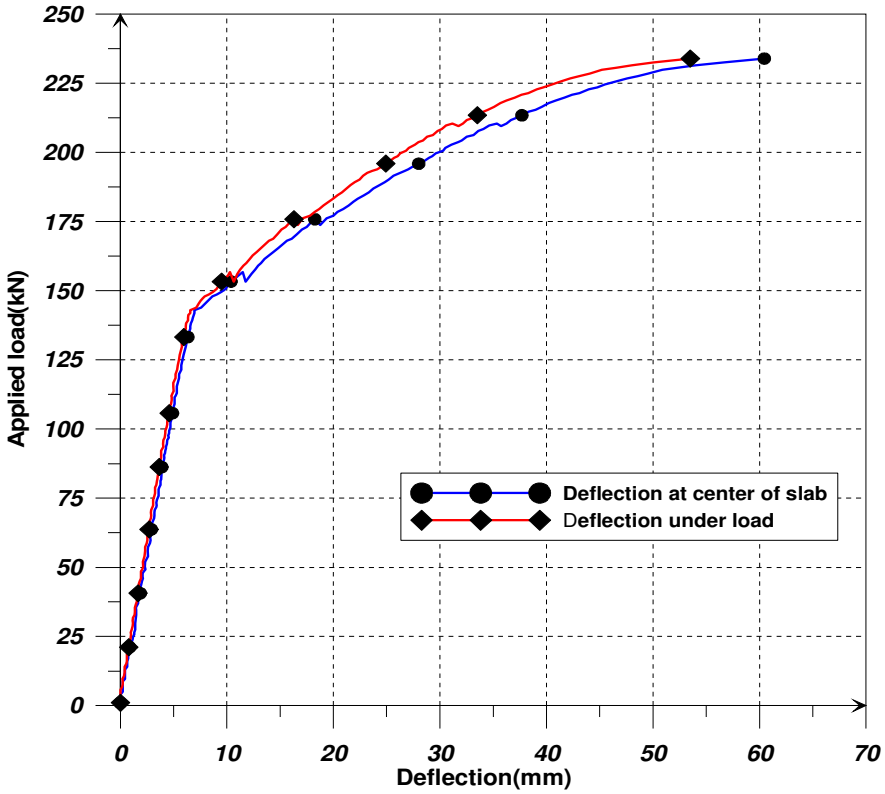

Figure 5.17: Load-Deflection Curves for Slab S4-B

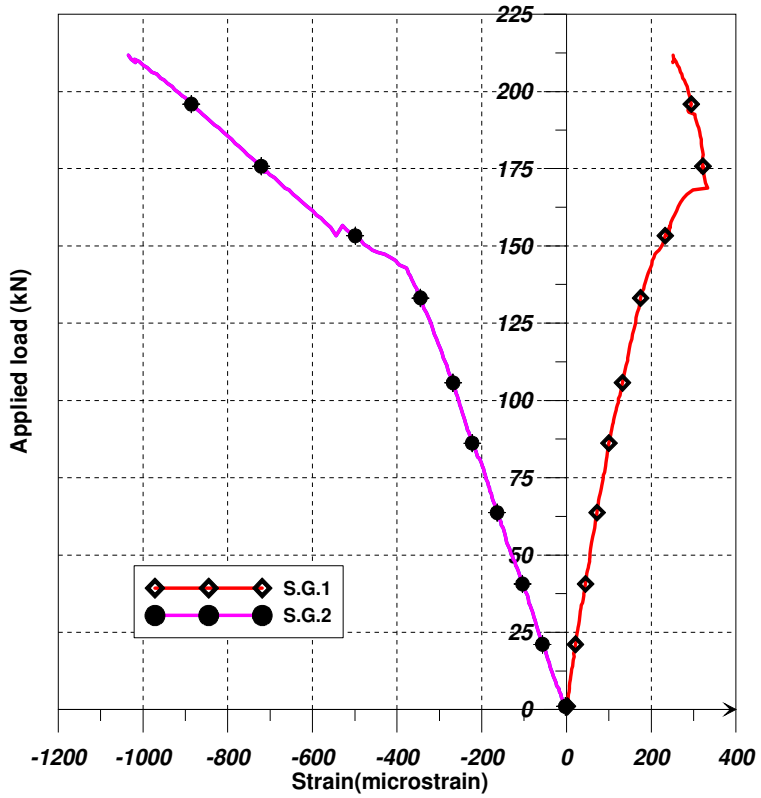

Figure 5.18: Load-Strain Curves for Slab S4-B

Table 5.6: The Maximum Strains in the slab S4-B

Strain Gauge No.	S.G.-1	S.G.-2
Strain(micro strain)	1555	255

5.2.2.5 Test results for specimen S5-C

The specimen has the overall length of 5000 mm and thickness of 300mm. During the test, the first crack appeared at a loading of 242.13 kN. The maximum load measured was 381 kN when the test was stopped. Flexural cracks were initiated in the region of constant moment between the two concentrated loads. As load increased, additional flexural cracks appeared within the shear span. The cracks within the shear span became progressively more inclined and propagated towards the load points leading finally to diagonal tension failure. In other words, the slab failed in flexural shear mode. Five cracks were marked in the constant moment zone at a varying

distance from one another, and four cracks outside the constant moment zone as shown in Figure 5.19. The maximum deflection at mid-span recorded in the LVDT was 75.68 mm. The maximum slip at strands recorded in the LVDT was 6.81mm. Strains at the concrete surface were measured using three strain gauges as shown in Figure 5.20. The maximum strains recorded in the strain gauges are listed in Table5.7.

Figure 5.19: Cracking During the Testing of Slab S5-C

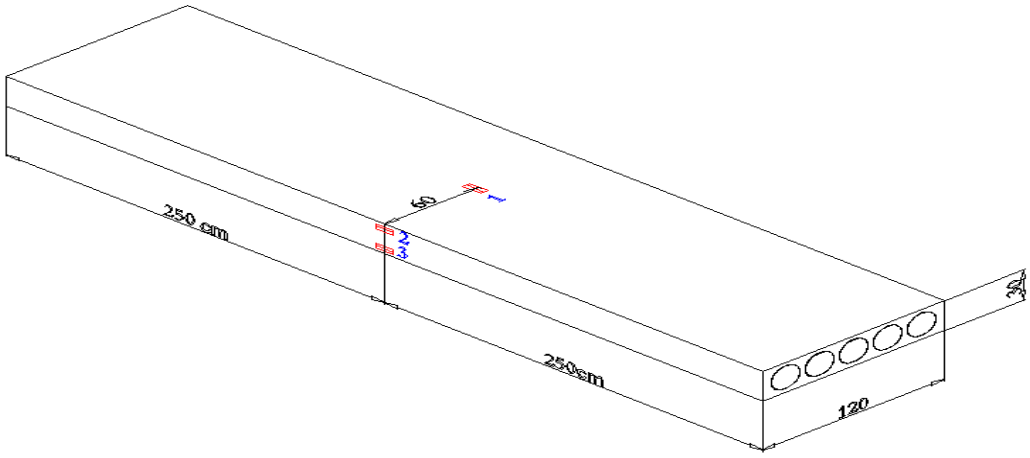

Figure 5.20: Location of Strain Gauges on Slab S5-C

The load-versus-deflection curves for the slab S5-C as shown in Figure 5.21. The load-strain curves for the gauges are shown in Figure 5.22.

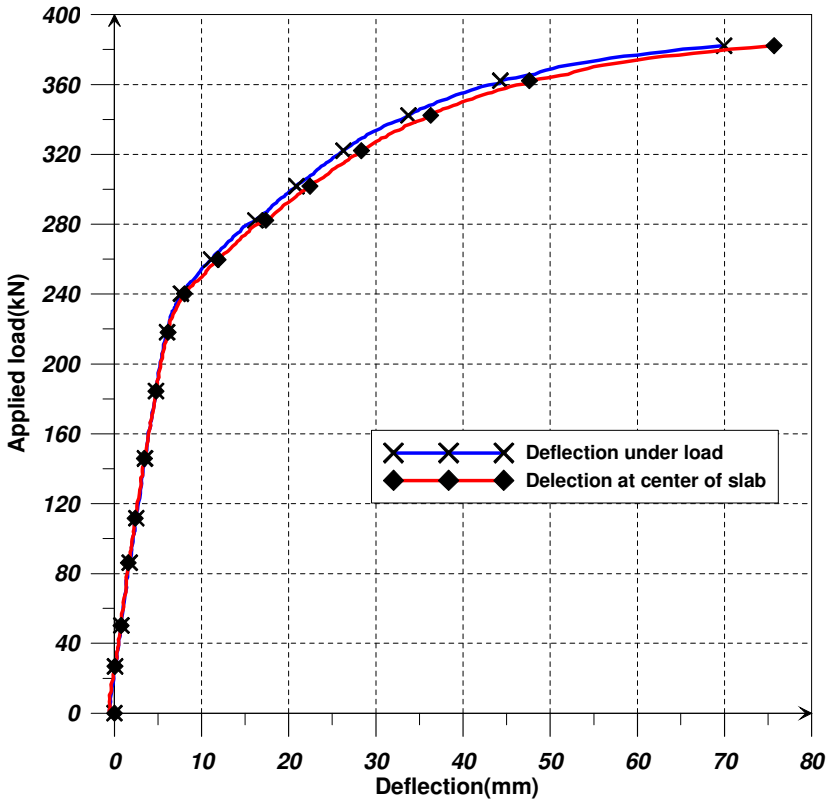

Figure 5.21: Load-Deflection Curves for Slab S5-C

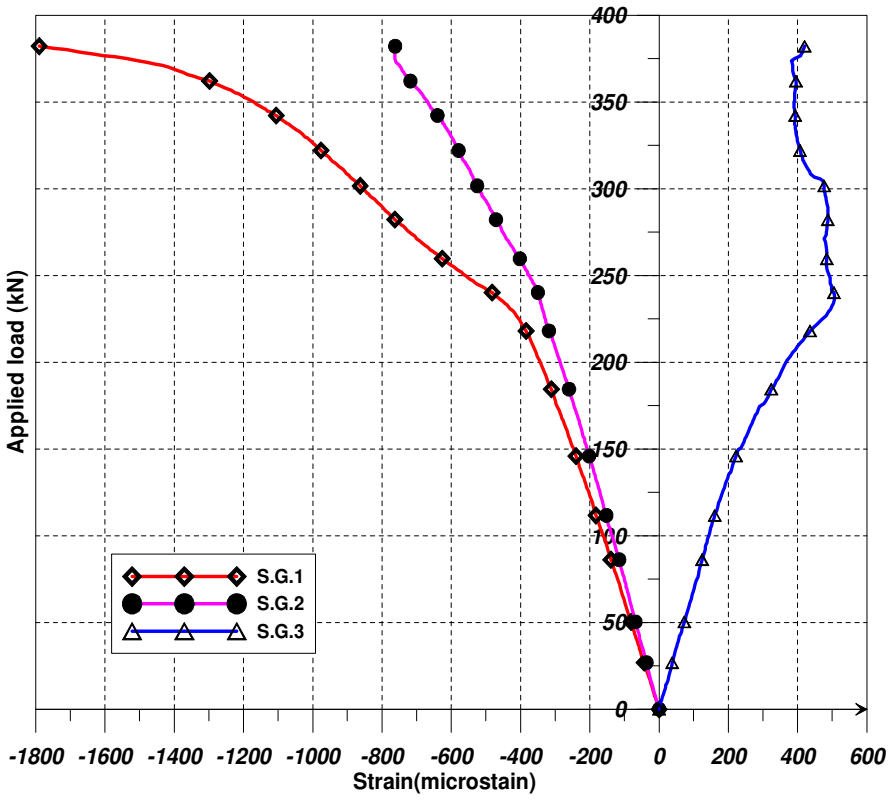

Figure 5.22: Load-Strain Curves for Slab S5-C

Table 5.7: Maximum Strains in The slab S5-C

Strain Gauge No.	S.G.-1	S.G.-2	S.G.-3
Strain(micro strain)	1790	762	420

5.2.2.6 Test results for specimen S6-C

The failure of this specimen was believed to be a bond failure, as the failure loads involved were far below the computed analytical flexural and shear failure loads. The initiation of shear cracks impairs the embedment of prestressing strands, and causes slippage of strands. This results in premature failure of precast prestressed hollow core slab. The first crack appeared at a loading of 152 kN. The maximum load measured was 202 kN when the test was stopped. When the bond failure occurred, a big crack formed and extended from line of load to the support as shown in Figure5.23. The maximum deflection at mid-span recorded in the LVDT was 34 mm. The maximum slip at strands recorded in the LVDT was 17.54 mm.

Figure 5.23: Cracking During the Testing of Slab S6-C

Three strain gauges were bonded on the concrete surface as shown in Figure 5.24.

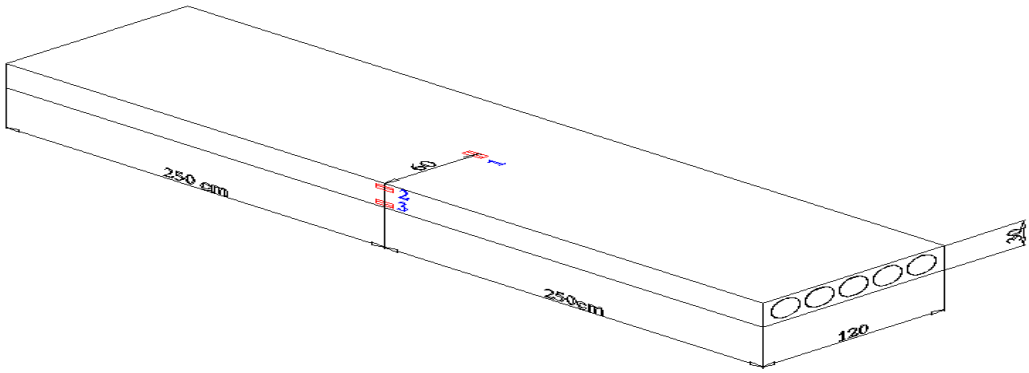

Figure 5.24: Location of Strain Gauges on Slab S6-C

The load-versus-deflection curves of the S6-C slab are shown in the Figure 5.25. The measured strains in the concrete versus the applied load for the S6-C slab are shown in Figure 5.26.

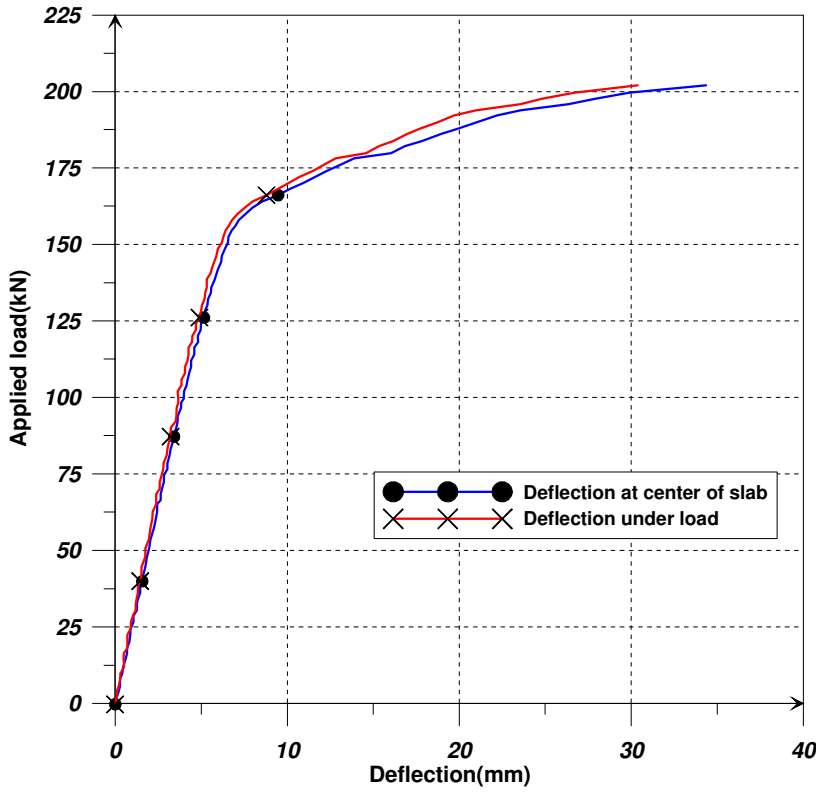

Figure 5.25: Load-Deflection curves for Slab S6-C

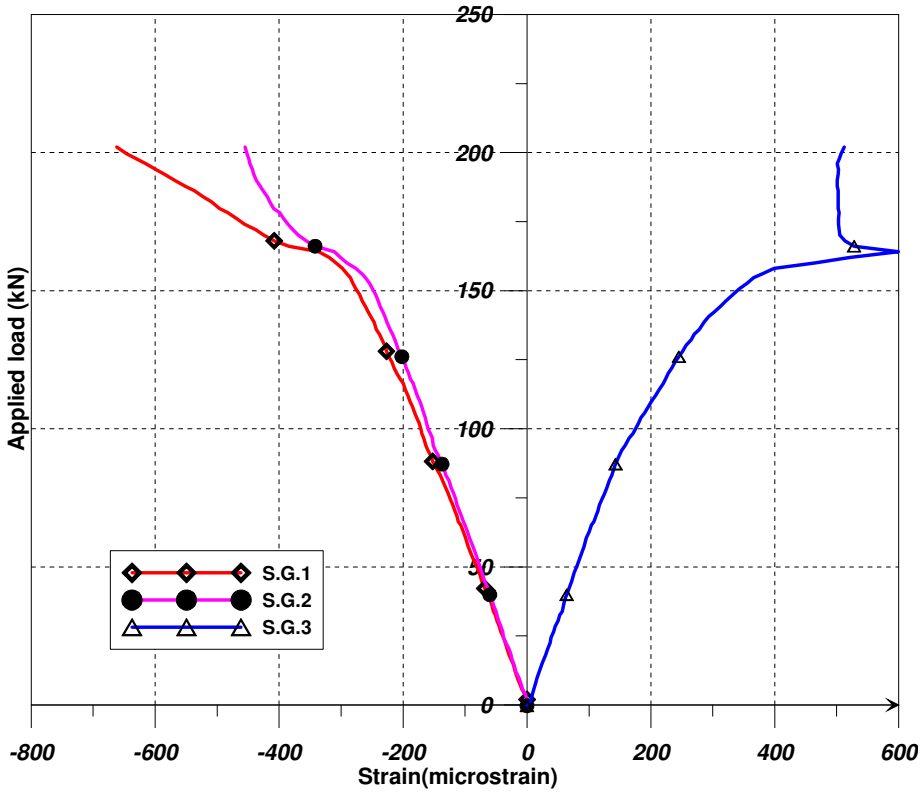

Figure 5.26: Load-Strain Curves for Slab S6-C

5.2.2.7 Test results for specimen S7-C

The specimen has the overall length of 5000 mm and thickness of 300mm. During the test, the first crack appeared at a loading of 250 kN. The maximum load measured was 383 kN when the test was stopped. At early stage of loading, flexural cracks were observed in the region of constant moment at different load levels. With a further increase in load, additional flexural cracks were formed in the shear spans between the applied load and the support. Because of the presence of shear stresses, these flexural-shear cracks became more inclined as shown in Figure 5.27. The slab S7-C failed in diagonal tension shortly after the formation of the critical diagonal crack. The maximum deflection at mid-span recorded in the LVDT was 75.75 mm. The maximum slip at strands recorded in the LVDT was 4 mm. Three electrical strain gauges were bonded on the surface of the slab to measure the concrete strains as shown in Figure 5.28. Table 5.8 gives the measured strains concrete at failure.

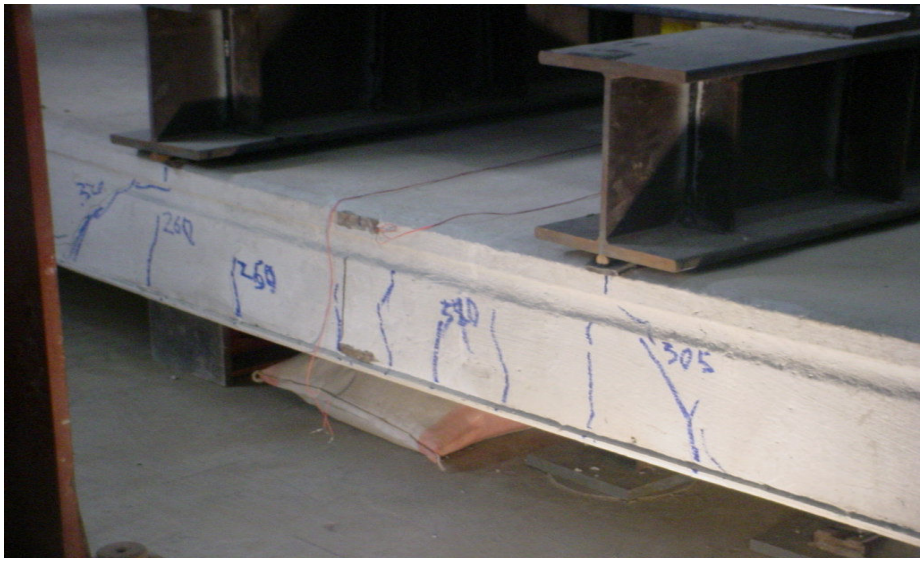

Figure 5.27: Cracking During the Testing of Slab S7-C

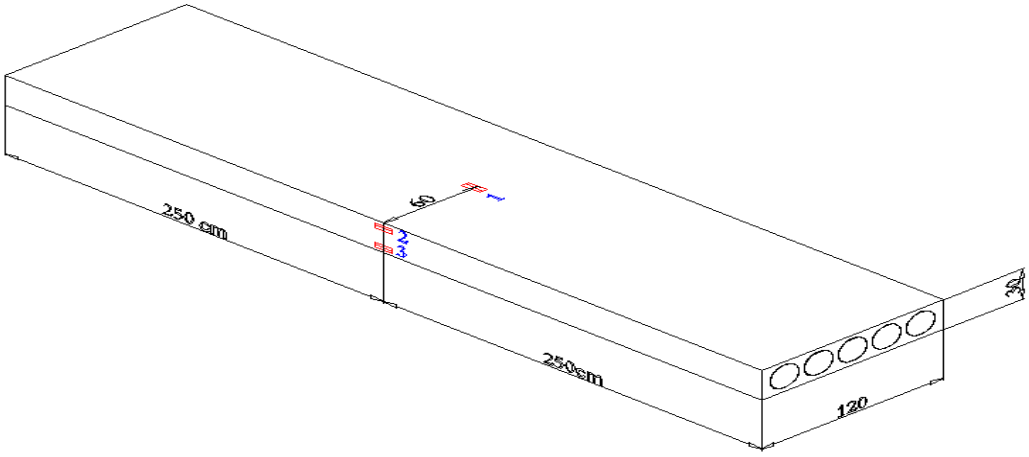

Figure 5.28: Location of Strain Gauges on Slab S7-C

The load-versus-deflection curves of the slab are shown in the figure 5.29. Figure 5 .30 shows the measured strains in the concrete versus the applied load for the slab S7-C.

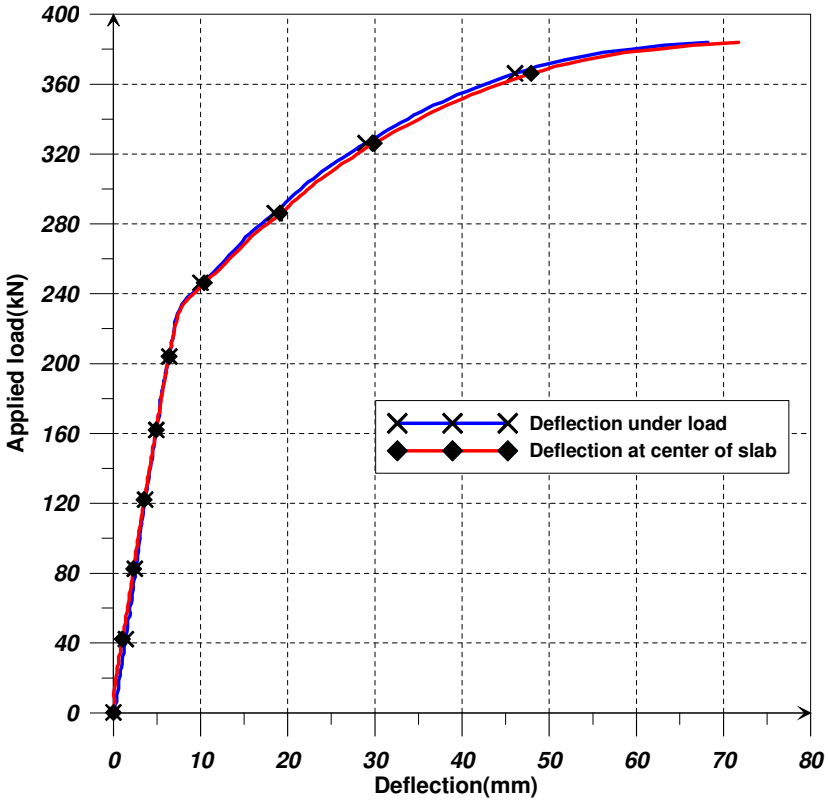

Figure 5.29: Load-Deflection Curves for the Slab S7-C

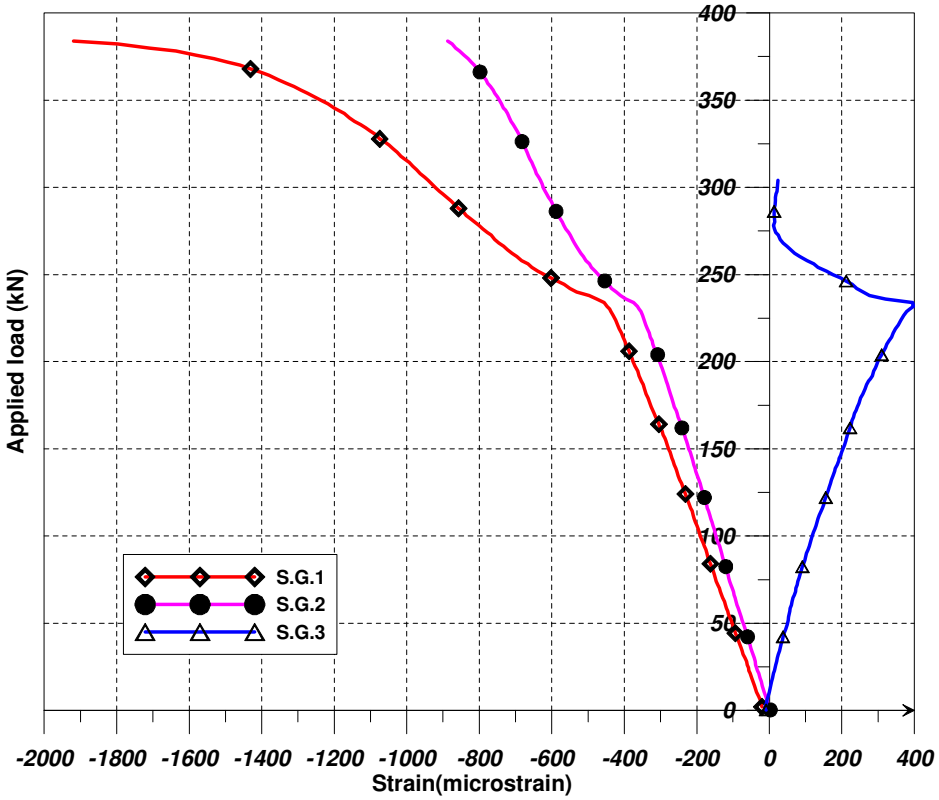

Figure 5.30: Load-Strain Curves for the Slab S7-C

Table 5.8: Maximum Strains in the Slab S7-C

Strain Gauge No.	S.G.-1	S.G.-2	S.G.-3
Strain(micro strain)	2119	881	397

5.2.2.8 Test results for specimen S8-D

This slab was strengthened by using one sheet of MAPE CFRP, 400 mm width, 0.167 mm thickness (67 mm^2), and 4.7 meter length as shown in Figure 5.31. During the application of loading, the first crack occurred at a load of 152 kN. The presence of CFRP did not affect the cracking load as expected. The maximum load was 219 kN before failure of slab. The corresponding deflection was 53 mm. The cracks were initiated in the constant moment region between the two concentrated loads before spreading along the span with increase of load. The cracks within the shear span became progressively more inclined and propagated towards the load points, leading finally to diagonal tension failure. A secondary concrete splitting failure occurred within the shear span at the level of the prestressed steel. This longitudinal splitting along the main prestressed steel occurred immediately after formation of the critical diagonal shear crack. Six flexural cracks occurred in the constant-moment zone at a distance of about 100 mm from each other, and two flexural shear cracks occurred outside the constant moment zone as shown in Figure 5.32. Because the slab was strengthened with CFRP in the flexural zone and not strengthened in flexural shear zone, no strength was gained in this slab when compared to the same slab without CFRP.

Figure 5.31: Strengthening the Slab S8-D with One Layer of CFRP

Figure 5.32: Cracking During the Testing of Slab S8-D

Five strain gauges were used to measure the strains in concrete and CFRP sheet as Shown in Figure 5.33.

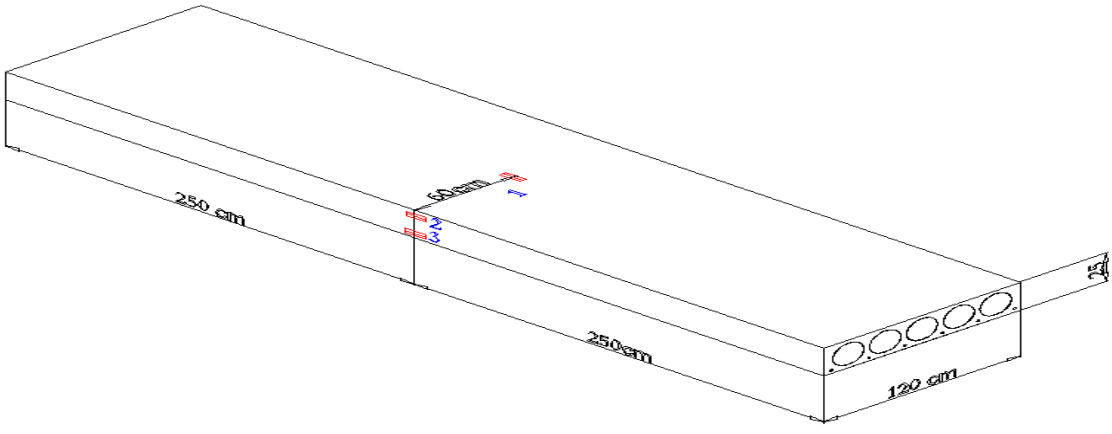

(a)

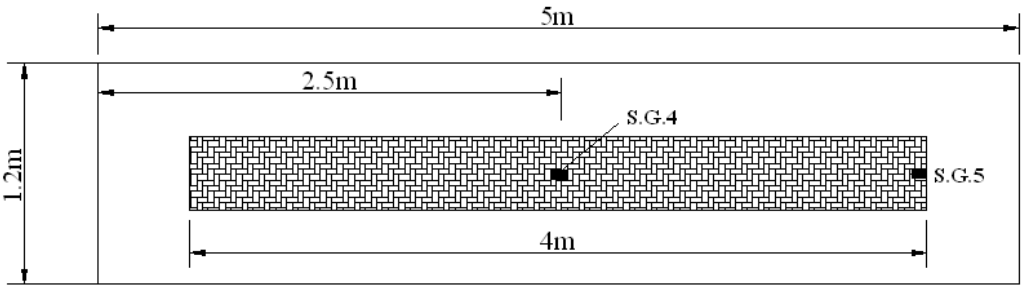

(b)

Figure 5.33: Locations of Strain Gauges: a) on concrete b) on CFRP

The load-versus-deflection curves are shown in the figure 5.34. The load-strain curves for the gauges are shown in Figure 5.35.

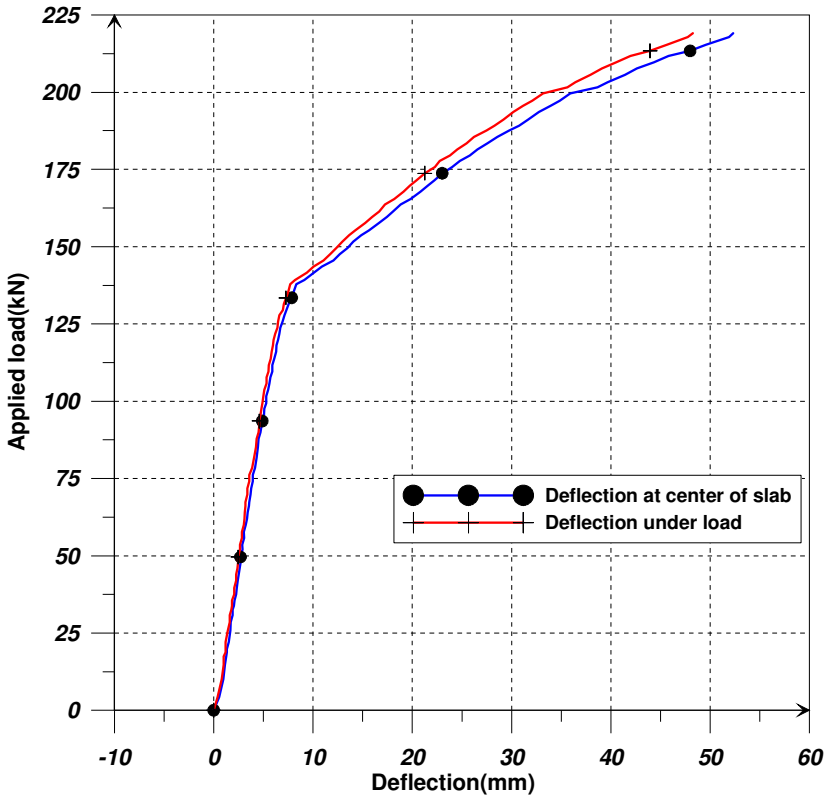

Figure 5.34: Load-Deflection curves for the Slab S8-D

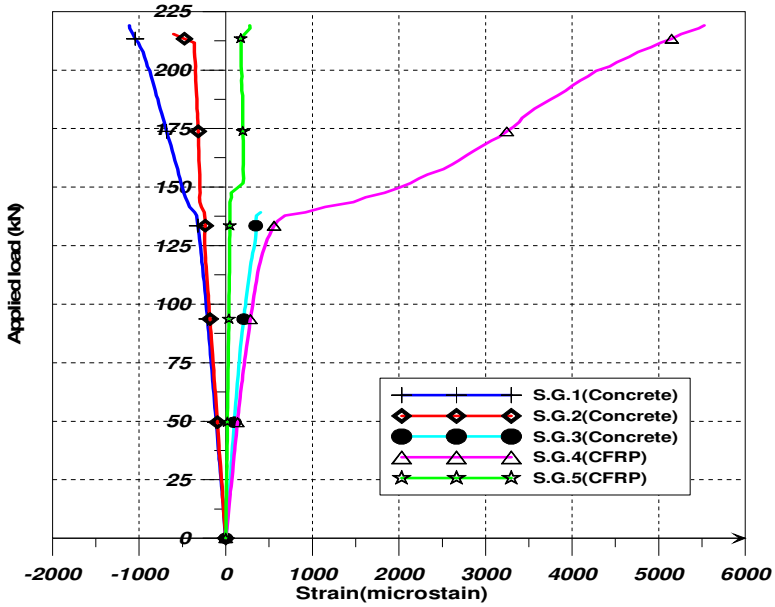

Figure 5.35: Load-Strain Curves for the Slab S8-D

5.2.2.9 Summary of the Experimental Results of PPHC Slabs with Length of 5m

The cracking load, ultimate load, deflection at maximum load and failure mode of the aforementioned slabs are summarized in Table 5.9.

Table 5.9: Summary of the Experimental Results for PPHC slabs with Length of 5m

Slab Code	Cracking Load(kN)	Failure Load(kN)	Deflection at Failure (mm)	Mode of Failure
S1-A	99	160	90	Flexure
S2-A	101	158	96	Flexure
S3-B	148	226.8	50.8	Flexural-shear
S4-B	148	233.9	60.45	Flexural-shear
S5-C	242.1	381	75.68	Flexural-shear
S6-C	152	202	34	Bond-slip
S7-C	250	383	75.75	Flexural-shear
S8-D	152	219	53	Flexural-shear

The applied load versus mid-span deflection relationships of the PPHC slabs 5M in span are presented in Figure 5.36.

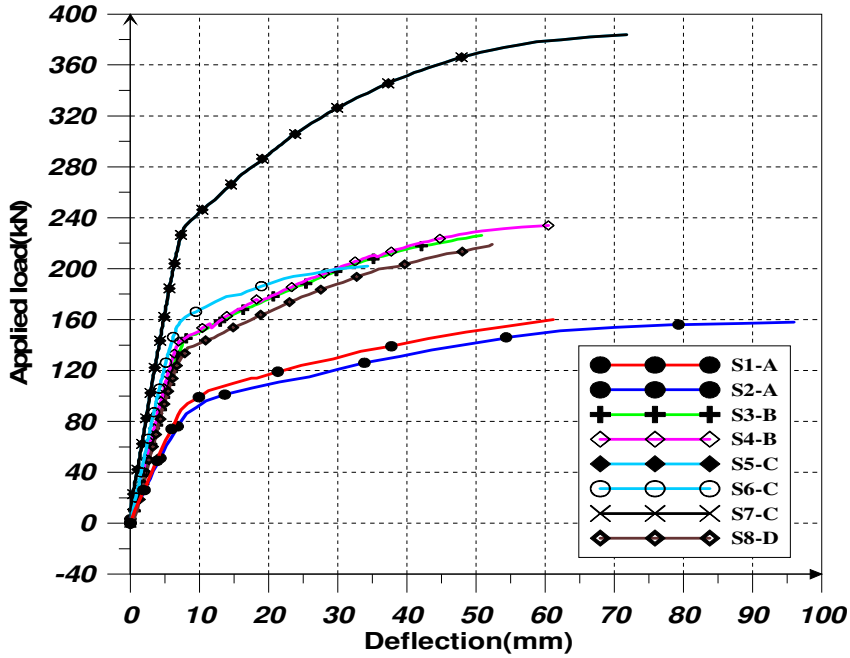

Figure 5.36: Load-Mid Span Deflection Curves for the PPHC Slabs with Length of 5m

The concrete compressive strains at mid-span for the PPHC slabs with 5m in span are shown in Figure 5.37.

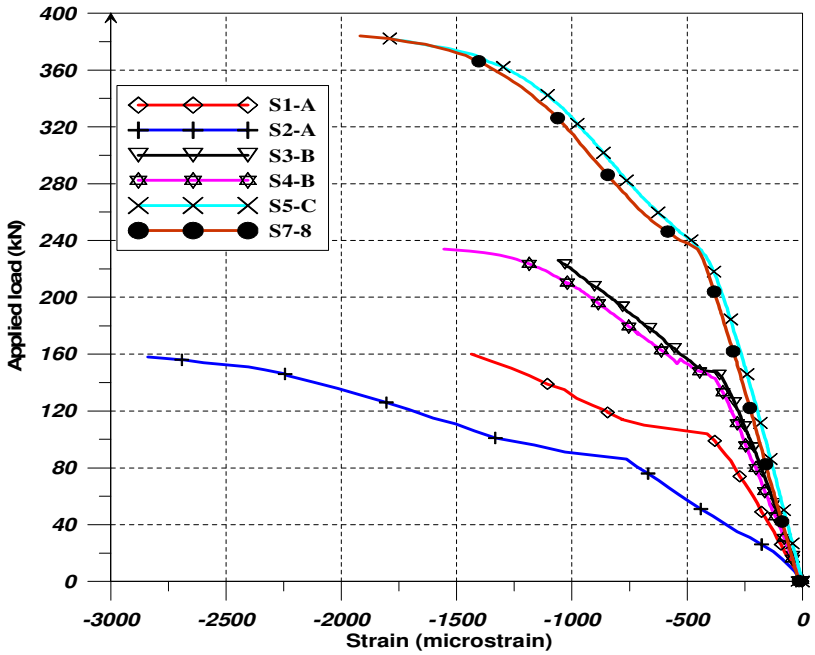

Figure 5.37: Load-Compressive Strains for the PPHC Slabs with Length of 5m

5.2.3 Test Results of PPHC Slabs with Length of 2.5m

5.2.3.1 Test Results for Slab S9-E

The specimen has the overall length of 2500 mm and thickness of 200mm. The shear span length is 600mm. During the test, the first flexural crack appeared at constant moment zone was at loading of 264 kN. With a further increase in load, additional flexural cracks were formed in the shear spans between the applied load and the support. The crack began to turn over and incline towards the loading point. Failure finally occurred when the concrete separated and the two planes of concrete slid past one another as shown in Figure 5.38. The failure load measured was 287 kN. It can be noticed that the difference between the cracking load and the failure load is small. The maximum deflection at mid-span recorded in the LVDT was 8.27 mm. The maximum slip at strands recorded in the LVDT was 5.85mm.To measure the strains on concrete, two strain gauges were bonded on the surface of concrete as shown in Figure 5.39.

Figure 5.38: Cracking During the Testing of Slab S9-E

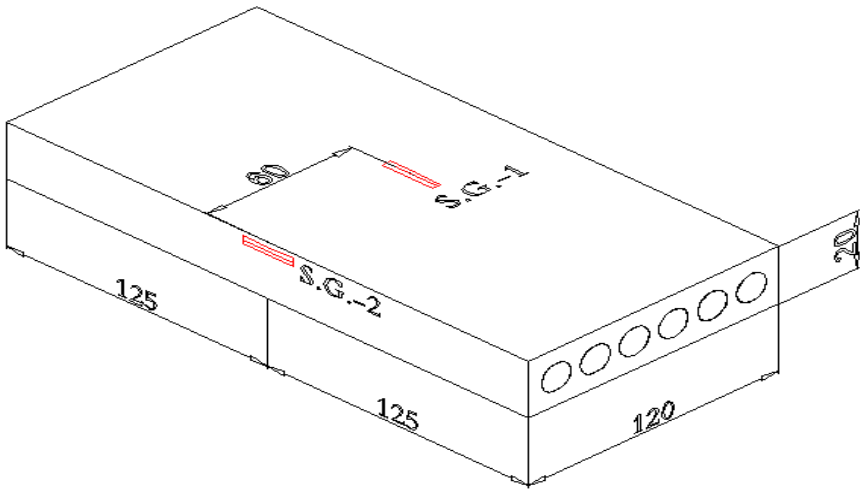

Figure 5.39: Location of Strain Gauges on Slab S9-E

The load-versus-deflection curves are shown in the figure 5.40. The load-strain curves for the gauges are shown in Figure 5.41.

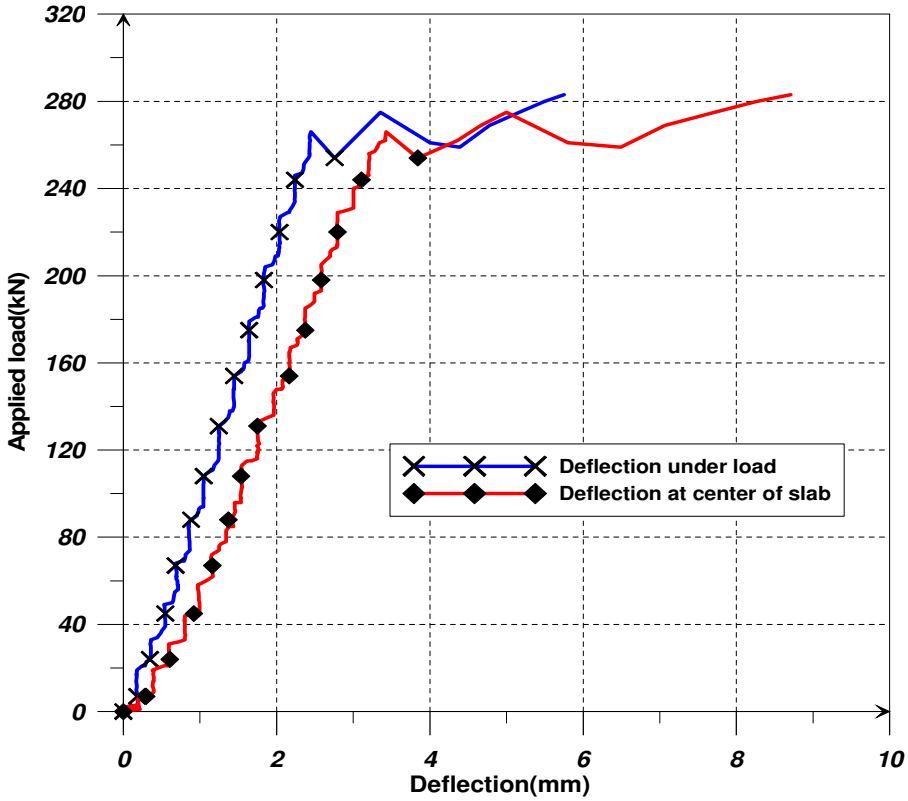

Figure 5.40: Load-Deflection Curves for Slab S9-E

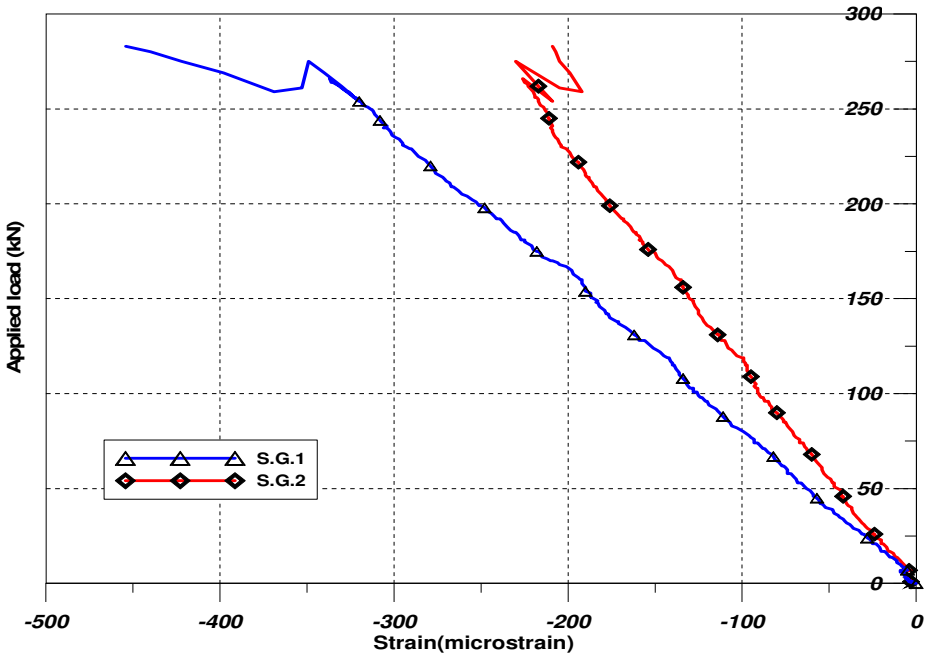

Figure 5.41: Load-Strain Curves for Slab S9-E

5.2.3.2 Test Results for Slab S10 -E

The specimen has the overall length of 2500 mm and thickness of 200mm. During the test, the first crack appeared at a loading of 245 kN. The maximum load measured was 301 kN when the test was stopped. The crack pattern and failure mode of this slab is similar to the slab S9-E as shown in Figure 5.42. The maximum deflection at mid-span recorded in the LVDT was 22.7 mm. The maximum slip at strands recorded in the LVDT was 6.15 mm. Four strain gauges were attached to the specimen to monitor the strains on concrete as shown in Figure 5.43.

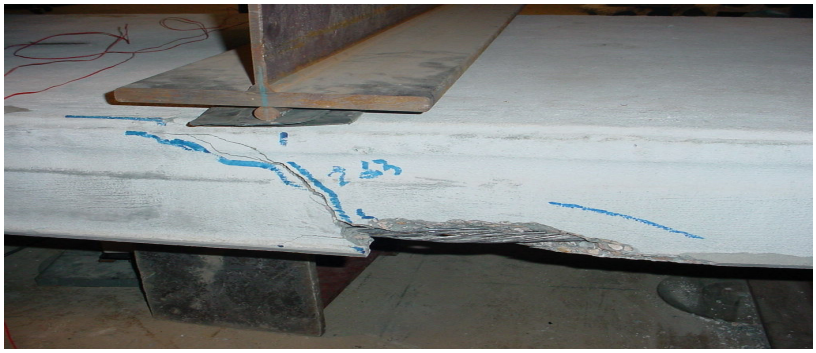

Figure 5.42: Cracking During the Testing of Slab S10-E

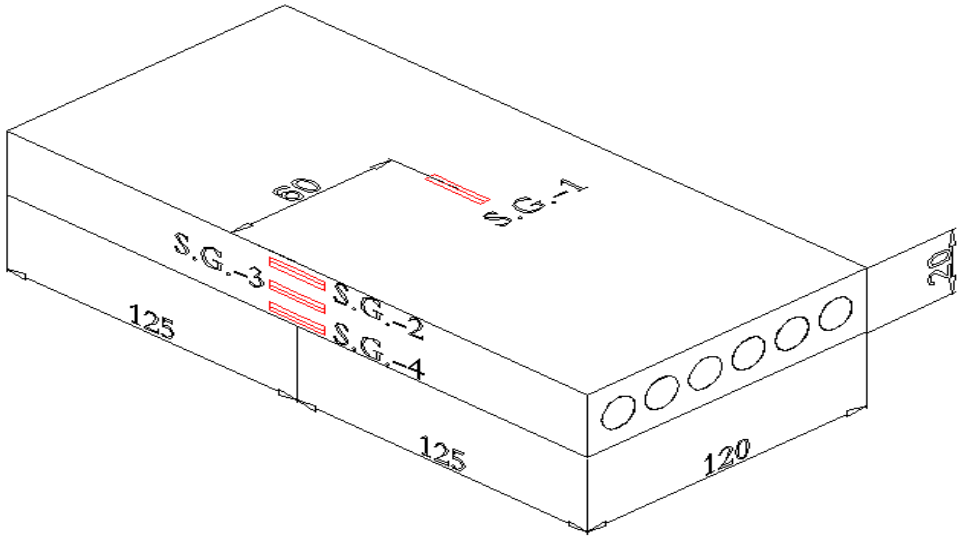

Figure 5.43: Location of Strain Gauges on Slab S10-E

The load-versus-deflection curves are shown in the figure 5.44. The load-strain curves for the gauges are shown in Figure 5.45.

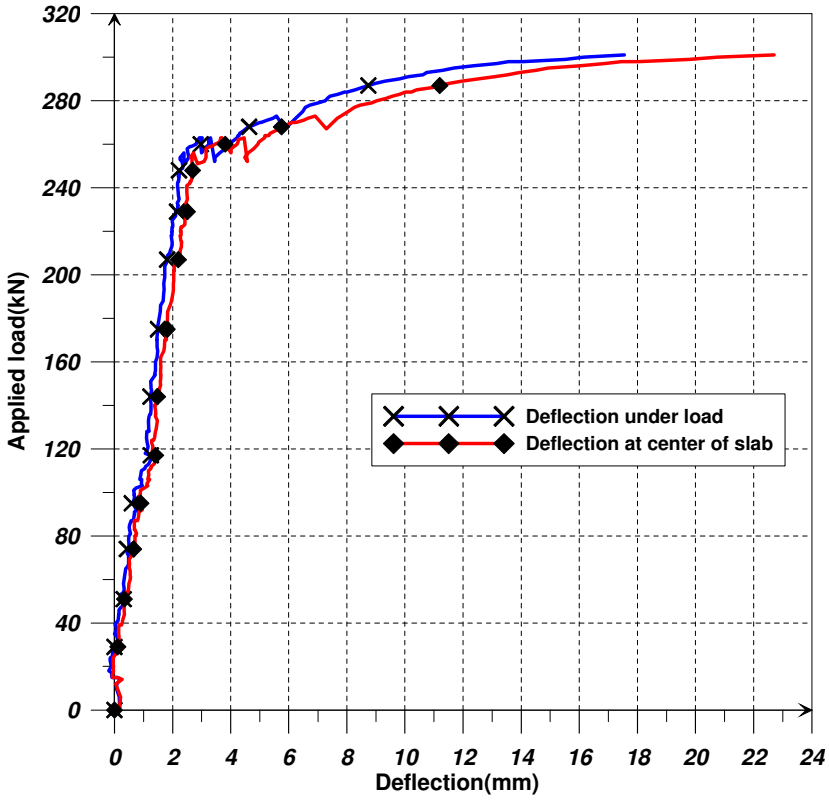

Figure 5.44: Load-Deflection Curves for Slab S10-E

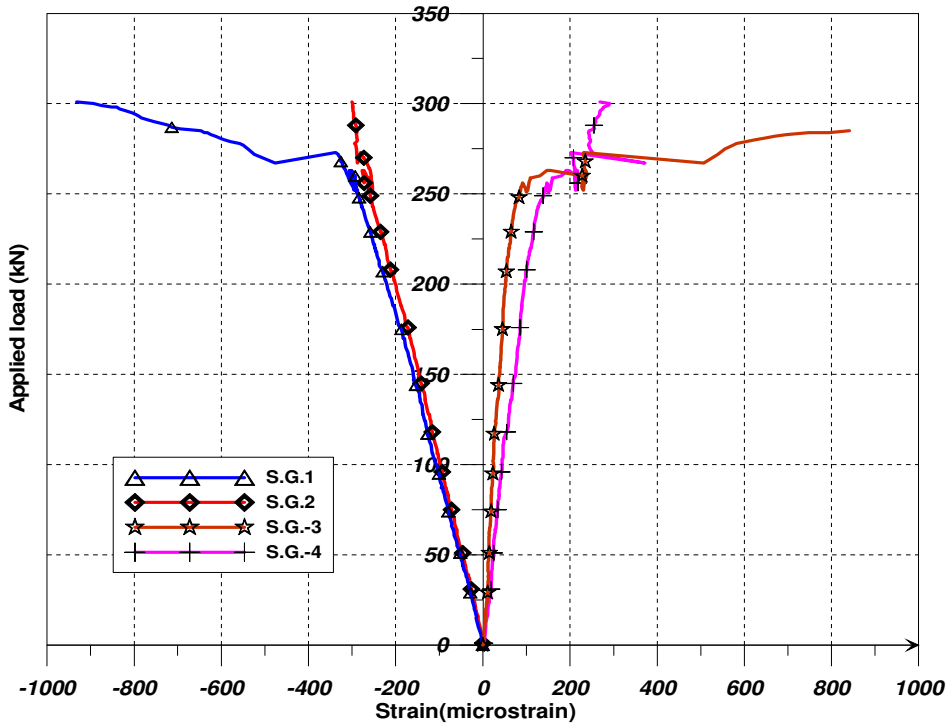

Figure 5.45: Load-Strain Curves for Slab 10-E

5.2.3.3 Test Results for Slab S11-E

The specimen has the same properties of slab S9-E and S10-E. During the test, the first crack appeared at a loading of 245 kN. The failure load was 259 kN. When the difference between the cracking load and failure load is small, it indicates the concrete is brittle and a few cracks may develop before the crack causes failure. The failure mode for this slab is a combination of web shear with flexural shear failure. Many factors produce the variation in results for the slabs that have the same characteristics, such as compressive strength of concrete and slip of strands. One side of slab failed in flexural shear mode, while the other side failed in web shear. The shape of slab when it failed is shown in Figure 5.46. The maximum deflection at mid-span recorded in the LVDT was 10.17 mm. The maximum slip at strands recorded in the LVDT was 5.46 mm. Two strain gauges were bonded on the concrete surface to provide the strain values as shown in Figure 5.47.

Figure 5.46: Cracking During the Testing of Slab S11-E

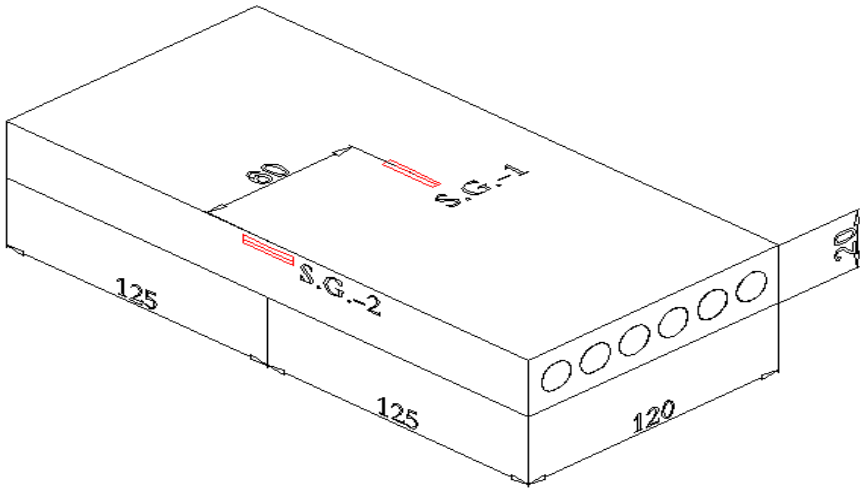

Figure 5.47: Location of Strain Gauges on the Slab S11-E

The load-versus-deflection curves are shown in the figure 5.48. The load-strain curves for the gauges are shown in Figure 5.49.

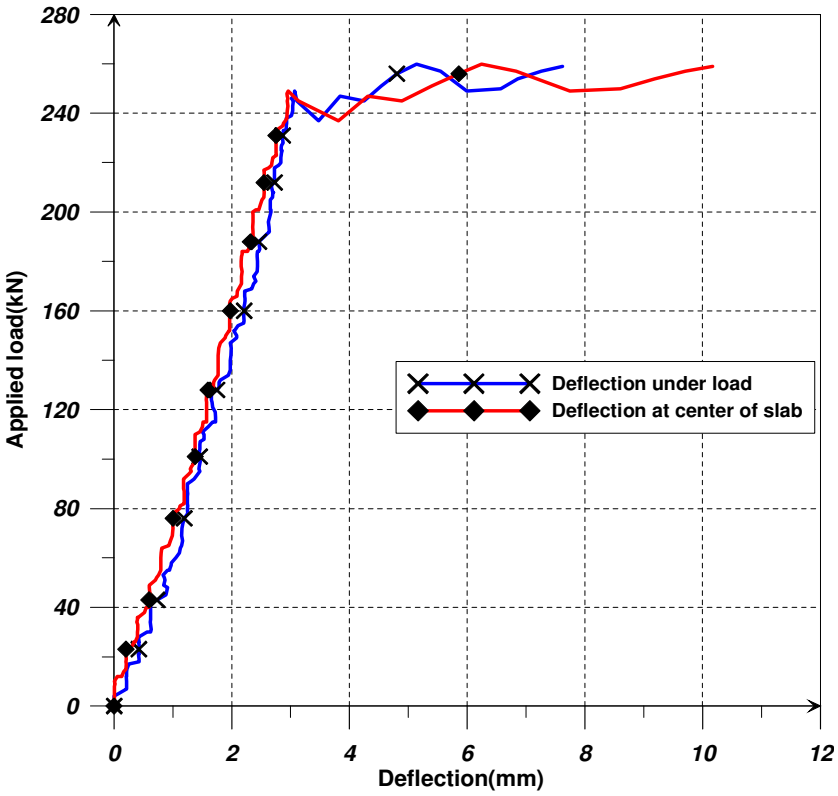

Figure 5.48: Load-Deflection Curves for Slab 11-E

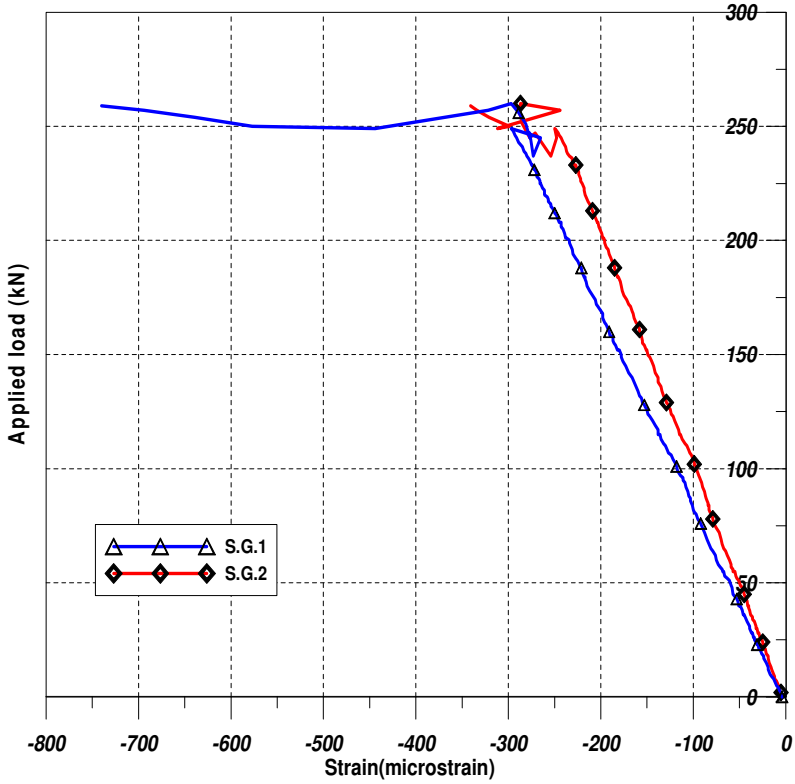

Figure 5.49: Load-Strain Curves for Slab S11-E

5.2.3.4 Test Results for Slab 12-F

The specimen has the overall length of 2500 mm and thickness of 250mm. The crack initiated in the web and grew upwards to the load and downwards to the support as shown in Figure 5.50. A shear tension failure took place in the web at the end of the hollow core slab. The failure load measured was 433 kN. The failure mode was tension failure in the web of the PPHC slab. The maximum deflection at mid-span recorded in the LVDT was 3.35 mm. The maximum slip at strands recorded in the LVDT was 7.5mm. The strains on concrete were measured by using three strain gauges as shown in Figure 5.51.

Figure 5.50: Cracking During the Testing of Slab 12-F

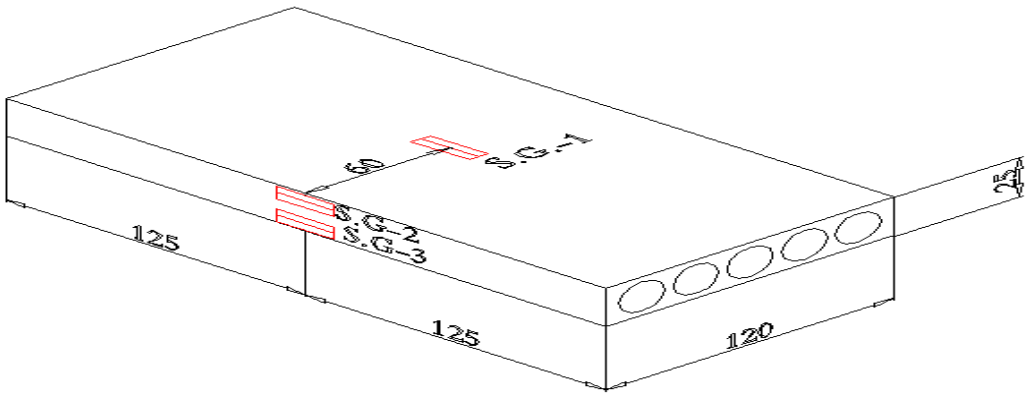

Figure 5.51: Location of Strain Gauges on the Slab S12-F

The load-versus-deflection curves are shown in the figure 5.52. The load-strain curves for the gauges are shown in Figure 5.53.

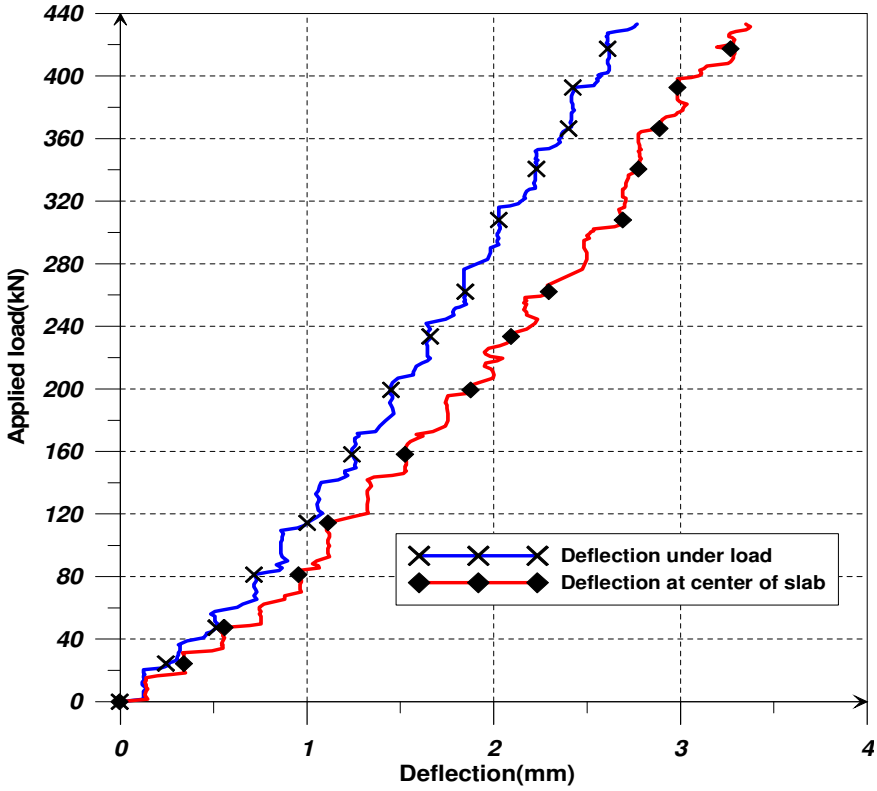

Figure 5.52: Load-Deflection Curves for the Slab S12-F

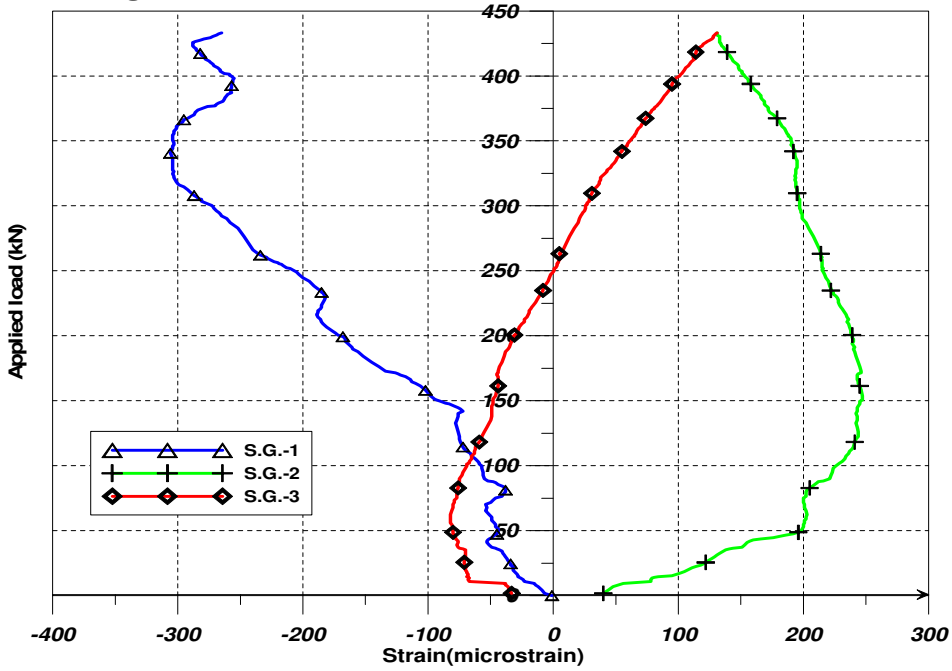

Figure 5.53:Load-Strain Curves for Slab S12-F

5.2.3.5 Test Results for Slab S13-F

The specimen has the overall length of 2500 mm and thickness of 250mm. During the test, the maximum load measured was 397 kN when the test was stopped. The slab failed due to web-shear cracking in shear span. The web shear cracking occurs when the principle tensile stress reaches the tensile strength of concrete. The slab had shear crack starting from the line of load to the support as shown in Figure 5.54. The maximum deflection at mid-span recorded in the LVDT was 2.55 mm. The maximum slip at strands recorded in the LVDT was 4.5mm.

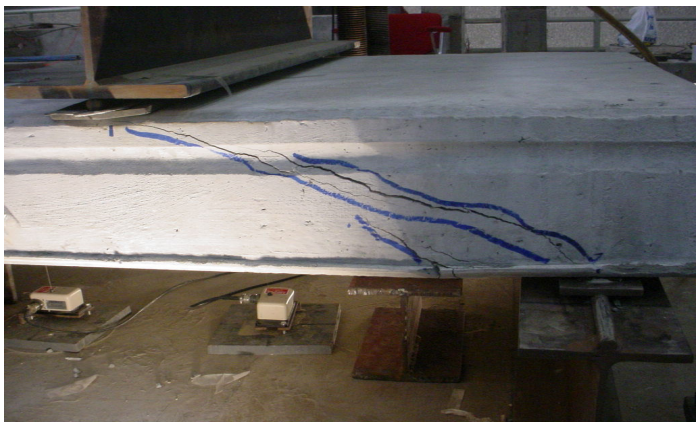

Figure 5.54: Cracking During the Testing of Slab S13-F

The locations of strain gauges attached to the concrete surface are illustrated in Figure 5.55.

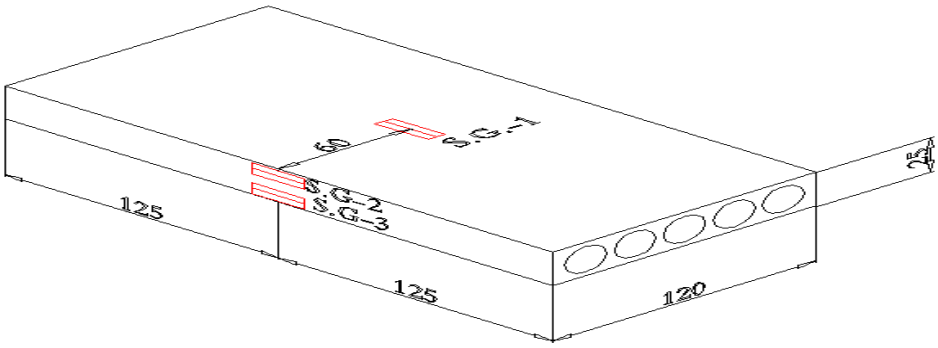

Figure 5.55: : Location of Strain Gauges on the Slab S13-F

The load-versus-deflection curves are shown in the figure 5.56. The load-strain curves for the gauges are shown in Figure 5.57.

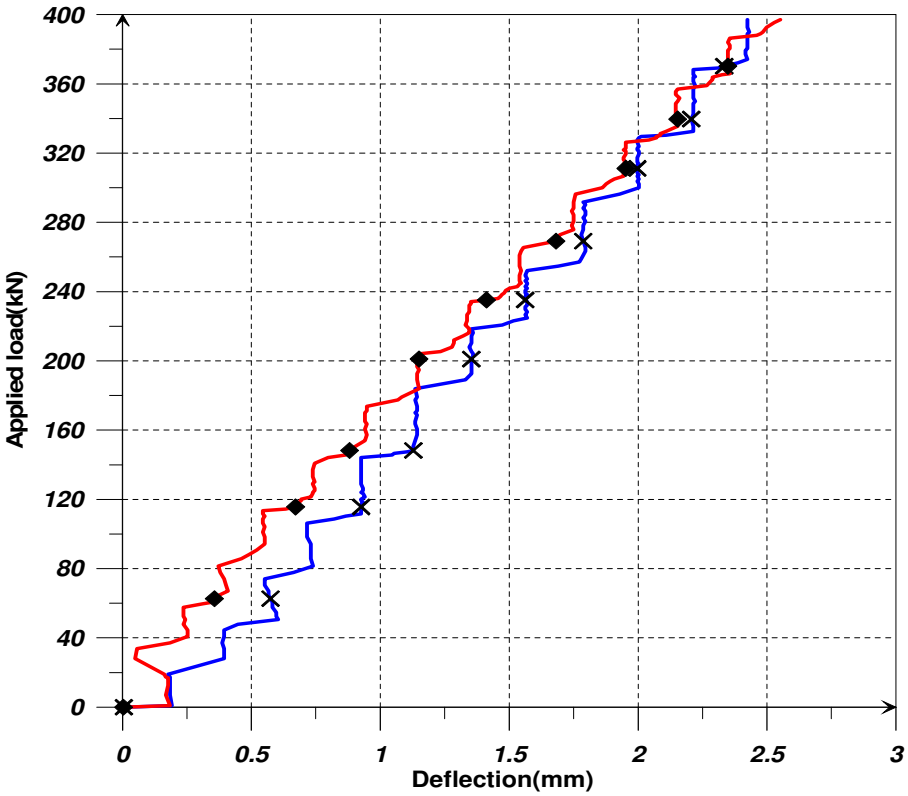

Figure 5.56: Load-Deflection Curves for slab S13-F

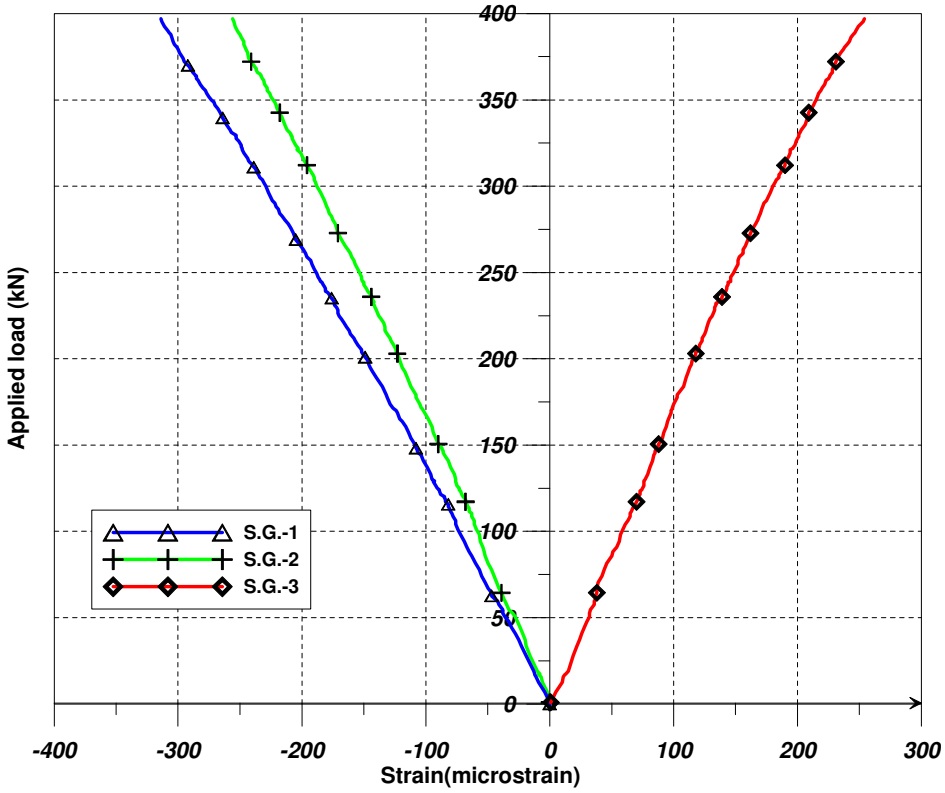

Figure 5.57: Load-Strain Curves for S13-F

5.2.3.6 Test Results for Slab S14-G

The specimen has the overall length of 2500 mm and thickness of 300mm. During the test, the maximum load measured was 529 kN when the test was stopped. The slab failed due to web shear crack. The shear crack initiated in the web and propagated upwards to the line of load and downwards to the support as shown in Figure 5.58. The maximum deflection at mid-span recorded in the LVDT was 3 mm. The maximum slip at strands recorded in the LVDT was 1.78mm. The strains on concrete were measured by using three strain gauges as shown in Figure 5.59.

Figure 5.58: Cracking During the Testing of Slab S14-G

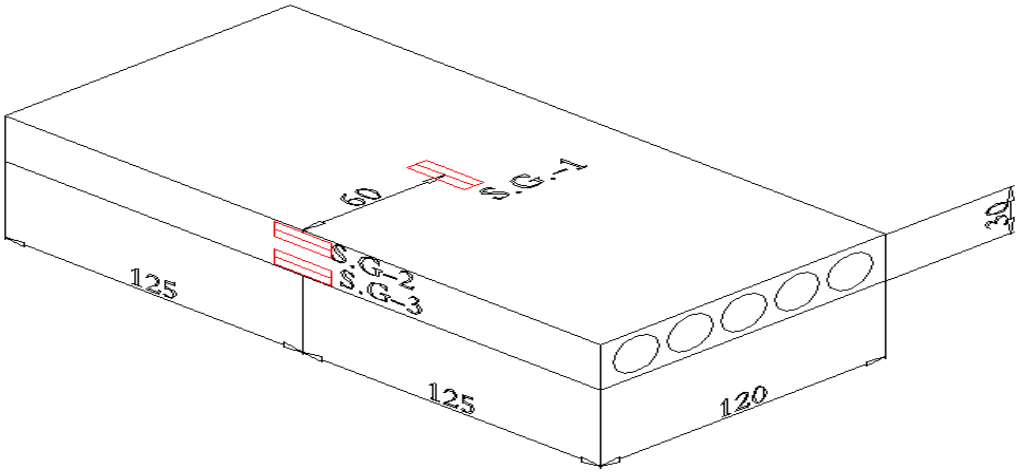

Figure 5.59: Location of Strain Gauges on the Slab S14-G

The load-versus-deflection curves are shown in the figure 5.60. The load-strain curves for the gauges are shown in Figure 5.61.

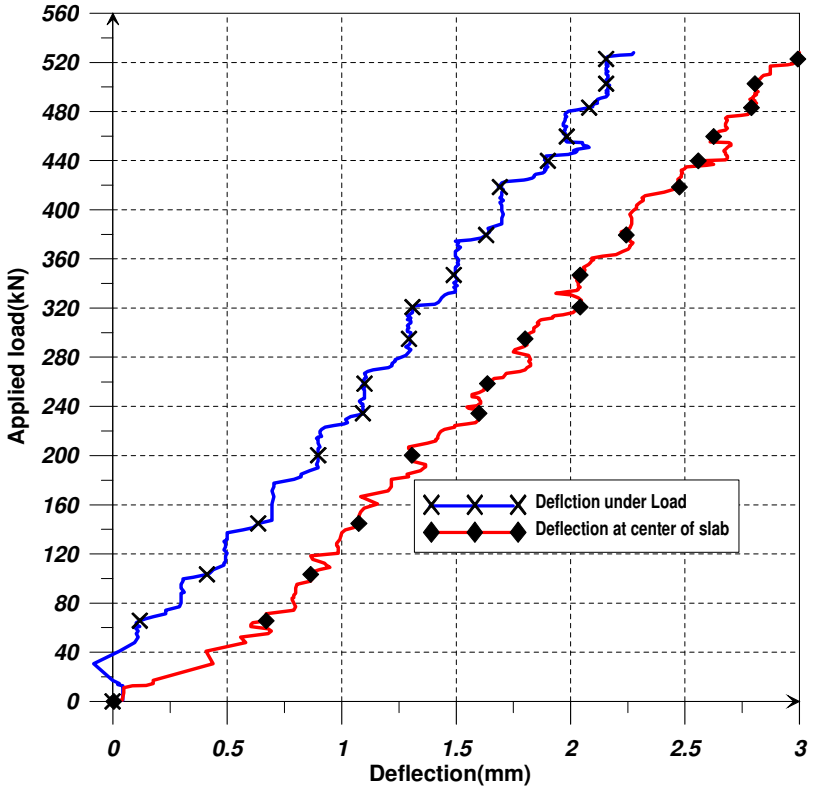

Figure 5.60: Load-Deflection Curves for Slab S14-G

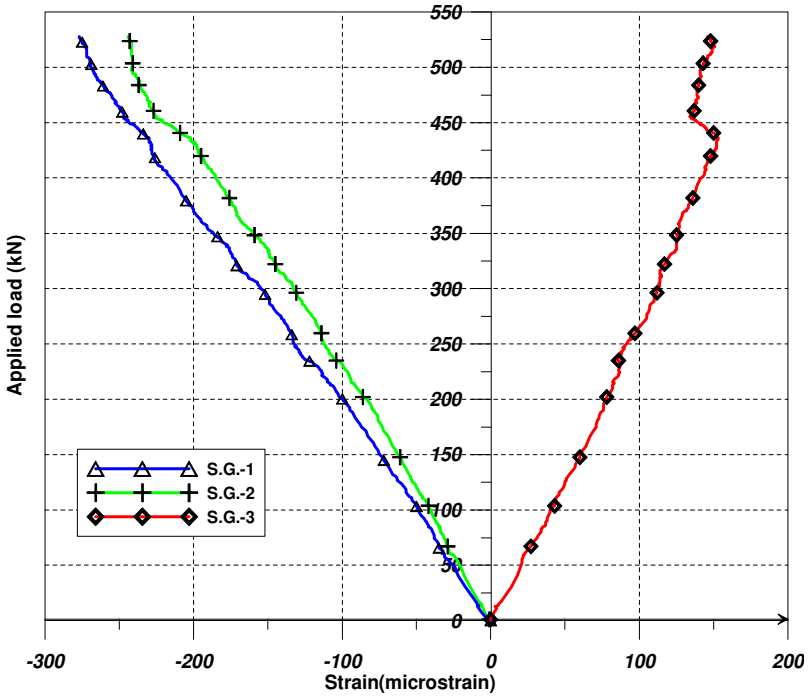

Figure 5.61: Load-Strain Curves for Slab S14-G

5.2.3.7 Test Results for Slab S15-G

The specimen has the overall length of 2500 mm and thickness of 300mm. During the test, the maximum load measured was 598 kN when the test was stopped. The concrete was brittle and failure occurred with no warning. Before a section cracked from flexure, the tensile stress exceeded the tensile strength of concrete at the shear span and web shear crack occurred. Web shear crack propagated to the support and load as shown in Figure 5.62. The maximum deflection at mid-span recorded in the LVDT was 3.77 mm. The maximum slip at strands recorded in the LVDT was 1.78 mm. Four strain gauges were used to measure the strains on concrete as shown in Figure 5.63 .

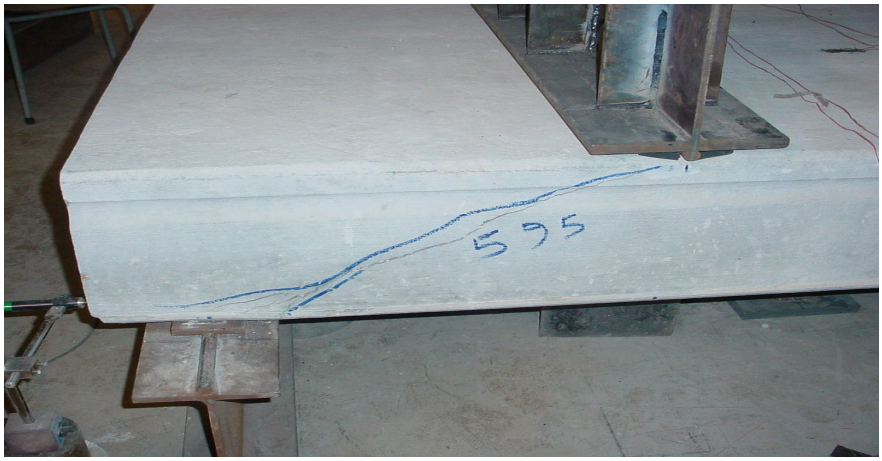

Figure 5.62: Cracking During the Testing of Slab S15-G

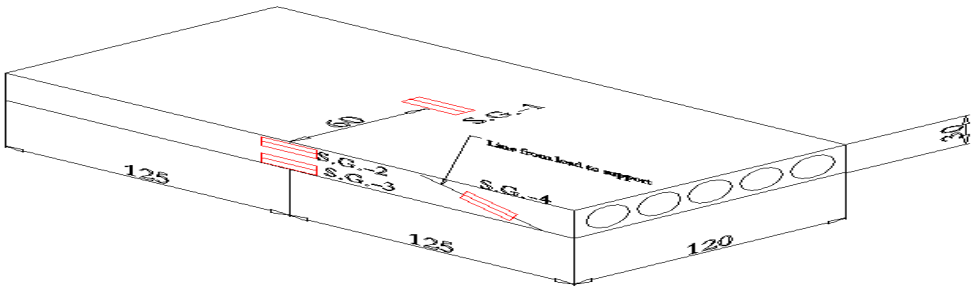

Figure 5.63: : Location of Strain Gauges on the Slab S15-G

The load-versus-deflection curves are shown in the figure 5.64. The load-strain curves for the gauges are shown in Figure 5.65.

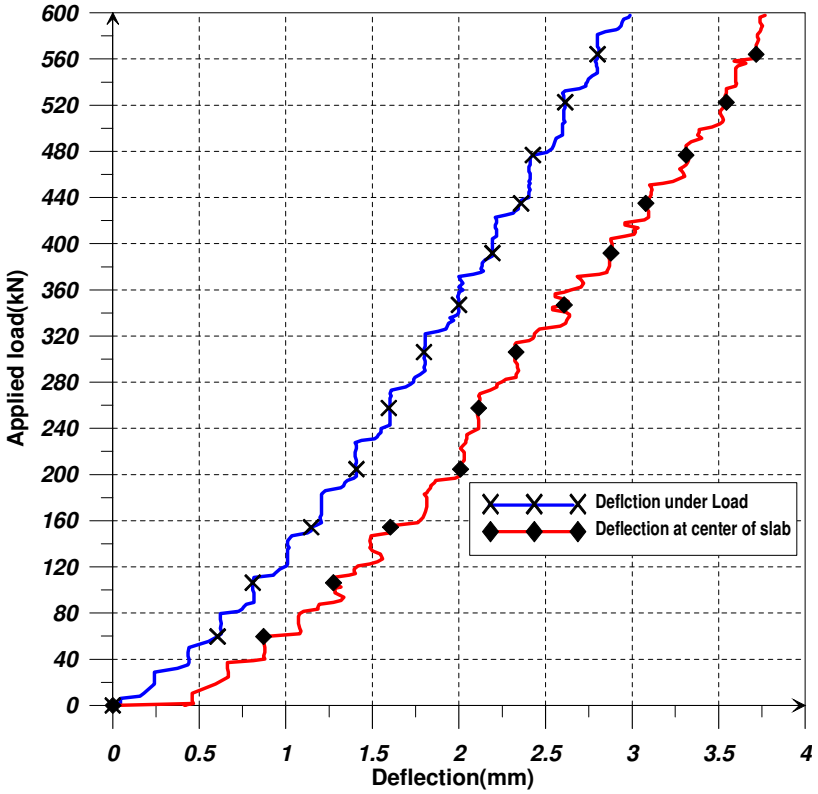

Figure 5.64: Load-Deflection Curves for Slab S15-G

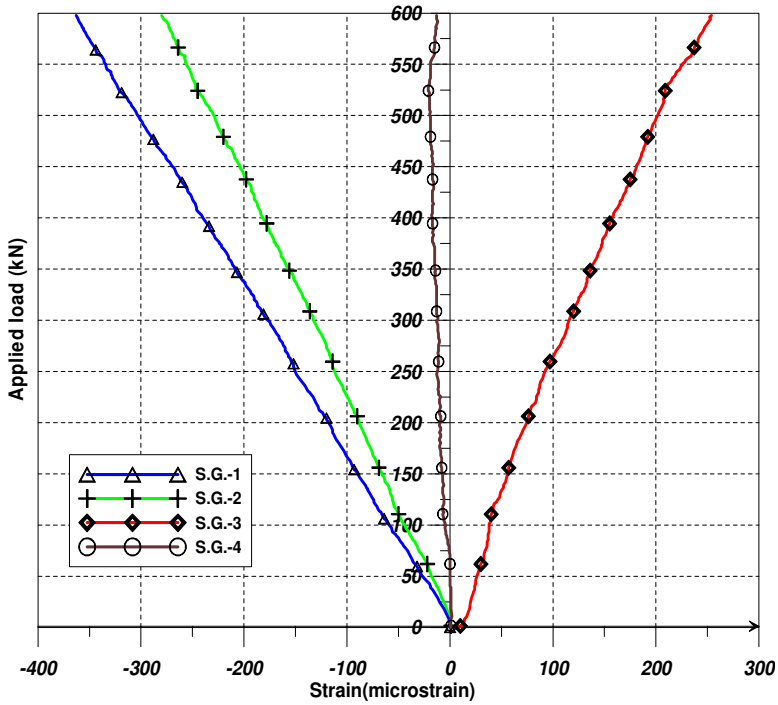

Figure 5.65: Load-Strain Curves for Slab S15-G

5.2.3.8 Test Results for Slab S16-G

This specimen has the same properties as slabs S14-G and S15-G . The failure load measured was 508 kN. The slab failed due to web shear cracking. The failure behavior of this slab was similar to the failure of slab S14-G and S15-G. The maximum deflection obtained was 3 mm. The maximum slip at strands recorded in the LVDT was 1.71mm. Three of strain gauges were bonded on the concrete surface as shown in Figure. The load-versus-deflection curves of this slab are shown in Figure 5.66. The load-strain curves for the gauges are shown in Figure 5.67.

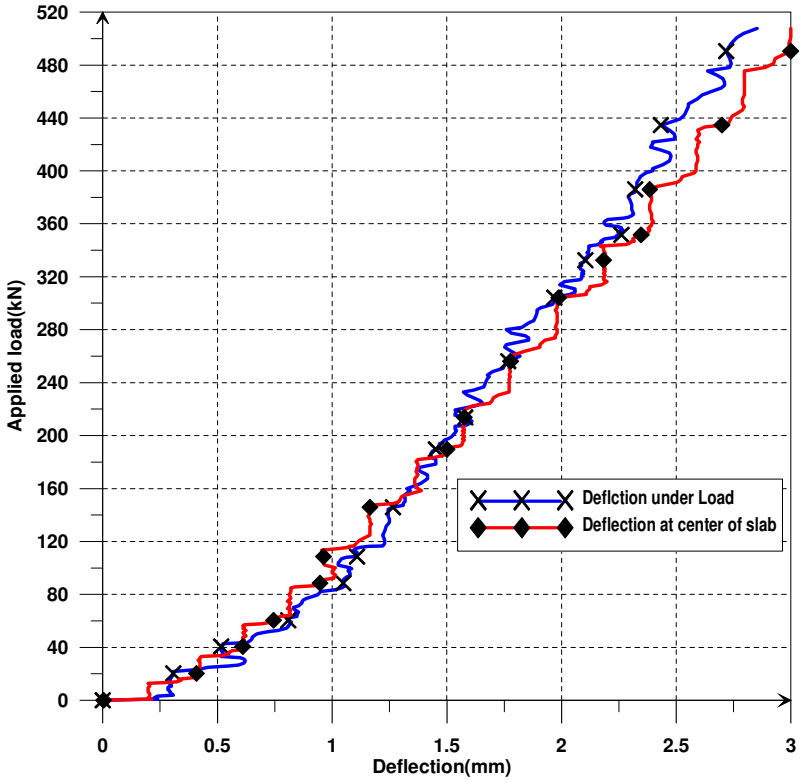

Figure 5.66: Load-Deflection Curves for Slab S16-G

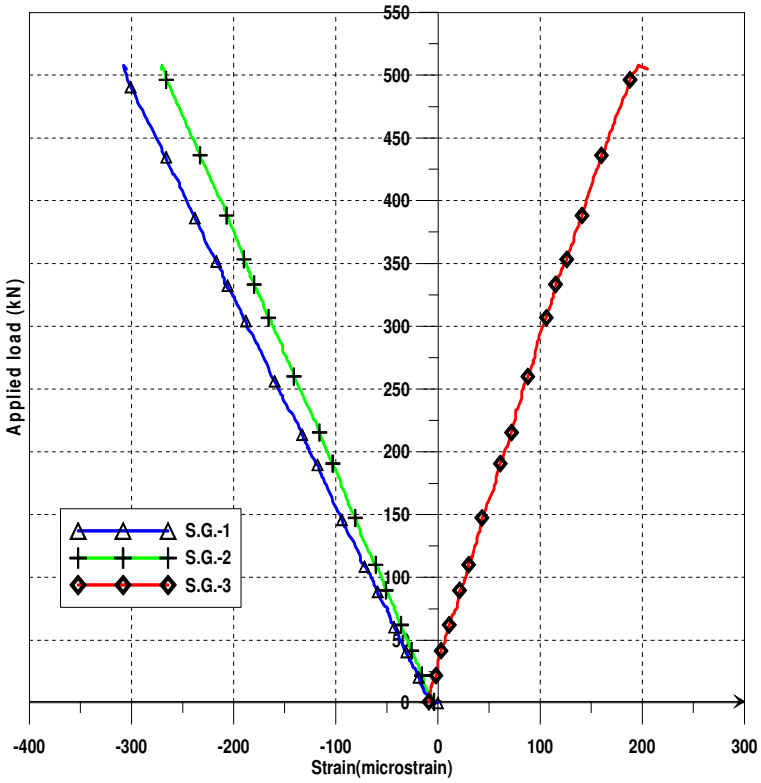

Figure 5.67: Load-Strain Curves for Slab S16-G

5.2.3.9 Test Results for Slab S17-H

The slab was strengthened in shear by wrapping the region of shear span with MAPE CFRP of 0.167 mm thickness as shown in Figure 5.68. The failure load measured was 350kN. When the load reached 281kN, a first vertical crack was observed under the left line of load as shown in Figure 5.69. The slab cracked and failed in load lower than expected. The slab failed due to strand slip before web-shear cracking. The slippage of strands caused the premature failure of slab before the CFRP took its role. The maximum deflection measured was 7.27 mm. Three strain gauges were used to measure the strains on the concrete, and two for measuring the strains in CFRP sheets.

Figure 5.68: Shear Strengthening of Slab S17-H

The load-versus-deflection curves are shown in the figure 5.70. The load-strain curves for the gauges are shown in Figure 5.71.

Figure 5.69: Cracking During the Testing of Slab S17-H

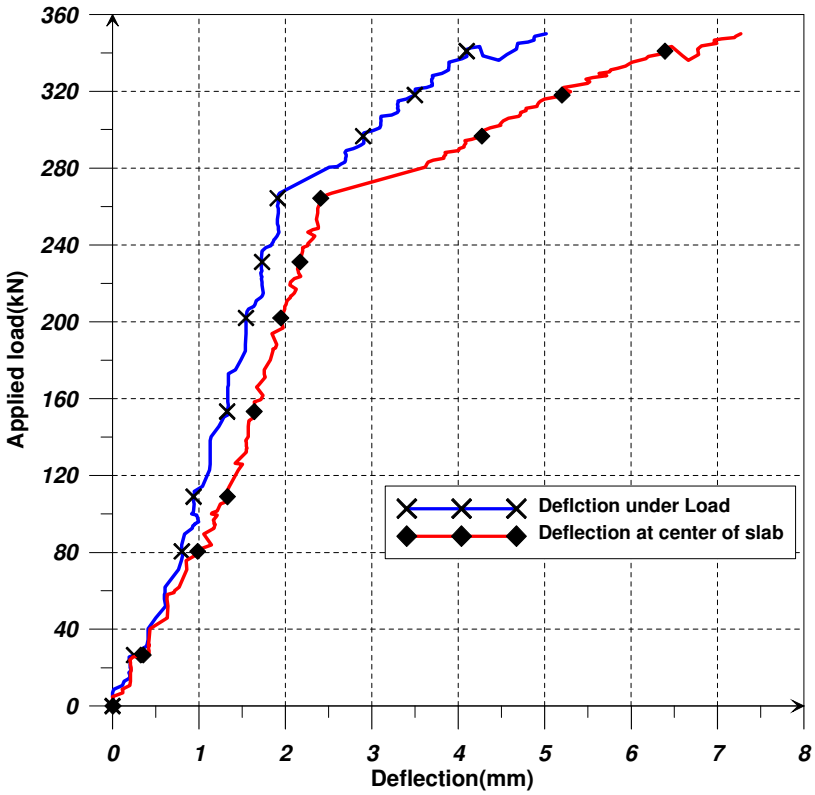

Figure 5.70: Load-Deflection curves for Slab S17-H

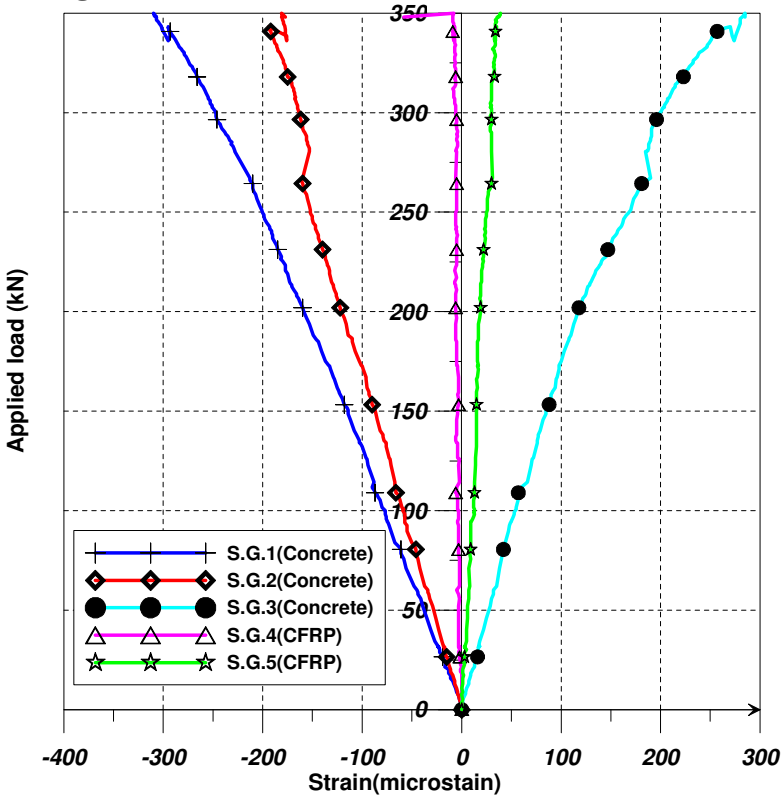

Figure 5.71: Load-Strain Curves for Slab S17-H

5.2.3.10 Summary of the Experimental Results of PPHC Slabs with Length of 2.5m

The cracking load, ultimate load, deflection at maximum load and failure mode of the second group of slabs are summarized in Table 5.10.

Table 5.10: Summary of the Experimental Results of PPHC Slabs with Length of 2.5m

Slab Code	Cracking Load(kN)	Failure Load(kN)	Max. Deflection (mm)	Mode of Failure
S9-E	264	287	8.27	Flexural-Shear
S10-E	245	301	22.7	Flexural-Shear
S11-E	245	259	10.17	Flexural-Shear
S12-F	433	433	3.35	Web-Shear
S13-F	397	397	2.55	Web-Shear
S14-F	529	529	3.00	Web-Shear
S15-G	597.7	597.7	3.77	Web-Shear
S16-G	508	508	3	Web-Shear
S17-F	350	281	7.27	Bond-Failure

When the depth of the hollow core slabs increases, the web shear strength decreases. The reduction in the web shear cracking strength with depth is related to the spread of prestressing force into the section and associated with a combination of effects due to shear lag, anchorage bond, prestress location, and the geometry of the cross section of the PPHC slabs.

The applied load versus mid-span deflection relationships of the PPHC slabs in second group are presented in Figure 5.72.

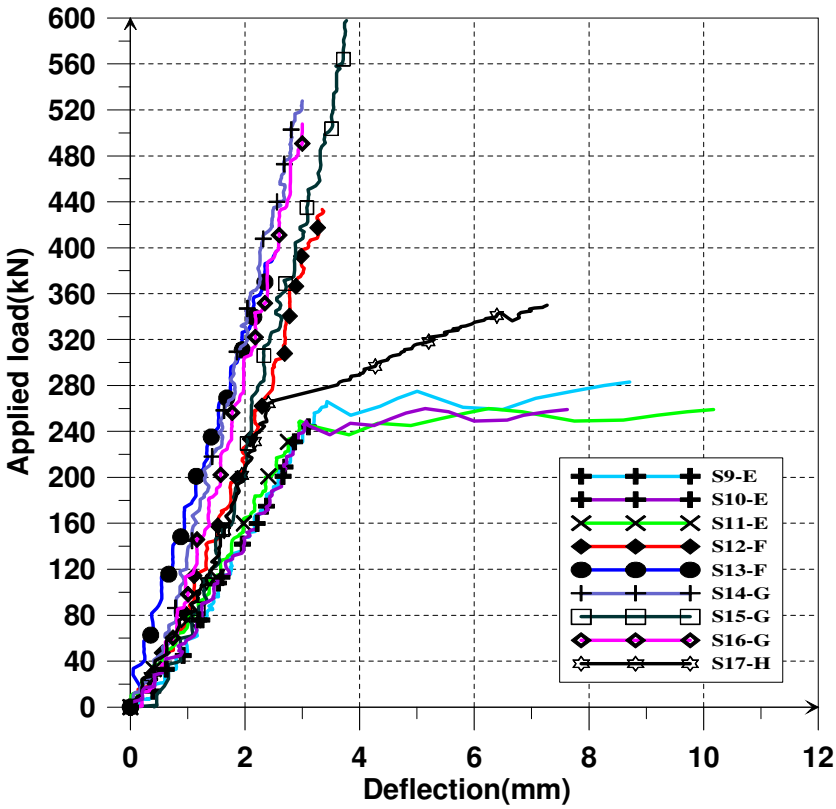

Figure 5.72: Load-Mid Span Deflection Curves for the PPHC Slabs with length of 2.5 m

5.3 The STRUT-AND-TIE MODEL RESULTS

The failure loads, and associated failure mode obtained by using the strut-and-tie model approach, are summarized in Table 5.11.

Table 5.11: Strut-and-Tie Model Results for Tested PPHC Slabs

Slab Name	STM Failure Load(kN)	Failure Mode
S1-A&S2-A	163	Flexural
S3-B&S4-B	206	Flexural-Shear
S5-C&S7-C	356	Flexural-Shear
S9-E&S10-E&S11-E	280	Flexural-Shear
S12-F&S13-F	400	Flexural-Shear
S14-G& S15-G	501	Web-Shear
S8-D	265	Flexural-Shear
S17-H	466	Web Shear

The analytical results computed by using ACI expression for flexural and shear and the experimental results are listed in Table 5.12.

Table 5.12: Comparison between the Analytical and Experimental Results

Slab Code	a/d	Test Failure Load (kN)	Flexural Failure Load ACI(kN)	Shear Prediction ACI(kN)			Difference %
				V_{ci}	V_{cw}	Shear Failure Load	
S1-A	11.42	160	167.42	74.55	226.256	149.1	6.81
S2-A	11.42	158	167.42	74.55	226.256	149.1	5.63
S3-B	8.73	226.8	226.41	96.515	224.625	193.03	14.89
S4-B	8.73	233.9	226.41	96.515	224.625	193.03	17.47
S5-C	7.06	381	354.61	148.02	302.505	296.05	22.30
S7-C	7.06	383	354.61	148.02	302.505	296.05	22.30
S9-E	3.7	287	361.22	143.2	191.89	286.4	0.21
S10-E	3.7	301	361.22	143.2	191.89	286.4	4.85
S11-E	3.7	259	361.22	143.2	191.89	286.4	-10.58
S12-F	2.83	433	698.03	253.5	224.625	449.25	-3.75
S13-F	2.83	397	698.03	253.5	224.625	449.25	-13.16
S14-G	2.3	529	1093.38	400.25	302.505	605.01	-14.37
S15-G	2.3	597.7	1093.38	400.25	302.505	605.01	-1.22
S16-G	2.3	508	1093.38	400.25	302.505	605.01	-19.1

The comparison between failure loads obtained from the experimental results and those obtained by using ACI 318-05 equations are shown in Table 5.13. The shear force (V_c) is limited to the lesser of flexure shear (V_{ci}) and web shear (V_{cw}). The most important observation from the Table is in respect of 200 mm thick hollow core slab for which the ACI-318 code equations had predicted a flexure-shear failure mode, but the actual failure observed in the test was a flexural failure mode. The ACI shear failure load is lower than the ACI flexural load capacity, indicating a flexure-shear failure. For 250 mm and 300 mm deep PPHC slabs of 5 m span, the ACI code predicts the correct failure mode i.e. the flexure-shear failure mode, which was also observed in the test. However, the flexure-shear capacity predicted by ACI equations is significantly lower than the measured experimental failure load. In Table 5.13, it is evident that for shear span to depth ratio $3 < a/d < 9$, the ACI code underestimates the flexure-shear capacity of PPHC slabs. For shear span to depth ratio $a/d > 9$, a flexure-shear failure is indicated by ACI code equations, whereas, in full-scale load tests, a

flexural failure was observed. From Table 5.13, it is clear that the PPHC slabs with *a/d* < 3 failed in web shear failure mode, and the shear capacity of these slabs predicted by the ACI code correlated well with the experimental results. The discussion above indicates that the existing ACI code recommendation concerning flexure-shear strength should be reassessed. Based on the comparison between ultimate loads from experimental results and ACI 318 equations, modification to the ACI code equation for flexure-shear of prestressed members is proposed. The nominal flexure shear strength given in Equation 5.12 can be modified, reincorporating the term *d/2* (see Equation 5.11) and varying the coefficient 1/20 for the shear force that exists when the flexure shear cracks are developed. The proposed equation for flexure-shear is

$$V_{ci} = k\sqrt{f_c'}\, b_w d + \frac{M_{cr}}{\frac{M_{max}}{V_i} - \frac{d}{2}} + V_d \qquad \text{where} \quad \frac{1}{20} \le k \le \frac{1}{12} \tag{5.16}$$

The regression for the results of flexure-shear failure loads was carried out to determine the magnitude of *k* factor. Figure 5.73 shows the relation between *k* factor and *a/d* ratio. The value of *k* can be obtained from the following equation:

$$k = \frac{1}{\sqrt{145}}\left(-0.00191\left(\frac{a}{d}\right)^{3} + 0.0391\left(\frac{a}{d}\right)^{2} - 0.183\left(\frac{a}{d}\right) + 0.841\right) \tag{5.17}$$

The experimental failure loads, and the flexure shear capacity of hollow core slabs obtained by using the modified new equation proposed, are shown in Table 5.13.

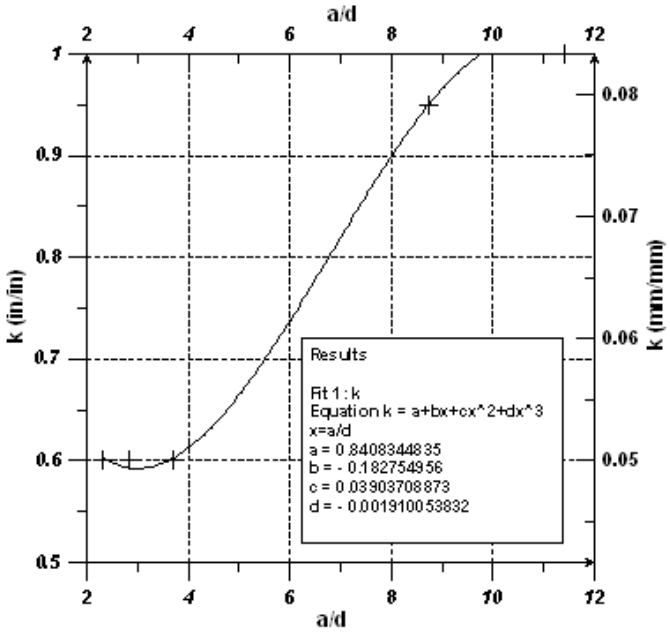

Figure 5.73: Relation between k Factor and a/d Ratio

The proposed equation for PPHC slabs with shear span depth ratio greater than 4 gives a more reasonable value for the flexure shear strength of hollow core slabs. It is evident from Table 5.13 that the proposed equation yields better agreement with the experimental results obtained in this experimental program. In accordance with the proposed equation, the flexure-shear strength of slabs with $a/d > 4$ increased, and the failure mode for slabs with $a/d > 9$ changed from flexure-shear mode to pure flexural mode.

When the depth of hollow core slab increases, the web-shear cracking strength decreases. The slab failed in web shear mode is not affected by new proposed equation. The relations between analytical and experimental results using ACI code expressions and the new proposed equations are illustrated in Figures 5.74 and 5.75 respectively.

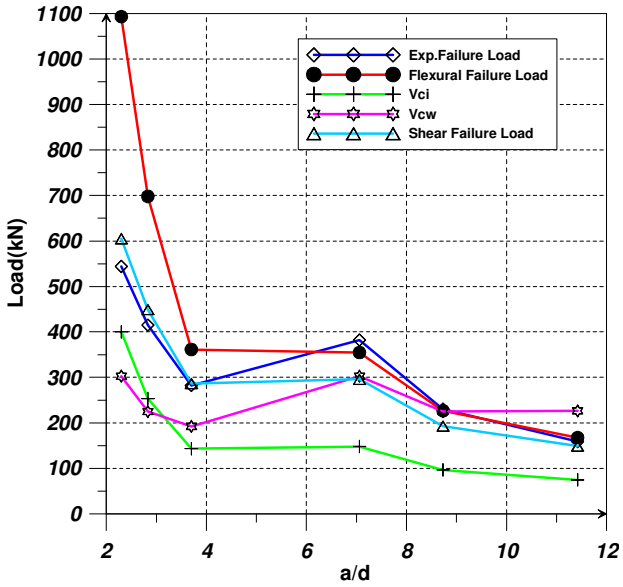

Figure 5.74: Relation between a/d and Applied Load by Using ACI Code Expressions

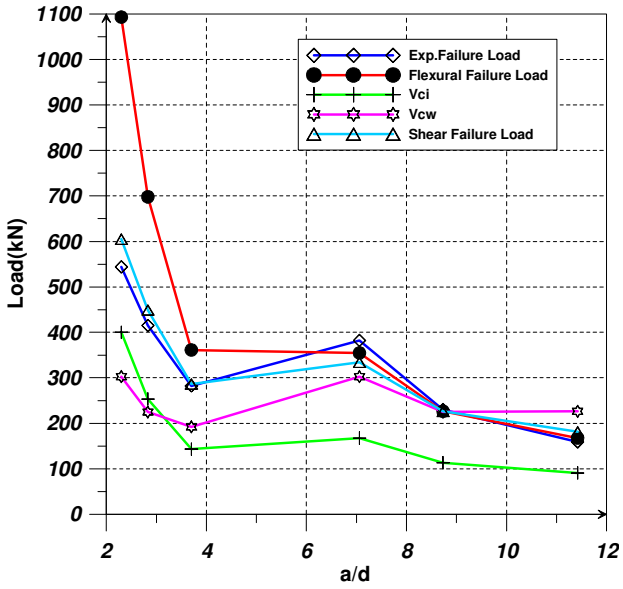

Figure 5.75: Relation between a/d and Applied Load by Using New Proposed Equation

The results obtained from the proposed strut-and-tie model are compared with these obtained from full-scale loading tests of prestressed precast hollow-core slabs of different shear span-to-depth ratio. The proposed strut-and-tie model provides a good correlation with the experimental results and, it indicates well to the associated failure mode as shown in Table 5.14.

Table 5.13: Comparison between the Experimental Failure Loads and the Results Obtained by New Proposed Eqn. (5.17)

Slab Code	a/d	Test Failure Load (kN)	Flexural Failure Load ACI(kN)	Shear Prediction ACI(kN)			Difference %
				V_{ci}	V_{cw}	Shear Failure Load	
S1-A	11.42	160	167.42	90.74	226.256	181.48	-4.64
S2-A	11.42	158	167.42	90.74	226.256	181.48	-5.96
S3-B	8.73	226.8	226.41	113.27	224.625	226.54	0.11
S4-B	8.73	233.9	226.41	113.27	224.625	226.54	3.15
S5-C	7.06	381	354.61	167.13	302.505	334.26	12.27
S7-C	7.06	383	354.61	167.13	302.505	334.26	12.27
S9-E	3.7	287	361.22	143.2	191.89	286.4	0.21
S10-E	3.7	301	361.22	143.2	191.89	286.4	4.85
S11-E	3.7	259	361.22	143.2	191.89	286.4	-10.58
S12-F	2.83	433	698.03	253.5	224.625	449.25	-3.75
S13-F	2.83	397	698.03	253.5	224.625	449.25	-13.16
S14-G	2.3	529	1093.38	400.25	302.505	605.01	-14.37
S15-G	2.3	597.7	1093.38	400.25	302.505	605.01	-1.22
S16-G	2.3	508	1093.38	400.25	302.505	605.01	-19.1

Table 5.14: Comparison between the STM Results and the Experimental Results

Slab Name	Average Experimental Failure Load kN	Failure Mode	STM Failure Load(kN)	Failure Mode	Diff. %
S1-A&S2-A	159	F*	163	F	-2.5
S3-B&S4-B	225	FS	206	FS	8.4
S5-C&S7-C	382	FS*	356	FS	6.8
S9-E&S10-E&S11-E	282	FS	280	FS	0.71
S12-F&S13-F	415	WS*	400	WS	3.6
S14-G& S15-G	545	WS	501	WS	8

* F: Flexural Failure FS: Flexural Shear Failure WS: Web Shear Failure

5.4 EFFECT OF STRANDS SLIP ON THE FAILURE MODE of PPHC SLABS

Under certain conditions, some of the typical machine processes for making hollow-core slabs may sometimes produce concrete with insufficient compaction or paste formation in the region surrounding the prestensioned strand. This can result in a deficiency in the bond capacity, which is evidenced by excess initial strand slip upon

transfer of the prestressing force through transverse saw-cutting of the product. As the specimens were loaded and the concrete section cracked, the stress in the strand increased abruptly. As loading continued, the stress in the strand increased until a limiting bond strength value was reached. At this point, some slippage between strand and concrete occurred at the region around the crack, reducing the bond stress in the crack region and increasing the bond stress at the adjoining regions. This process continued, creating a flexural bond stress wave moving away from the point of loading. Whenever the flexural bond stress wave overlapped the transfer length, bond failures were observed. The failure of S6-C and S17-H slabs was believed to be a bond failure, as the failure loads involved were far below the computed analytical flexural and shear failure loads. The initiation of shear cracks impairs the embedment of prestressing strands, and it causes slippage of strands. This results in premature failure of precast prestressed hollow-core slabs. The measured slip versus applied load charts of some tested slabs is shown in Figure 5-76 to Figure 5-79.

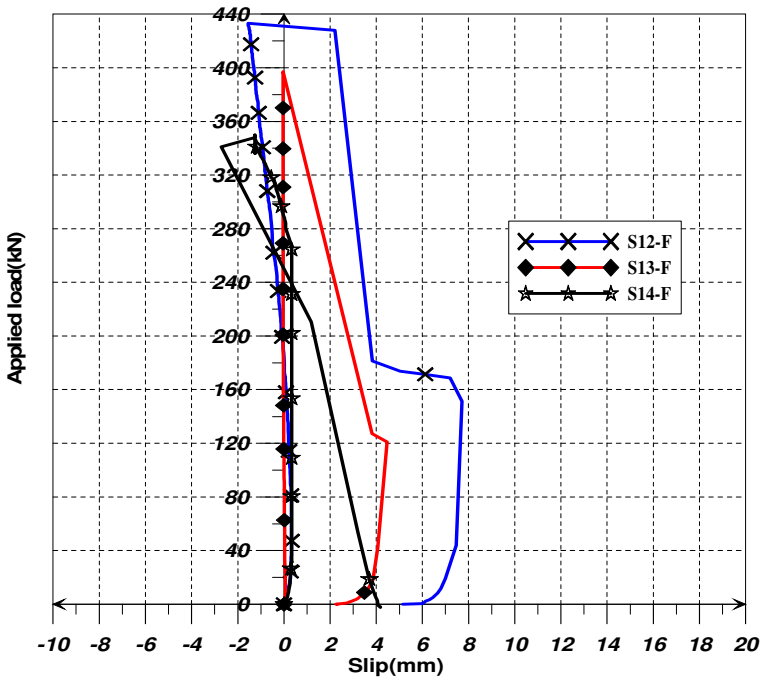

Figure 5.76 : Load-Slip Curves for Slabs S12,S13&S14

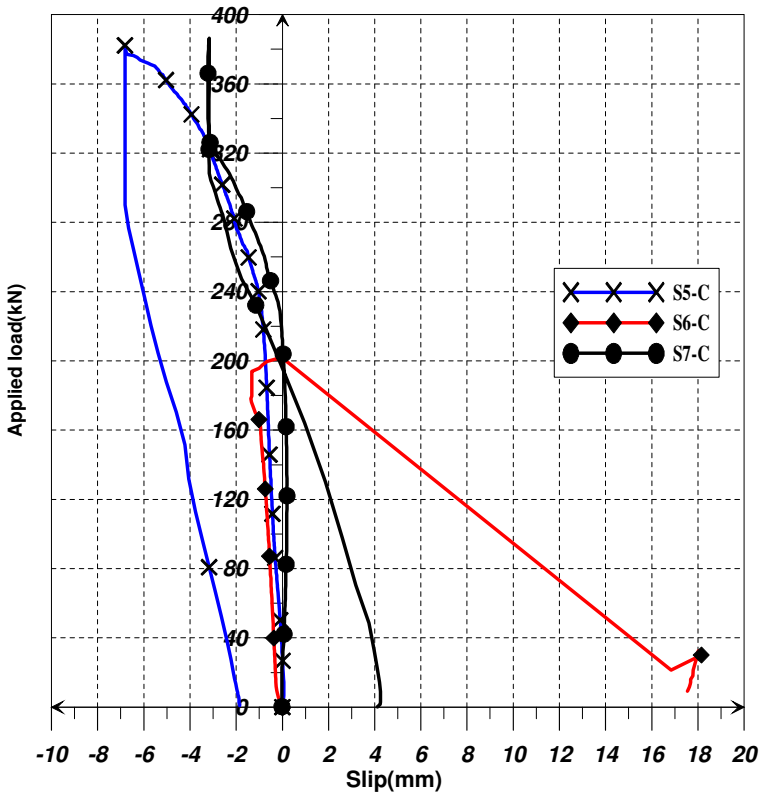

Figure 5.77: Load-Slip Curves for Slabs S5, S6 &S7

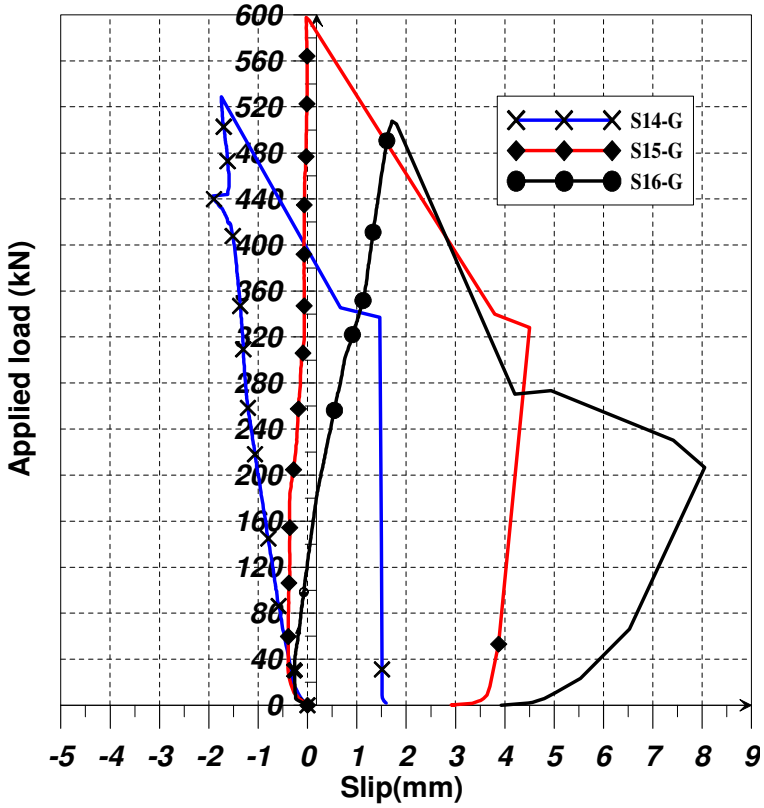

Figure 5.78: Load-Slip Curves for Slabs S14 ,S15 &S16

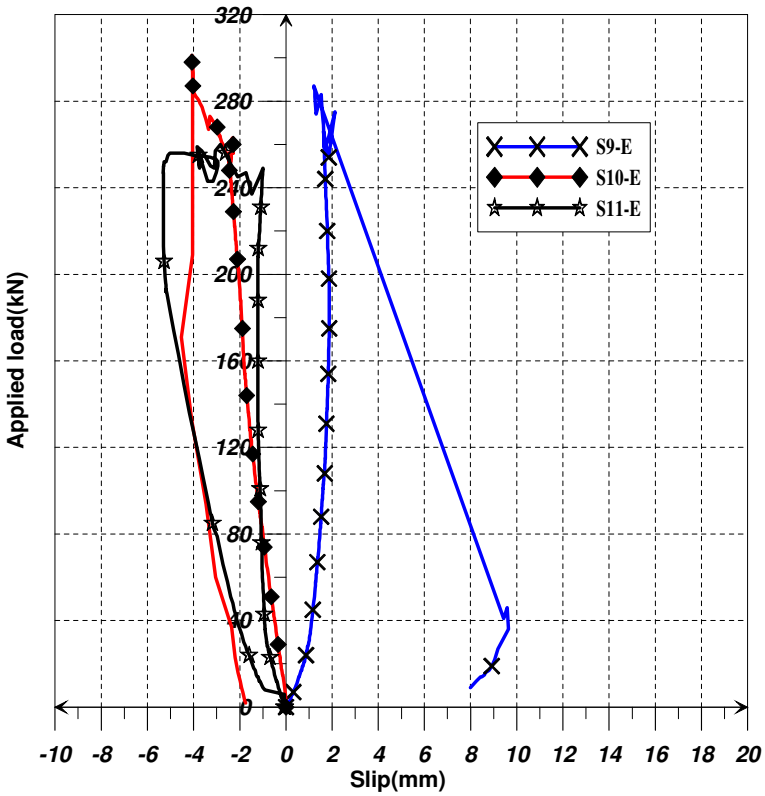

Figure 5.79: Load-Slip Curves for Slabs S9, S10 &S11

CHAPTER 6

SUMMARY,CONCLUSION & RECOMMENDATIONS

6.1 SUMMARY

A Strut-and-Tie method for PPHC slabs with and without CFRP strengthening was developed and proposed. The proposed STM starts by selecting the initial centerline of a truss consisting of concrete tension ties, concrete compression struts and steel tension ties. The iterating procedure is repeated until a geometric compatibility has been reached, and the stress levels in the struts and ties have also reached their limits. The vertical positioning of the struts and ties was determined on the basis that the change in strains of both bottom tensile prestressing steel and CFRP sheets are the same. In dimensioning the area of tension ties, it is assumed that the strength reduction factor for bottom prestressed tensile steel reinforcement and for CFRP sheet is 0.75. Prestressing forces represented by equivalent external loads are gradually introduced along the tendon's transfer length in the nearest strut-tie model joints. After selecting a centerline of the Strut-and-Tie model and dimensioning the struts and ties, structure analysis was conducted to obtain stress ratios for each strut, tie, and nodal face. A total of 17 experimental test results are compared to the proposed STM approach with ACI effective factor model. The results from the analytical study, experimental tests, and STM model are summarized in Table 6.1.

Table 6.1: Summary of Analytical, Experimental and STM Failure Loads, kN

Slab Name	Experimental		Analytical		STM model	
	Failure Load	Mode of Failure	Flexural Failure	Shear Failure	Failure Load	Mode of Failure
S1-A	160	F	167	149	163	F
S2-A	158	F	167	149	163	F
S3-B	226.8	FS	226	193	206	FS
S4-B	233.9	FS	226	193	206	FS
S5-C	381	FS	354	296	356	FS
S6-C	202	B	354	296	356	FS
S7-C	383	FS	354	296	356	FS
S8-D	219	FS	270	271	265	FS
S9-E	287	FS	361	286	280	FS
S10-E	301	FS	361	286	280	FS
S11-E	259	FS	361	286	280	FS
S12-F	433	WS	698	449	400	WS
S13-F	397	WS	698	449	400	WS
S14-G	529	WS	1093	605	501	WS
S15-G	597.7	WS	1093	605	501	WS
S16-G	508	WS	1093	605	501	WS
S17-H	350	B	696	579	466	WS

* F Flexural Failure FS Flexural Shear Failure WS Web Shear Failure B bond failure

6.2 CONCLUSIONS

Based on the analysis of experimental results, the following conclusions can be drawn:

- The Strut-Tie approach is instrumental in understanding the function of both concrete and steel reinforcement in reinforced and prestressed concrete members. It allows the engineer to visualize the flow of internal forces and provide an adequate structural system to carry those forces.
- It has been proven that the proposed Strut-and-Tie method approach is a useful tool for analyzing the PPHCS slabs with and without CFRP strengthening.
- For prestressed concrete members without web reinforcement, such as prestressed precast hollow core slabs, concrete tension elements (concrete ties) are used to resist the tension forces in these members

- The analysis of the experimental results showed that flexural shear strength of the slabs with shear span to depth (a/d) ratio > 4 is greater than strengths as computed by using the ACI expression for flexure-shear failure. Modification of the ACI equation is proposed for predicting the flexural shear capacity that yields better agreement with the test results
- For the slabs S6-C and S17-H, some of the strands experienced additional slip during application of increasing test load. Despite this partial bond loss, these slabs were able to carry additional load, suggesting that the strands which exhibited additional slip were able to sustain tensile capacity, while the remaining strands were able to continue to carry increasing tensile load, until they too lost bond, and general bond loss failure resulted.
- In the proposed Strut-and-Tie Model, the effective prestressing forces represented by equivalent external loads are gradually introduced along the tendon's transfer length in the nearest strut-tie model joints. The friction at the interface of main diagonal shear cracks is modeled by diagonal struts along the direction of the cracks in strut-tie model. Additional positioning of concrete ties perpendicular to concrete struts is incorporated.
- The initiation of shear cracks impairs the embedment of prestressing strands, and it causes slippage of strands. This results in premature failure of precast prestressed hollow-core slabs.
- The strength reduction factor of 0.75 for Prestressed steel and CFRP sheets is used in this study.
- ACI 318-08 effective factor model gives a good correspondence to experimental test results.

- The results obtained in the proposed strut-and-tie model has been compared with experimental results of a total of 17 prestressed precast hollow core slabs with depths ranging from 200mm to 300mm. The proposed model provides a good agreement with the experimental results.

6.3 RECOMMENDATIONS FOR FUTURE STUDY

- In this study, explanatory tests were conducted for shear strengthening of hollow core slab with thickness of 250 mm. No strength was gained due to CFRP strengthening in that slab. An extensive study is needed to study the influence of CFRP strengthening on hollow-core slabs with thickness greater than 200mm and especially for slabs which failed in web shear failure.
- Further study is needed on the strengthening of hollow core slabs which failed in flexural shear mode with CFRP sheets.

REFERENCES

1. AASHTO, "LRFD Bridge Design Specifications," 2nd ed., American Association of State Highway and Transportation Officials, Washington, D.C., 2005.
2. AbdulKadir, B.A., "Analysis and Design of Hammerhead Bridge Pier Using Strut and Tie Method," M.S. Thesis, Civil Engineering Dept., University of Technology, Malaysia, April 2005.
3. ACI 318-05, "Building Code Requirements for Structural Concrete and Commentary," American Concrete Institute, Farmington Hills, Michigan, 2005.
4. Alshegeir, A., Ramirez, J., "Computer Graphics in Detailing Strut-Tie Models," *Computing in Civil Engineering Journal*, Vol. 6, No. 1, April 1992, pp. 220-231.
5. Bakir, P.G. and Boduroglu, H.M., "Mechanical Behavior and Non-linear Analysis of Short Beams Using Softened Truss and Direct Strut & Tie Models," *Engineering Structure Journal*, Vol. 27, 2005, pp. 639-651.
6. Basil, G., "A Variable Angle Space Truss Model for Structural Concrete Beams," Ph.D. Dissertation, Civil Engineering Dept., University of Toronto, March 1974.
7. Chun, S.C., "Three-Dimensional Strut-and-Tie Analysis for Footing Rehabilitation," *Structural Engineering Journal*, Vol. 7, No. 2, Feb. 2002, pp. 14-25.
8. Collins, M.P. , Mitchell, D., Adebat, p. and Vecchio, F.J. "A General Shear Design Method," *ACI Structural Journal* , January-Febraury, 1996,pp36-45.

9. Colloti, V., Spadea, G., and Swamy, R.N., "Structural Model to Predict the Failure Behavior of Plated Reinforced Concrete Beams," *Composite of Construction Journal*, Vol. 8, No. 2, April 2004, pp. 104-122.

10. Ebead, U. and Marzouk, H., "Fiber-Reinforced Polymer Strengthening of Two-Way Slabs," *ACI Structural Journal*, Vol. 122, No. 5, 2004, pp. 650-659.

11. EC2: Eurocode 2, "Design of Concrete Structures, Part 1, General Rules and Regulations for Buildings," *British Standards Institution*, London, 1992.

12. Eraki, M.A. and Heffernan, P.J., "Reinforced Concrete Slabs Externally Strengthened with Fiber-reinforced Plastic Materials," *Proceedings, 2nd International Symposium, FRPRCS-2*, 1995, pp. 509-516.

13. Hawkins, N.M. and Ghosh, S.K., "Shear strength of hollow core slabs," Prestressed Concrete Institute Journal, Vol. 30, 2006, pp. 110-114.

14. Hong, G. and Jeung-Hwan, D., "Development of Strut and Tie Models in Deep Beams with Web Openings," *Structural Engineering Journal*, Vol. 10, No. 6, 2007, pp. 697-711.

15. Hosny, A.H., Abdelrahman, A., and Elarabi, A., "Strengthening of Prestressed Concrete Slabs Using CFRP," *Composites in Construction*, Vol. 23, 2003, pp. 355-359.

16. Hsu, T.T.C. and Mo, Y.L., "Softening of Concrete in Low-rise Shear Walls," *ACI Journal*, Vol. 82, No. 6, 1985, pp. 883-889.

17. Hwang, S.J., Fang, W.H., Lee, H.J., and Yu, H.W., "Analytical Model for Predicting Shear Strength of Squat Walls," *Journal of Structural Engineering*, Vol. 127, No. 1, 2001, pp. 43-50.

18. Hyo-Gyoung, K. and Sang-Hoon, N., "Determination of Strut-and-Tie Models Using Evolutionary Structural Optimization,"*Engineering Structures Journal*, Vol. 28, 2006, pp. 1440-1449.

19. Kolizadeh, M.T. and Saadatmanesh, H., "Strengthening of Steel-Concrete Composite Girders Using Carbon Fiber Reinforced Polymer Sheets," *Journal of Structural Engineering, ASCE*, Vol. 129, No. 1, 2003, pp. 30-40.

20. Liang, J.L., Chang, W.H., Chuin, S.C., and Ying, P.L., "Strut-and-Tie Design Methodology for Three-Dimensional Reinforced Concrete Structures," *Structural Engineering Journal*, Vol. 132, No. 6, 2006, pp. 929-938.

21. Limam, O., Foret, G., and Ehrlacher, A., "RC Two-way Slabs Strengthened with CFRP Strips: Experimental Study and Limit Analysis Approach," *Composite Structures Journal*, Vol. 60, 2003, pp. 467-471.

22. MacGregor, J.G., "Derivation of Strut-and-Tie Models for the 2002 ACI Code,"*ACI SP-208: Examples for the Design of Structural Concrete with Strut-and-Tie Models*, K.-H. Reineck, ed., American Concrete Institute, Farmington Hills, Michigan, pp. 7-40.

23. MacGregor, J.G., "Reinforced Concrete-Mechanics and Design," *3rd edition ,Prentice Hal,*1997.

24. Mahmud, I., "Modeling of Precast Prestressed Hollow-Core Slabs Strengthened with CFRP," Ph.D. Dissertation, Civil Engineering Dept., KFUPM, Jan. 2008.

25. Marco, A., "Impact of Steel Fiber in Compression Strut Capacity," M.S. Thesis, Civil Engineering Dept., University of Nevada, Dec. 1994.

26. Marti, P., "Truss Model in Detailing," Concrete International, December, 1985,pp 66-73.

27. Mohiuddin, J., "Flexural Behavior of Prestressed Precast Hollow Core Slabs Strengthened with CFRP Sheets," M.S. Thesis, Civil Engineering Dept., KFUPM, Jan. 2006.

28. Mosallam, A.S. and Mosallam, K.M., "Strengthening of Two-way Slabs with FRP Composite Laminates," *Construction and Building Materials*, Vol. 17, 2002, pp. 43-54.

29. Nielson, M.P., *Limit Analysis and Concrete Plasticity*, 2nd Edition, CRC Press, 1998.

30. Nielson, M.P., Braestrup, M.W., and Bach, F., "Rational Analysis of Shear in Reinforced Concrete Beams," *LABSE Periodic, Proceedings*, P-15/78, No. 2, May 1978, p. 18.

31. Ning, Z. and Kang, H.T, "Direct Strut-and-Tie Model for Single Span and Continuous Deep Beams," *Engineering Structure*, Vol. 27, 2007, pp. 2987-3001.

32. Ong, K.C., Hao, J.P., and Parmasivam, P., "A Strut-and-Tie Model for Ultimate Loads of Precast Concrete Joints with Loop Connections in Tension," *Construction and Building Materials Journal*, Vol. 20, 2004, pp. 169-176.

33. Pajari, M., "Shear resistance of PHCC slabs supported on beams. II: Analysis," *Journal of Structural Engineering*, ASCE, Vol. 124, No. 9, 1998, pp. 1062-1073.

34. PCI Design Handbook, 6th Edition, Precast/Prestressed Concrete Institute, Chicago, IL, 2005

35. Pisanty, A., “The Shear Strength of Extruded Hollow Core Slabs.” Materials and Structures, Vol. 25, No. 4, 1992, pp. 224-230.

36. Ramirez, J. and Breen, J., “Evaluation of a Modified Truss-Model Approach for Beams in Shear,” *ACI Journal*, Vol. 88, No. 5, Sept.-Oct. 1991, pp. 562-571.

37. Richard, W., “Strut and Tie Model for Punching Shear of Concrete Slabs,” M.S. Thesis, Civil Engineering Dept., University of Newfoundland, Aug. 1995.

38. Ritter, W. “The Hennebique Design Method (Die Bauweise Hennebique),” 1899.

39. Rong, Q., “Theoretical Analysis of Reinforced and Prestressed Concrete Bridge Members Strengthened with CFRP Laminates,” M.S. Thesis, Civil Engineering Dept., Florida Atlantic University, Dec. 1994.

40. Schlaich, J. and Anagnostou, G., “Stress Fields for Nodes of Strut-and-Tie Models,” *Journal of Structural Engineering*, ASCE, Vol.116, No.1, January, 1990, pp. 13-23.

41. Schlaich, J. and Weischede, D., “Detailing Reinforced Concrete Structures,” *Canadian Structural Concrete Conference*, Department of Civil Engineering, University of Toronto, Toronto, 1981, pp. 171-198.

42. Schlaich, J., Schafer, K. and Jennewein, M., “Toward a Consistent Design of Structural Concrete,” *Prestressed Concrete Institute Journal*, Vol. 32, No. 3, May 1987, pp. 74-150.

43. Tan, K.H., Tong, K., and Tang, C.Y., “Direct Strut-and-Tie Model for Prestressed Deep Beams,” *Journal of Structural Engineering*, Vol. 127, No. 9, 2001, pp. 1076-1084.

44. Tan, K.H., Tang, C.Y., and Tong, K., "A Direct Method for Deep Beams with Web Reinforcement," *Magazine of Concrete Research*, Vol. 55, No. 1, 2003, pp. 53-63.

45. Tjhin, T.S. and Kuchma, D.A. "Computer-Based Tools for Design by Strut-Tie Method: Advances and Challenges," *ACI Structural Journal*, September-October, 2002, pp. 586-594.

46. Tong, K., "Strut-and-Tie Approach to Shear Strength Prediction of Deep Beams," MEng. Thesis, Nanyang Technological University, Singapore, 1997.

47. Wight, R.G. and Erki, M.A., "Prestressed CFRP Sheets for Strengthening Concrete Slabs in Fatigue," *Advances in Structural Engineering*, Vol. 6, No. 3, 2003, pp. 175-181.

48. Vecchio, F.J. and Collins, M.P., "Compression Response of Cracked Reinforced Concrete," *Journal of Structural Engineering*, Dec., 1986, pp. 3590-3611.

49. Yang, L., "Design of prestressed hollow core slabs with reference to web shear failure," *Journal of Structural Engineering*, ASCE, Vol. 120, No. 9, 1992, pp. 2675-2696.

50. Young, M.Y., "Computer Graphics for Nonlinear Strut-Tie Model Approach," *Computing in Civil Engineering Journal*, Vol. 14, No. 2, April 2000, pp. 127-133.

51. Young, M.Y. and Julio, A.R., "Strength of Struts and Nodes in Strut-Tie Model," *Journal of Structural Engineering*, Vol. 122, No. 1, 1996, pp. 20-29.

52. Yun, Y.M. and Ramirez, J.A., “Strength of Struts and Nodes in Strut-Tie Model,” *ASCE Journal of Structural Engineering*, Vol. 122, No. 1, 1996, pp. 20-29.

VITA

NAME : **Muneer Kaid Said Abdo**

ADDRESS: **Almekhlaf- Sharaab Alsalam**

Taiz City

Yemen

E-MAIL: **Mounir _Almekhlafi@ hotmail.com**

EDUCATIONAL QUALIFICATIONS

M.S (Civil Engineering – Structures)

February 2005-April 2009

King Fahd University of Petroleum and Minerals, Dhahran, Saudi Arabia

GPA- 3.906/4.00

B.E. (Civil Engineering)

September 1996-April 2001

Tishreen University – Syria